Summer 8-18-2023

Linkages Among Hydrodynamics, Biofouling, & Sea Scallops on an Aquaculture Farm

Elisabeth Younce
University of Maine, elisabeth.younce@maine.edu

LINKAGES AMONG HYDRODYNAMICS, BIOFOULING, & SEA SCALLOPS ON AN AQUACULTURE FARM

By

Elisabeth Younce

A THESIS

Submitted in Partial Fulfillment of the

Requirements for the Degree of

Master of Science

(in Civil & Environmental Engineering)

The Graduate School

The University of Maine

August 2023

Advisory Committee:

Kimberly Huguenard, Associate Professor, Department of Civil and Environmental Engineering, Advisor

Lauren Ross, Associate Professor, Department of Civil and Environmental Engineering

Damian Brady, Agatha B. Darling Associate Professor of Oceanography

LINKAGES AMONG HYDRODYNAMICS, BIOFOULING, & SEA SCALLOPS ON AN AQUACULTURE FARM

By Elisabeth Younce

Thesis Advisor: Dr. Kimberly Huguenard

An Abstract of the Thesis Presented
in Partial Fulfillment of the Requirements for the
Degree of Master of Science
(in Civil & Environmental Engineering)
August 2023

Understanding the linkage between hydrodynamics, biofouling and shellfish growth enables Maine aquaculture farmers to optimize their net profit. This thesis focuses on lantern-net based Atlantic Sea Scallop farming, which is a relatively new industry in Maine with excellent economic potential. This study characterized and quantified the hydrodynamics, biofouling, and shellfish growth along a scallop longline at the Darling Marine Center experimental aquaculture farm from July-Oct 2021. Its purpose was to investigate farm-wide associations of water, scallops and biofoulants that can be applied by aquaculture farmers to improve cultivation methods and act as foundational work for future research. Hydrodynamics were quantified with monthly tidal surveys with an underway Acoustic Doppler Current Profiler (ADCP) and a vertical profile and incident current angles from a moored ADCP near to the longline. Methods to measure in-water weights of biofouling on lantern nets were developed and applied on a monthly time scale, and scallop heights and weights were also recorded in parallel. Velocities local to the farm generally showed flow reduction in space and over time in the farm layer as

lantern net mass and solidity increased due to biofouling and scallop growth, while flows accelerated underneath the farm- a phenomenon that occurred due to conservation of mass. The effects of friction imposed by the farm structure (inclusive of biofouling and scallops) upon the ambient hydrodynamics, were directly quantified as tidal asymmetries (ratio of D4/D2 tidal energy bands) and as normalized magnitudes of the after-farm velocities. Accumulated biofouling weight and scallop weight were shown to have a significant, linear relationship that varied throughout the water column on both the tidal asymmetries and normalized magnitudes, controlling for oceanographic conditions. The northern half of the longline (farthest into Lowes Cove) presented lower velocity magnitudes throughout the tidal cycle ($\leq$1 cm/s) than did the southern half ($\geq$1cm/s), and it also demonstrated lower shellfish growth but higher biofouling settlement and accumulation than the southern half. The orientation of ambient current relative to the longline (incident angles) and farm wake generation were examined to determine if farm orientation was a factor in this reduction in velocity moving northwards up the longline. It was discovered that the Darling Marine Center aquaculture farm was in its own wake for 65% of flood tide velocities. This likely effected shellfish growth negatively and biofouling accumulation positively, as downstream nets would experience decreased flow speed inside the wake of upstream nets. Further study is recommended to determine if rotating the farm would be beneficial to cultivation goals. This study demonstrated that the connection of hydrodynamics, shellfish growth, and biofouling in semi-sheltered lantern net farms is quantifiable and statistically significant. Findings underscore the importance of knowledge about incident current angles in farm siting and mooring orientation decisions, as well as providing foundational information on how biofouling, scallop cultivation, and local flow interact.

ACKNOWLEDGEMENTS

"Guess what?? We get to do math today, all day!"

– Dr. Eric Sullivan

I would like to thank my advisor, Dr. Kim Huguenard for the opportunity to become an engineer, and her support throughout this entire journey. Also, thank you to the U.S. Army Engineer Research and Development Center (ERDC) and the Advanced Structures and Composites Center (ASCC) for funding of my master's degree. Thank you as well to Dr. Damian Brady, Dr. Lauren Ross, Dr. Neil Fisher, and Dr. Toby Dewhurst, and Dr. Jon Yoder for their insights and guidance. There are many others I would like to thank, especially Cristian Rojas, Engiliyage (Nalika) Lakmali, Sam Rickerich, Anthony Flores, Nicolas Cyr, Christopher Abela, Aidan Carlson, Lucy Slattery, and others who have lent data advice, and talked through analyses with me. To all the students who helped me with field work, I literally could not have completed this without you (Liam, Alyson, Reilley, Matt, Sam (again), Casey, Will, Leah, Nick (again), and Preston). I am extremely indebted to Tom Kiffney, Struan Coleman and Rob Cuddy for their aid, guidance, and implementation of the biological field experiment. Staff, professors and students at the Darling Marine Center all took an active role in actualizing the project and I am the author is incredibly grateful for their collaborative spirit and support. Without them this never would have gone from idea to reality. Additionally, I would like to thank all my friends and "family" in Orono, Maine, including my coworkers and supervisors at the ASCC and the University of Civil & Environmental Engineering Department. You mean the world to me, and I relied on your support throughout this process. Hopefully you weren't too tired of my ocean jokes by the end.

Finally, I would like to dedicate this thesis to my recently passed undergraduate advisor, Dr. Eric Sullivan and the people of Comau Fjord, Hualihué, Región de Los Lagos, Chile. Dr. Sullivan lost a battle to brain cancer in early 2023 at the age of 47. He was the best math teacher I ever had the honor to study with, and always pushed us to appreciate 100% of life in career and in the outdoors, often by covering every assignment in red ink then encouraging us to try again: with his boundless energy, positivity and patience. The uncertainty analysis used in this work is based on a method he and I brainstormed after I came to office hours, stuck on how to get the necessary parameters for sensitivity analysis of an Optimization project. This resultant, modified Monte Carlo will always be special to me. Comau Fjord was my home for over a year and the people of Hornopirén, Huinay, Leptepu, and the Camanacha salmon pontoon, 'Llongchochagua' were especially welcoming. We have many memories together from asados to soccer matches, to early mornings drinking maté and catching rides on the *Serenade*. These people and our shared fjord, including its natural inhabitants, are what inspired me to pursue a career in aquaculture engineering. Someday I hope to see them again.

TABLE OF CONTENTS

LIST OF TABLES

LIST OF FIGURES

CHAPTER 1: INTRODUCTION

The world population is now almost 8 billion people (United States Census Bureau, 2023), and each individual needs daily nutrition. The United Nations lists their second Sustainable Development Goal as “End hunger, achieve food security and improved nutrition and promote sustainable agriculture” (United Nations, n.d.). Sustainable in this context implies a net neutral or net positive impact on both the socioeconomic and ecological climate of the earth (United Nations, n.d.); an application or process that, by its essence, can exist indefinitely. Not only does the human population need to thrive, but it must also do so while allowing and enabling the other living inhabitants, as well as the natural biotic and abiotic processes, to thrive as well. Seafood is known, in general, for its high nutritive content, especially regarding protein (Reames, 2012; Washington State Department of Health, n.d.), as well as its efficiency in the production of those nutrients through natural processes. This efficiency within nature makes seafood a sustainable food source, however, climate change and the short-sighted consumption of humanity have created instability in the wild fisheries of the world (Harte, Tiller, Kailis, & Burden, 2019; Government of Canada, 2009). Therefore, agricultural seafood, or aquaculture, is left to fill that gap.

Around the world, aquaculture has existed in some form for millennia. In the Pacific Northwest of North America, the five Pacific salmon species, Chinook, coho, pink, chum and sockeye have dictated the way of life of Native Americans for centuries (Anderson & Connolly, 2022; NOAA Fisheries, 2022). For example, their traditional respect and care for sustenance of the wild population of salmon, including traditional fishing methods, limitations of catch, annual

rituals, stories, and songs, (NOAA Fisheries, 2022; Squamish Tribe, 2023; Loy & Cai, 2017), all demonstrate the roots of aquaculture, by abstract definition. From this perspective, aquaculture is a nurturing, respectful relationship of humans with a species whose population they maintain for food, and in the case of the first nations, many other life necessities. However, the Native American tribes were unable to maintain this sustainable "aquaculture" when they lost primary ownership of the fisheries and lands that had been under their control for centuries due to initial colonization and now urban/suburbanization of the Puget Sound region. Today, a more typically defined version of aquaculture is practiced to prevent those five species from disappearing (Anderson & Connolly, 2022). Hatcheries managed by the federal and state governments cultivate fish annually (Anderson & Connolly, 2022). As Native American tribes have regained more of their original rights regarding salmon, they have taken an increasingly active role in this modern aquaculture to fulfill the goals of their original "aquaculture", to respectfully take and give from the marine species that sustain their way of life (Anderson & Connolly, 2022).

In Maine, there is a long history of respectful dependence on aquatic species. As with salmon in the Pacific Northwest, a respectful necessity for Brook Trout led the Aroostook Band of Micmacs to initiate modern aquaculture efforts through a recirculating aquaculture facility (Bagnall, 2022; Harder, 2020). They seek to maintain the population of Brook Trout in northern Maine as climate change and pollution threaten the wild population in lakes and ponds (Bagnall, 2022; Harder, 2020). Yet, it is more than just the Native Americans of Maine that maintain a respectful and caring relationship with marine life. The lobster fishermen of Maine are known worldwide in political science and economics fields as a counterexample to the "tragedy of the

commons" (Corson, 2009) which occurs when everyone takes as much as they want from a shared resource (often nature-based), without regard for the wellbeing of the resource itself or for their shared stakeholders (Hardin, 1968). The "tragedy" is the subsequent collapse of the shared resource (Hardin, 1968). In contrast, the Maine lobster fishery is known for the collaboration of its fishermen; fishing grounds and quotas per group are not only well-communicated and respected, but also enforced by lobstermen upon each other, albeit sometimes violently (Corson, 2009). If lobstermen break trust and do not follow the common agreements, their fellow constituents enforce consequences (Corson, 2009). This culture of accountability to community and nature has been a factor of prevention of overfishing of the lobster population and ensured mutual economic waterfront welfare in the region for generations (Perry, 2010). An additionally notable demonstration of respectful dependence on aquatic species within the region occurred when the wild Atlantic Sea Scallop population in the Gulf of Maine almost collapsed due to lack of population monitoring in the mid-1990s (Hart & Rago, 2006). At that time, the state of Maine worked with wild scallop fishermen to create a network of rotating protected areas closed to fishing (Hart & Rago, 2006). The scallop population was able to recover for sustainable fishing and ecosystem health in the present day (Hart & Rago, 2006). However traditional fishing industries in the Gulf of Maine, including lobsters and sea scallops, are experiencing increasing instability due to warming water temperatures (Pershing, et al., 2021, and references therein; Zang, et al., 2023). As waters warm, lobsters are migrating (Tanaka, Torre, Saba, Stock, & Chen, 2020), and growth of the Atlantic Sea Scallop is being inhibited (Zang, et al., 2023). Expansion of modern aquaculture presents a potential solution.

The known history of modern aquaculture in Maine began in the same century as that of the Pacific Northwest, and, as exemplified with the Brook Trout, it is the natural next step in the history of respectful dependence on marine life. The mid-20th century saw the beginnings of European oyster and soft-shell clam cultivation, as well as implementation of a shellfish hatchery at the Darling Marine Center (Schmitt & Hartin, 2016). Since then, partnerships with Maine Sea Grant and the University of Maine have fostered cultivation of various species (Schmitt & Hartin, 2016). One such program was to replace the once endemic oyster population through aquaculture (Schmitt & Hartin, 2016). This was especially significant for the Damariscotta River estuary, where the Whaleback Shellfish Midden has been a testament for millennia of the role of the species in the lives of the Native Americans of the coast (Maine Department of Agriculture, Conservation & Forestry, 2021). Today, the wild oyster population in Maine has continued to increase, and the Damariscotta River Estuary is the capital of cultivated oysters in Maine (Thompson et al., 2006). In the same way that aquaculture has been vital in regenerating the oyster population and maintaining that of Brook Trout, farming of Atlantic Sea Scallops is emerging as a way to (a) potentially aid long term population preservation of the wild stock of the same species and (b) provide an economic supplement for fishermen of lobster and other species, whose livelihoods are at risk from stock die-offs and migration due to climate change. Scallop aquaculture has been encouraged and developed with cross cultural exchange of knowledge with the Aomori state in Japan, the sister state of Maine, and has included various methodologies. The farming method of using lantern nets (Fig. 1)

Figure 1. Scallop lantern nets hung on land prior to use at the Darling Marine Center (DMC) experimental aquaculture lease. Photo used by permission from S. Coleman.

for sea scallops was learned from Aomori (NOAA Fisheries, 2020) and is also common in China, which is the largest producer of farmed scallops (not Atlantic Sea Scallops) at a global level (Guo & Luo, 2016). Another farming method is ear-hanging of scallops, also learned from Aomori and applied in Maine (Morse et al., 2020). In January 2021, the Scallop Research Collaborative hosted its first meeting that brought farmers, researchers, and other government and industry stakeholders together to discuss successes, challenges, and the future of scallop aquaculture in Maine. A primary concern of farmers was reiterated throughout the program, and as of the 2023 Maine Aquaculture R&D&E Summit remained: how to mitigate biofouling on farms while maximizing stock yield and maintaining efficiency for both monetary and human capital.

Biofouling is the growth of water-based organisms on surfaces, living and non-living, that are submerged in water both continuously and infrequently. Though the larger definition includes freshwater, it is the organisms that colonize surfaces in the marine environment which are important to sea scallop farmers (and the larger marine aquaculture industry worldwide). Overall, fouling is dictated by fluid dynamics and particle transport on all scales, as larvae and other plankton, often with little self-motility, are transported by circulating currents to a submerged surface, where the microscopic organisms will colonize based on the texture, slope, fluid critical stresses, fluid temperature and chemical characteristics to said surface, as well as seasonal patterns (Abarzua & Jakubowski, 1995; Bullard et al., 2013; Edmondson & Ingram, 1939; Menesses et al., 2017; Newell & Branch, 1980; & Okubo, 1978). More chronologically, within minutes of submersion of a surface, a conditioning film of organic molecules will form, which is (in general) a required base for colonization of subsequently larger and biologically complex organisms. Considering a successional model of biofouling: an initial film thickens from adhesion of proteins (in minutes), to bacterial colonization of a surface (over days) and then grows into a secondary film (microfouling) from the addition of diatoms, macroalgae, and protozoa in the first few weeks after submersion (Abarzua & Jakubowski, 1995; Nurioglu et al., 2015; Vinagre et al., 2020; Wahl, 1989). Afterward, larger organisms, i.e. macrofoulants such as algae, animal larvae,spores and fully-developed organisms are able to colonize the surface (Abarzua & Jakubowski, 1995; Nurioglu et al., 2015; Vinagre et al., 2020; Wahl, 1989). It is important to note that in the initial weeks of fouling, fluid dynamics are one of the primary factors of foulant settlement and growth, as they not only dictate the critical stress levels (Menesses et al., 2017) but also have larger impacts through circulation patterns which effect the

abiotic conditions, such as chemical and temperature (Abarzua & Jakubowski, 1995; Edmondson & Ingram, 1939) as well as transport of particles to a location (Okubo, 1978); in this sense, particles refers to the micro-organisms themselves and to the nutrients necessary for their growth. Sunlight is also an important factor in fouling, as plant foulants, such as Cladophora spp., themselves utilize photosynthesis (Michalak & Messyasz, 2021, and references therein) or feed on autotrophs such as algae (Petersen, Schou, & Thor, 1997). This makes the depth that a surface is submerged, inclusive of tidal range, an indirect factor in fouling. Regardless, after development of macrofouling and especially as surface roughness increases, the weight and structure of the foulants will be altered (Abarzua & Jakubowski, 1995; Nurioglu et al., 2015; Vinagre et al., 2020; Wahl, 1989), which will have effects on the ambient fluid dynamics (Cengel & Cimbala, 2018) and therefore an aquaculture farm. These hydrodynamics in turn dictate local processes including (but not limited to): nutrient transport, abiotic properties such as pressure and temperature, overall flow speed and structure , and hydrodynamic and hydrostatic forcing on the surface (Bashevkin & Mahardja, 2022; Cengel & Cimbala, 2018; Davidson, 2015; Hammack et al., 2009; Okubo, 1978). These effects are important to aquaculture farmers not only because they impact the farming equipment (hydrostatic and hydrodynamic forcing) but also because (a) many foulants compete with cultivated shellfish for nutrients, (b) occluded nets mitigate the ambient flow to shellfish, and (c) some foulants attach to and therefore inhibit growth of the cultivated shellfish directly (Bannister et al., 2019, and references therein; Palanisamy et al., 2018; Fitridge et al., 2012, and references therein). As sea scallops are a more sensitive species to external stressors, these typical impacts are magnified (Morse, et al., 2020) and references therein. Within Maine, common hard macrofoulants include barnacles and

mussels, which regionally colonize during May/June (Scrosati & Holt, 2021) and July/August (Petraitis, 1991), respectively. Many common microfoulants belong to a collection of ascidians, some invasive, that have soft structures which expand to full shape in water and deflate when removed from the sea. Some of these, such as *Ciona intestinalis*, are rounded and tube-like (Trotter, 2018) and others, such as *Didemnum vexillum*, are flatter and carpet like (Kaplan, et al., 2017). The highest recruitment of ascidians in the Gulf of Maine is during August/September (Bullard, Davis, & Shumway, 2013).

This thesis seeks to address the request of Maine sea scallop farmers for research in biofouling mitigation by studying the linkages between biofouling and hydrodynamics on a lantern-net based Atlantic Sea Scallop farm, while also monitoring shellfish growth on that same farm. This larger goal to connect hydrodynamics, biofouling, and shellfish growth was constructed with three objectives. Primarily, (1) to plan and perform a foundational study on biofouling and hydrodynamics (and shellfish) around a lantern net farm in Maine. Secondly, (2) to create a method for collecting in-water weights on a lantern-net farm and an analytical model connecting hydrodynamics with biological growth. Finally, (3) to determine what implications these findings yield for (a) the Darling Marine Center experimental farm and the larger scallop farming industry in Maine with respect to farm siting, farm and orientation, and local flow patterns, and (b) further research on hydrodynamics and biofouling for Maine aquaculture. As with many of the historical aquaculture initiatives in the Pine Tree State, partnership with the Darling Marine Center (DMC) was central to this research work. The experimental aquaculture farm of the DMC facilitated the longline of scallop-filled lantern nets, while the research vessel of the DMC, as well as the skiff were utilized for hydrographic data collection. This study was,

to my apparent knowledge, the first of its kind in the Gulf of Maine and was meant to be foundational, providing data and ideas for further studies with larger impacts that will enable expansion of the Atlantic Sea Scallop aquaculture industry in Maine. This work is presented across two material chapters and one implications chapter, with Chapter 1 being (this) introduction. Chapter 2 encompasses the study and results. Chapter 3 describes the biological field methods and analytical model for quantifying biofouling and sea scallops over the time series. The final, concluding chapter (Chapter 4) describes recommendations for the Darling Marine Center, as well as larger Maine aquaculture stakeholders and future regional research on this topic.

CHAPTER 2: BIOLOGICAL FIELD & QUANTITATIVE ANALYSIS METHODS

Introduction

Interactions of hydrodynamics and ecology make the calculation of in-water weights of suspended (biological) objects difficult, especially of objects with varying surfaces, densities, and a biological need to stay in seawater, such as scallop farm lantern nets that contain live scallops. More importantly, the high monetary and logistic cost of hydrodynamic instrumentation, as well as necessity for specialized knowledge in data interpretation, are barriers to knowledge on small-scale aquaculture farms. This Aug-Oct 2021 biofouling study created a novel method for collecting in-water weights of scallop-filled lantern nets that utilized a control object of a known in-air weight, constant mass, and structure to create a relative weight scale that is collected in tandem with in-water net weights throughout the extent of the experiment. The costliest equipment was a ~$50 industrial crane scale. The time series of the control item weights quantifies variations in both the hydrodynamic environment (assuming all weights are taken in a sheltered, low-energy area) and the scale functionality. A time series of whole-net weights, R_W, was calculated per lantern net by utilizing unit multipliers to scale the measured in-water weights (of the whole lantern nets) to the control item time series. A relation developed from basic physics then yielded the estimated biofouling weight per net, $E_B *$, from R_W and the estimated total submerged weights of scallops per net, E_S.

Methods

Experimental Setup

On the first day of the study, nine lantern nets (10 tiers each) were filled with 15 scallops per tier and given a numerical tag. Scallops were randomly selected from overflow/stock farm nets and were approximately two years of age (personal communication, T. Kiffney). Each net had a total of 150 scallops, for a total of 1350 scallops in the entire experiment. Before placement on the longline, the in-water weight was taken of each lantern net, as detailed in *Whole Net Weights*, and the heights and submerged weight of 4 scallops per tier were also recorded as detailed in *Scallop Measurements*. The in-air weight of the control object was also measured and recorded. For the next three months, measurements of in-water weights, scallop heights, submerged scallop weights, and photos of biofouling were recorded per lantern net, per sample group within 72 hours of the second neap tide for consistency of tidal conditions.

Whole Net Weights

Nets were transported from the longline to the floating dock one sample group at a time. Care was taken to drive slowly both to not (a) stress the animals in the nets or (b) knock off the biofouling accumulated on the nets. Nets were tied off to keep them in their environment while not actively being measured. Per group, the leeward side of the dock was determined and used as the location for all whole net weights to ensure the calmest (lowest energy) environment possible for measurements. Using the same location for all weights per sample group reduced error. This was feasible because the hydrodynamic conditions were relatively constant for the 30-45 minutes

per sample group measured. However, the control item time series was collected in tandem with all in-water weights to quantify any variations in the hydrodynamics, including during the 30-45min windows. This control item (approx. 1 m of 2.5 cm chain for first half of time series) was weighed in air with the crane scale on the first day of measurements.

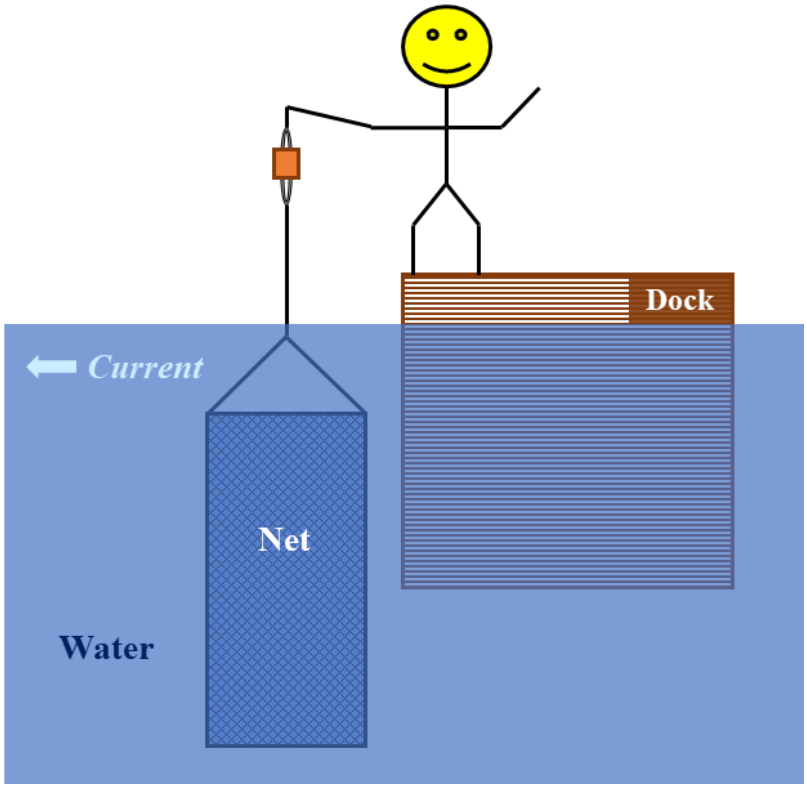

Figure 2. Diagram of how in-water weights were measured.

The in-water weight of the lantern nets, inclusive of biofouling and scallops, was measured with a RoMech 660lb Mini Digital Hanging Scale to the nearest 0.01kg. The control item was weighed in the water immediately before or after each net was weighed. The crane scale reading fluctuated even with small water movements, so a delay of approximately 30-60s was needed to let the scale reading converge. If the scale reading oscillated consistently

(generally oscillations were ≤0.1kg), it was up to the data collector's best judgement to estimate the median weight of the digits fluctuating on the scale. Error introduced from these oscillations was accounted for by the uncertainty analysis (see Chapter 3: Uncertainty Analysis).

The original control item (chain) was lost during September data collection. Fortunately, multiple weight measurements were already recorded from that day, and several bricks were used as a new control object. Their in-air weight was recorded, and they were utilized as the control object for the remainder of the experiment. Calculating the ratio of the mean of the in-water bricks to the mean of the in-water chain from that collection day enabled correction of future measurements to the original scale. However, this did introduce more error into the scaling, making the uncertainty analysis more important (see Chapter 3: Uncertainty Analysis). There was relatively low variation of weight values measured of the control item over the time series. The amount of water that may have been absorbed by the bricks throughout each measurement day was considered negligible.

Scallop Measurements

A random subsample of 4 scallops per tier was selected for heights and submerged weights (40 scallops total per net). The heights of the four selected scallops per tier were measured with scientific calipers. The heights were the shellfish growth measurements over time, and enabled calculation of an average scallop size per tier per net.

For submerged weights, a bucket was filled to approximately 2/3 volume with seawater and weighed by suspension with the crane scale over the floating dock. To maintain tier differences and track progress through the net tiers as heights were measured, the shellfish

subsamples were placed in mesh oyster bags labeled by tier. The bags of shellfish subsamples were then placed in the same bucket of seawater that was already weighed with the crane scale. The bucket was emptied and refilled per lantern net. Once all ten oyster bags of shellfish were fully submerged in the bucket, it was weighed again with the crane scale. The weight of the water and bucket would be subtracted by the bucket with the shellfish to leave only the submerged shellfish weight. This submerged weight of the scallops was multiplied by the ratio (150/40), to estimate the total submerged shellfish weight (E_S) per lantern net (*Relative Weights: Calculation*); the ratio was the count of total scallops (150) to the count of sampled scallops (40).

More scallops had to be added to several lantern nets at the end of the first month, due to a mishap with a boat propeller. Care was taken to get approximately the same size scallops as those remaining in the tiers. However, the most damaged net (Net 39, from Center sample group) was removed from the analysis to mitigate outliers and confounding variables. Additionally, the bagged shellfish + seawater bucket weight was not recorded for Net 41 (from North sample group) in October. However, as there was complete shellfish height data from that day, this missing value for the shellfish weight was interpolated from a multiple of the shellfish heights, because shellfish weight is directly proportional to shellfish height (Hennen & Hart, 2012).

Photography

Prior to shellfish measurements, photos were taken of each net, the tag of the net and 4 side photos which covered 90-deg each of the cylindrical lantern net. These were used for identification of biofouling organisms, visual tracking of biofouling changes over time, as well as detection of trends in biofouling communities per sample group.

Calculation of Relative Weights

The relative weight of net i on month j was $R_{W_{ij}}$, calculated as:

$$R_{Wi,j} = \frac{W_{ij}}{C_{ij}} \frac{\overline{C_{ij}}}{C_0} \quad (1)$$

Where W_{ij} was the whole net weight, C_{ij} was the control object weight, and $\overline{C_{ij}}$ was the mean control object weight from a particular date of measurement, while $C_0$was the in-air weight of the control object from the first day of measurements. The estimated total submerged weight of the scallops per lantern net was given by:

$$S_{Bucket_{ij}} - S_{Sbucket_{ij}} = S_{Scallops_{ij}} \quad (2)$$

$$\frac{150}{40} \times S_{Scallops_{ij}} = E_{S_{ij}} \quad (3)$$

Where $S_{Bucket_{ij}}$ was the weight of the bucket of seawater suspended from the crane scale, $S_{Sbucket_{ij}}$ was the weight of the seawater filled bucket including the 10 oyster bags of 4 scallops each, and $E_{S_{ij}}$ was the estimated weight of scallops in the *i*th whole lantern net. The fraction $\frac{150}{40}$ was the unit multiplier for the total scallops in the net (150) relative to the count of scallops in the sample (40). The relation among submerged biofoulant weight, $E_{B_{ij}}$, the whole net relative weight, $R_{W_{ij}}$ and the submerged weight of all scallops in the net, $E_{S_{ij}}$, was found as:

$$R^2_{W_{ij}} \approx K_i \left[E_{S_{ij}} + E_{B_{ij}}\right] \quad (4)$$

where the factor K_i accounted for the impact of hydrodynamics of R_{Wij}, squaring R_{Wij} accounted for interaction terms of the net and hydrodynamic forces, and the submerged weight of the lantern net was counted negligible. The factor K_i was calculated per net *i* from the initial date of measurement, since $E_{B_{ij}}$ was zero at the start of data collection. These K_i values were then utilized to calculate $E^*_{B_{ij}}$, which was a non-density corrected estimate of the real $E_{B_{ij}}$, for the rest of the time series. The initial model utilized $R_{W_{ij}}$ in place of $R^2_{W_{ij}}$, however, as detailed later in this chapter, the uncertainty analysis (see Chapter 3: Uncertainty Analysis for methods) created instability for the initial model, as there were unpredictably large variations in results

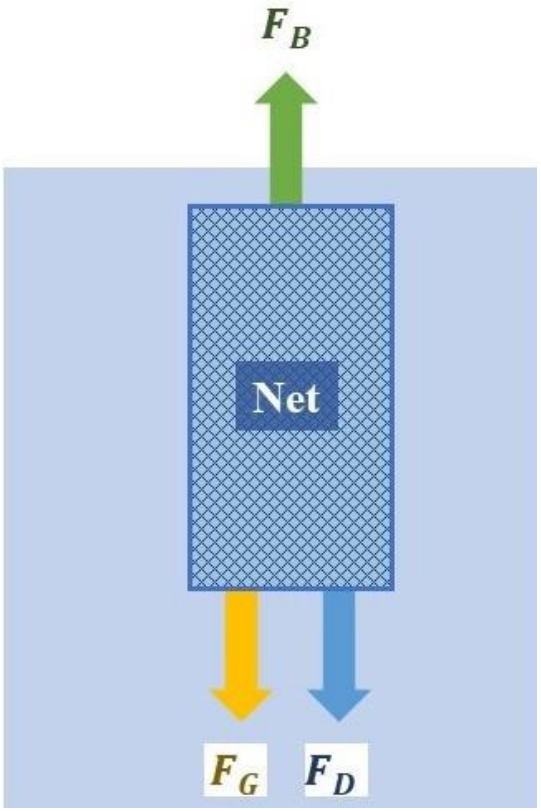

Figure 3. Free Body Diagram of nets for the in-water weight measurement by crane scale, where F_B is the buoyant force (positive up), F_D is the drag force (positive down), and F_G is gravity force (positive down).

when n and/or p were increased. Expansion of the final model in Equation (4), including a free-body diagram (*Figure 3*), list of variables (*Table 1*), relevant assumptions, and derivation of the empirical hydrodynamic constant, *K*, continues:

Table 1. Definition of variables in analytical model and derivation

Term	**Definition**
F_G	Gravity force
F_D	Drag force
F_B	Buoyant force
m_B	Biofoulant mass
m_S	Sea scallop mass
$\overline{\rho_S}$	Mean density of a sea scallop
$\overline{\rho_B}$	Mean density of a biofoulant
m_S^*	Estimated biofoulant mass
g	Acceleration due to gravity
R_W	Relative weight from the crane scale measurements, corrected to control object
K	is the factor for conversion of F_G to $\Sigma^{\downarrow+}F_Y$ for in-water weights, calculated per net on the first measurement day (i.e. when $m_B = 0$)

Relative Weights: Assumptions

The following assumptions are required for applicability of the analytical model expressed in Equation (4). Variables are those that are defined in Table 1 but are also stated in the text.

1. The mass of the lantern net is negligible relative to the mass of sea scallops (m_S) and biofoulants (m_B) such that the force of gravity, $F_{G,}$ acting on a lantern net with scallops and biofouling is equal to: $F_G = (m_B + m_S)g$, as from Newton's Second Law force is the product of mass and acceleration (and g is acceleration due to gravity).
2. When the lantern nets were deployed, there was no biofouling mass (m_B) on the experimental nets, therefore at the first set of measurements, $m_B = 0$.
3. For the entire time series, the square of the relative weight of a net (R_W^2) was equal to the empirical hydrodynamic constant (K) multiplied by the sum product of the masses (in the case of the biofoulants, the estimated mass) of the biofoulants (m_B^*) and sea scallops (m_S) and gravity (g) such that: $R_W^2 = K(m_B^* g + m_S g)$. At the first measurement, when the lantern nets had no biofouling accumulation, this simplified to, $R_W^2 = K(m_S g)$, and therefore the total gravitational force on a lantern net was a function of the sea scallop mass, such that $F_G = m_S g$.
4. The relation of mass to size, which affects displaced water volume (for F_B), cross-sectional area and drag coefficient (for F_D) is approximately constant for scallops and biofoulants in the study, such that the density of the scallops in the *i*th net ($\rho_{S,i}$) should approximate the mean density of all scallops on the longline ($\overline{\rho_S}$), and the density of

biofoulants (per species) on the net ($\rho_{B,i}$) should approximate their respective mean densities ($\overline{\rho_B}$), such that: $\rho_{S,i} \approx \overline{\rho_s}$ and $\rho_{B,i} \approx \overline{\rho_B}$ for any *i*th lantern net.

5. Sea scallops inside the lantern nets are settled in the 30-60 seconds as the crane scale converges during in-water weight measurements (i.e. they were not swimming).
6. Since volume displaced, cross-sectional area, and drag coefficient are related to mass through density, the rate of change of these with respect to mass for biofoulants (m_B) versus scallops (m_S) is proportional to the ratio of their average densities, $\left(\frac{\overline{\rho_B}}{\overline{\rho_S}}\right)$, leading to assumption (7).
7. If the mean density of the sea scallops in a lantern net ($\overline{\rho_S}$) is equal to the mean density of the biofoulants ($\overline{\rho_B}$) on that same net, $\overline{\rho_S} = \overline{\rho_B}$, then $m_B = m_B^*$ so that the true biofoulant mass (m_B) is equal to the estimated biofoulant mass (m_B^*). Otherwise, the true biofoulant mass (m_B) is equal to the estimated biofoulant mass (m_B^*) multiplied by the ratio of the mean density of the biofoulants ($\overline{\rho_B}$) to the mean density of the scallops ($\overline{\rho_S}$), expressed as $m_B = m_B^* \left(\frac{\overline{\rho_B}}{\overline{\rho_S}}\right)$.

Relative Weights: Derivation

To derive the meaning and force-composition of the hydrodynamic empirical constant, K, from the relative weights taken at the first measurement, where $R_W^2 = K(m_S g)$ and $R_W = F_G + F_D - F_B$, the following derivation applies:

At the first measurement: $$R_W^2 = K(m_S g) \quad (5)$$

Through substitution let: $$(F_G + F_D - F_B)^2 = K(m_s g) \quad (6)$$

And as: $$(A + B + C)^2 = A^2 + 2AB + 2AC + B^2 + 2BC + C^2 \quad (7)$$

let: $A = -F_B, B = F_D$, and $C = F_G$ such that:

$$(-F_B)^2 + 2(-F_B F_D) + 2(-F_B F_G) + F_D^2 + 2F_D F_G + F_G^2 \approx K(m_S g) \quad (8)$$

recall that for month one: $F_G = m_S g$. It follows that:

$$\frac{F_B^2 - 2F_B F_D + F_D^2}{F_G} + \frac{-2F_B F_G + 2F_D F_G + F_G^2}{F_G} = K \quad (9)$$

$$\frac{\mathrm{F_B^2 - 2F_B F_D + F_D^2}}{\mathrm{m_S g}} + 2\mathrm{F_B} + 2\mathrm{F_D} + \mathrm{m_S g} = K \quad (10)$$

And finally, for the first month of measurements:

$$R_W^2 = ([F_B^2 - 2F_B F_D + F_D^2][m_S g]^{-1} - 2F_B + F_D m_S g)(m_S g) \quad (11)$$

It is important to note that as $E^*_{B_{ij}}$ is on a scale unique to its location and time series, and should not be reported in lbs, kgs, or other typical units of mass or weight unless corrected with densities of biofouling organisms and scallops. Also note that calculation of the relative weights for this Aug-Oct 2021 study utilized more multipliers of control items to account for (a) change

in control item during September measurements, (b) having to take August measurements split between two days.

Results

As part of model development, derivation of the monthly means, including uncertainty analysis were calculated with data divided into north and south halves of the longline and (initially) without squaring the left side of Equation (4). However, without squaring the left-hand side of Equation (4), the estimated biofoulant weight (E_B^*) curves fluctuated unpredictably when simulated from even the lowest precision level (p) and confidence intervals were wide enough to encompass the entire vertical range of the time series (*Figure 4*, left panel). After the left-hand

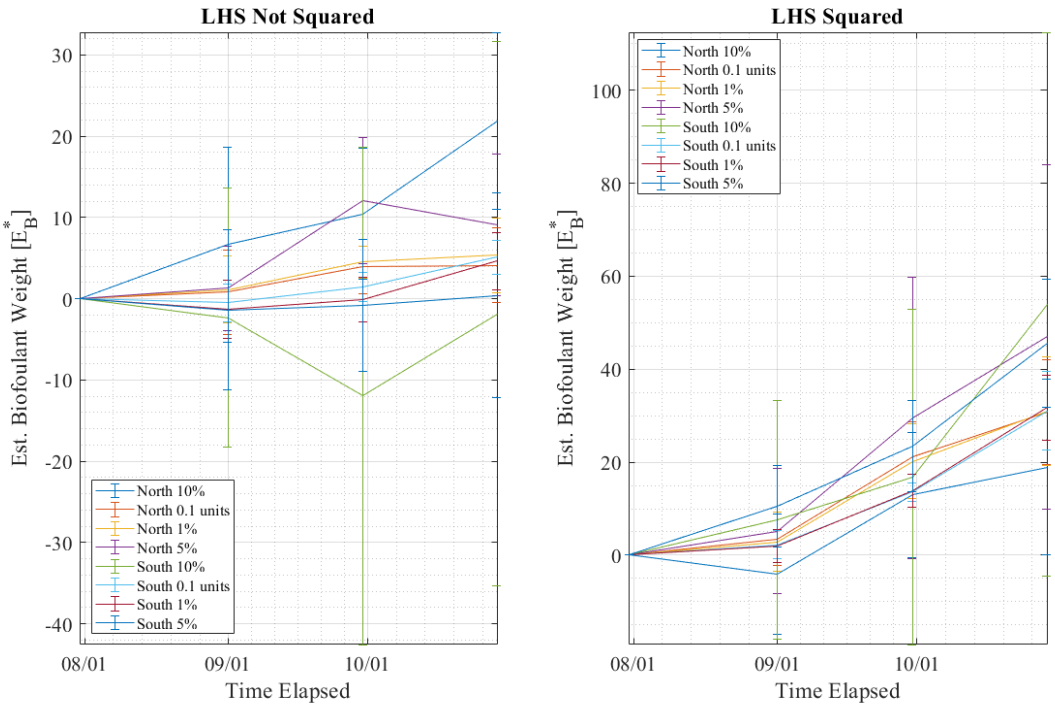

Figure 4. Comparison of the estimated biofoulant weight time series (E_B^*) split between north and south halves of the longline for a squared vs non-squared left-hand-side (LHS) of Equation (4), for all levels of uncertainty analysis (categories in legend). Note that the left panel, where the LHS of Equation (4) was not squared, demonstrates instability (i.e. unpredictable fluctuations when original values are varied) and extremely wide confidence intervals. In contrast, the right panel, where the LHS of Equation (4) was squared, shows far less instability yet retains wide confidence intervals, likely from low sample size.

side (LHS) of Equation (4) was squared, instability was lessened as all test results now showed similarity to the beginning of a logistic curve, regardless of the iteration count *(n*) and precision level (*p*) used in the uncertainty analysis. However, the wide confidence intervals (*Figure 4*, right panel) demonstrated that the sample size per group was still too small to avoid large scale uncertainty in the model over time. To triple the sample size and thus narrow the confidence intervals, the mean of nets from all groups combined was utilized for the final estimated weight of biofouling per month. Using the mean of all nets on the longline, versus the mean of the north and south halves of the longline separately, also negated the necessity to calculate two versions of the results (to check for the effect of switching Net 38 and Net 40 between north and south categories).

Both Figure 5 and Figure 6 (following page) present shellfish heights from each as the center group was split between the north and south groups to enable larger sample size for more statistically strong results of north versus south. Net 39 was torn after the first month of sampling, leaving only two nets for the center group which could inhibit interpretation. Nets 38 and 40 were traded between groups to test if the results were dependent on their classification.

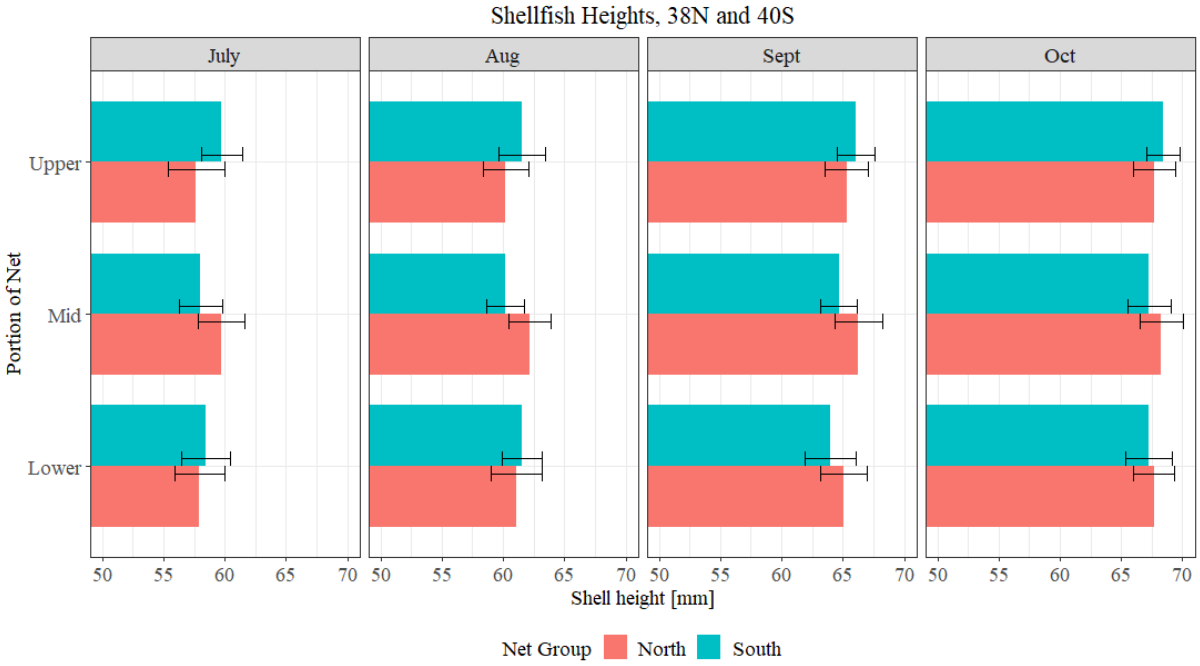

Figure 5. Monthly measurements of sea scallop shell heights (mm) per group and vertical bin, with Net 38 classified as North, and Net 40 classified as South.

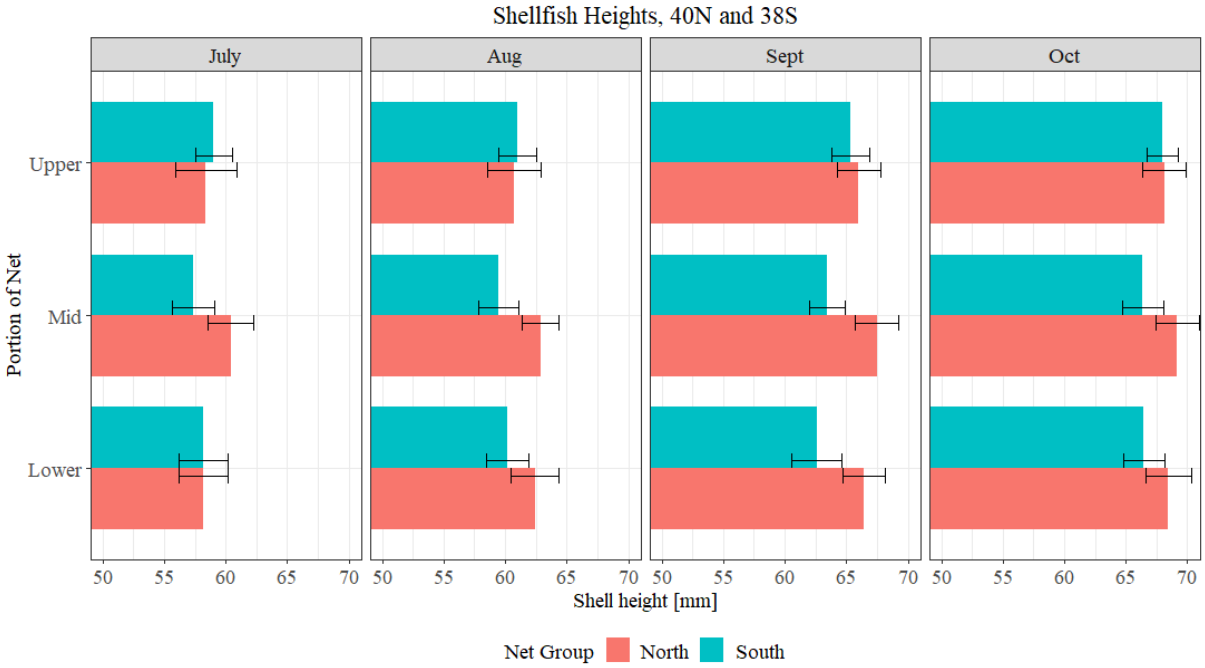

Figure 6. Monthly measurements of sea callop shell heights (mm) per group and vertical bin, with Net 40 classified as North, and Net 38 classified as South.

Discussion

These methods are worth refinement as they enable measurement of biofoulant weight in water, which is preferable to in-air measurements for three reasons. First, in-water weights eliminate the need to suspend the 60kg+ nets at a height adequate to weigh the net, and with little enough motion for a reliable instrument reading. Second, extended removal from seawater is harmful to both the sea scallops and biofoulants, since they are marine animals. Third, in-water weights account for the forces on biofoulants in their natural environment when water is a part of their inflated physical structure (Harbo, 2022), versus the frequent deflation that resulted when the net was removed from the water (observed). However, if a mass of foulants is all that is desired, weighing in air with a hydraulic winch would be preferable to duplicating the many tasks of this experiment. The biofoulant weights could be fit to the start of a logistic growth curve, however the logistic form was not well-developed by the end of the 90-day study since nether species had a large enough population have growth limited by environmental carrying capacity, so the data followed an exponential curve. This functional form, for the first 90-days of fouling, agrees with the results of Uzun (2019) and the wider knowledge of biofouling (Uzunet al., 2019). Shellfish heights are not reported in Chapter 3 due to the lack of significant growth patterns seen over the time series but were still important to the context of this study so are included in this chapter. Literature and conversations with scallop experts revealed that during the time series, shellfish would be preparing for reproduction (personal communication, C. Noren, 2023). Scallops in deep water environments spawn in October, while in shallower water they spawn a month earlier, around September (Barber et al., 1988). Both months are toward the end of data

collection. As such, the scallops in the study would have increased in mass, as they utilized nutrients and energy to grow larger reproductive organs in preparation to spawn but would have mitigated resources allocation for increase in shell height (Hart & Chute, 2004).

CHAPTER 3: LINKAGES OF AQUACULTURE & HYDRODYNAMICS

Introduction

As fisheries migrate or even disappear due to climate change, the economic stability of working waterfront communities is at risk. Local-scale aquaculture of shellfish such as the Atlantic sea scallop, *Plactopecten magallenicus,* provides (1) an alternative income source for fishermen, (2) an additional source of seafood for the larger public, (3) improved ambient water quality, and (4) in the case of Atlantic sea scallops in the Gulf of Maine, a potential way to support the wild population of native species (Clark, 2021). A hinderance to aquaculture of any form is colonization of unwanted marine organisms on farm equipment and cultivated stock, collectively known as biofouling. Linkages between hydrodynamics, biofouling, and shellfish growth on lantern net farms are not well-studied or understood. However, a relationship between water flow and biofouling exists. For example, high water velocities can both reduce settling of biofouling organisms and inhibit their growth (Doochin, 1951; Smith, 1946). Biofouling organisms may directly impact scallop growth by settling onto shells, or they may indirectly affect shellfish by settling on surrounding equipment changing the flow of water and food available, as well as stressing farm equipment (Fitridge et al., 2012, and references therein).

Biofouling, in general, is a financial burden to aquaculture farmers around the world. According to Bannister et al (2019) biofouling organisms affect farms and cultivated stock physically (mass and dimensions), chemically (material degradation) and biologically (stock competition and mortality) as found in topic reviews (Bannister et al., 2019; Fitridge et. al, 2012). A 2011 study found that an average of 14.7% of annual operating costs were used for

biofouling control (Adams et al., 2011). However, it is accepted that overall costs of biofouling through indirect impacts on shellfish production are far higher than quantified amounts suggest (Fitridge et al., 2012, and references therein). Antifouling coatings, such as Netminder®, modify equipment surfaces to reject recruitment of biofouling organisms (Tettelbach et al., 2012; MacKenzie et al., 2021). Though these coatings can delay occlusion of nets by weeks (MacKenzie, et al., 2021), they may transfer epibionts to the shells of cultivated bivalves, thereby reducing survival rate (Tettelbach et al., 2012).

Various studies have measured biofouling on aquaculture equipment to aid in mitigation. Image analysis, as well as dry and wet weights are common tools among researchers (Gansel et al., 2015; Gansel et al., 2017; Tettelbach et al., 2012; Uribe & Etchepare, 2002). Image analysis is the least accessible for industry growers due to constraints of time, labor, and equipment. Scallops are a marine species with a low survival time outside of ambient water, therefore dry weight assessments of lantern net biofouling are unideal unless farmers have replacement nets or another form of catchment readily available for shellfish during measurements (personal communication, R. Taylor, 2020; personal communication, T . Kiffney, 2021). Therefore, wet weights are the most applicable method of biofouling level assessments for a typical aquaculture farmer. Wet weights could be confounded by where and how measurements are taken (i.e. what phase of the tide, ambient currents, changing weight of the growing shellfish), leaving a gap between what is measurable and what is practical, especially on small scale farms with less human and monetary capital.

Regardless of biofouling, the hydrodynamics of the flow ambient to a farm affects the fitness of sea scallops. Scallops are filter feeders and are impacted by the volume of

phytoplankton available for consumption and ambient water currents (Côté et al., 1994; Kirby-Smith, 1972; Wildish & Saulnier, 1993). The primary mode of plankton transport is through environmental drivers of water movement, though some have local motility (Morgan et al, 2018; Schuech & Menden-Deuer, 2014). Ambient current velocity has been linked to positive and negative growth effects of both bay and sea scallops (Kirby-Smith, 1972; Wildish & Saulnier, 1993). Low velocities (~0.21cm/s or < 0.03 m/s) may not transport an adequate volume of plankton to sustain ideal scallop growth along a cultivated area due to feeding shadow, while high velocities (~0.125 m/s or > 0.06 m/s) may flush plankton past the bivalves before there is time for consumption (Kirby-Smith, 1972; Wildish & Saulnier, 1993). Wildish & Saulnier (1993) found optimal sea scallop growth from velocities of 0.03-0.06 m/s, and that past 0.3 m/s, scallops close their openings and cease feeding (Wildish & Saulnier, 1993). Nutrient uptake impacts scallop growth, which in turn impacts the livelihood of North American aquaculture farmers as scallops are sold in the United States per pound of the abductor muscle (Rbouvier Consulting, 2019).

The interaction of hydrodynamics and aquaculture farms is most directly quantified through the drag force, in both open and sheltered environments. Basic drag force, with respect to the surfaces of an aquaculture farm, is calculated as:

$$F_D = \frac{1}{2}\rho v^2 C_D A \tag{12}$$

Where for a particular farm object: F_D is quantified drag force acting upon the object, ρ is density of water surrounding the object, v is the velocity of the object relative to the surrounding water, C_D is the drag coefficient specific to the object and A is the cross-sectional area of the

object (Cengel & Cimbala, 2018). Drag impacts farms directly through tensions on mooring lines and forcing on equipment and shellfish, as well as indirectly through alterations of the local flow field that can modify particle transport, effecting shellfish nutrient uptake and flux of detritus through the system. In wave-exposed conditions, waves add further force on the lantern net longline in addition to pre-existing drag from tides and currents. Forcing from waves is traditionally calculated from the Morison equation, where the drag force term is similar to Equation (12) but an inertial term is also included. The horizontal component wave force on a pile in the original Morison equation is calculated by:

$$dF = \left[C_M \left(\rho \frac{\pi D^2}{4}\right) \frac{\partial u}{\partial t} \pm C_D \frac{\rho D}{2} u^2\right] dz \quad (13)$$

Where D is pile diameter, ρ is water mass density, C_M is the coefficient of mass, C_D is the coefficient of drag, dF is the force corresponding to the length of pile section, dz, time is t, and u is the horizontal component of wave orbital velocity (Morison et al., 1950). The first term of Equation (13) is the inertial force term, and the second term is the drag force term (Morison et al., 1950). Empirical studies have found that wave induced drag force increases as flow velocity increases (Wang, et al., 2023) and mooring tensions are inversely related to wave period (Zhao, et al., 2019). When the wave period is large, forces on lantern net longlines are higher with increased incident wave angle (angle between wave direction and farm longline), as there is more contact with the farm area over the longer wavelengths (Zhao, et al., 2019). The reaction of local flow to an aquaculture farm, with regards to drag force, is expressed through friction. Friction from a floating mussel farm in open coastal environment has been shown to reduce tidal velocities and cause downwelling, both of which decrease ambient seston for shellfish nutrition

(Lin et al., 2016). This modification of ambient flow field is also present in the semi-sheltered environment of estuaries, where frictional effects from floating farms have been found to modify lateral circulation (Liu & Huguenard, 2020) and reduce tidal current velocity up to 45% within farms, which in turn negatively affects shellfish nutrition (Jiang et al., 2023). The friction associated with drag force in turn causes the farm to impact the surrounding waters through tidal asymmetry, in this case when friction induces an energy exchange among tidal frequencies, creating an imbalance in the duration and strength of flood and ebb velocities relative to each other (Walton, 2002). Suspended aquaculture farms, independent of species being cultivated, have been shown to redirect ambient flow fields around and underneath their structures, accelerating flow at their edges and decelerating flow inside farms themselves through friction (Gibbs et al., 1991; Loland, 1991; Plew et al., 2005). As these effects are altered by farm siting, density, and cage type, they mandate serious consideration for farmers and ecologists with a goal of sustainable aquaculture (Jiang et al., 2023; Valle-Levinson, 2013).

The overall goal of this study is to support the development of the scallop aquaculture industry through foundational research on the link between hydrodynamics, biofouling, and shellfish growth on lantern net longlines in semi-sheltered environments. By understanding how variations in hydrodynamics link to biofouling and shellfish growth, farmers are more able to make informed decisions to help optimize returns on cultivated stock. These decisions may include the location of a scallop lease, equipment selection, farm orientation, and more. The objectives of this research are to: connect the orientations of flow and farm longline to accumulation of biofouling and growth of shellfish over time and to link farm drag effects to changes in the biofouling and sea scallop population on the farm through changes in tidal

asymmetries and normalized magnitudes of local velocities flowing orthogonal to the farm. The research was conducted in a semi-sheltered environment where both the incident angle of the principal component of flow and the mean incident angle of the instantaneous local velocity were considered. Results demonstrate differences in biofouling and shellfish growth both within and among sample groups, corresponding with variations in their hydrodynamic surroundings, and implying that incident flow angles are an important consideration for farmers in the absence of high wave loadings. Additionally, as tidal asymmetries grew from frictional drag of the farm, velocity was accelerated underneath the farm on both immediate and monthly times scales, which has implications for shellfish cultivation, most importantly with regards to dispersal of shellfish waste and potential benthic scour.

Methods

Study Area

The Damariscotta River forms a north-south oriented, convergent estuary in midcoastal Maine, that extends approximately 29 km from Inner Heron Island at its mouth to Great Salt Bay at its head; it hosts the small communities of Newcastle, Damariscotta, and South Bristol on its banks (McAlice & Petrie, 1969; Lieberthal et al., 2019). Freshwater inflow is low in magnitude and originates principally from Damariscotta Lake at the head of the estuary where it is managed through the Newcastle Dam owned by KEI Power, (McAlice & Petrie, 1969; Lieberthal et al., 2019). Discharge of the estuary varies throughout the year based on precipitation; flow ranges from 0.1 m^3/s in the dry season to 12 m^3/s in the wet season (Lieberthal et al., 2019). Tidal range

at the estuary mouth is 2.2-3.6 m, depending on spring or neap tide (Lieberthal et al., 2019). Subtidal regime varies throughout the estuary: nearer to the mouth, vertical shear is controlled by baroclinic forcing, midway up-estuary, lateral and vertical shear mixed with main channel inflow and shoal outflow, while farther up-estuary, the lateral shear pattern is reversed due to channel morphology and frictional effects (Bears, 2018). A study of tidal asymmetry in velocities throughout the length of the estuary indicated ebb dominance (Friedrichs & Aubrey, 1988) across multiple sites, inclusive of Clark Cove (near the Darling Marine Center) where flood amplitudes averaged 0.119 m/s while those of ebb averaged 0.129 m/s (Lieberthal et al., 2019). The region is well known for shellfish production and the Damariscotta River specifically is the highest producer of oysters in Maine (Thompson et al., 2006).

Field methods

Experimental Farm Layout

Data were collected on the longline of an experimental aquaculture lease from July-Oct 2021 at the University of Maine Darling Marine Center in the Damariscotta River estuary. The longline was approximately ~61 m long.

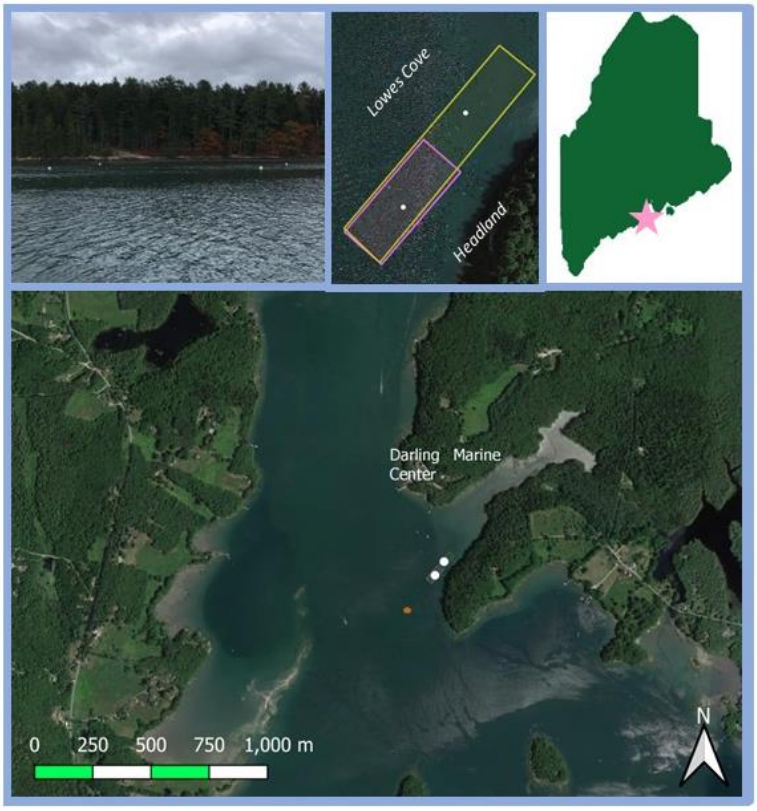

Figure 7. (Upper middle) Aerial map of study site with the two aquaculture leases active at the time of the experiment as yellow and pink rectangles and the two mooring buoys as white dots. (Upper right) State of Maine cartoon with pink star at approximate location of the study. (Lower) aerial view of the Damariscotta River with LOBO buoy as orange dot and mooring buoys as white dots. (Upper right) above water view of the farm, with mooring buoys visible as white dots.

Throughout field work operations the longline hosted multiple lantern net experiments in addition to the one outlined in this paper, as well as multiple bottom oyster cages on the northeast end (Figure 8). As the scope of this work did not include oyster cages, the upper-cove or "north" bound of the longline studied was the last lantern net of the experiment, which was measured by an underway ADCP (Acoustic Doppler Current Profiler) at around 50m from the south mooring buoy. The orientation of the farm longline was 48.2 degrees clockwise from true North.

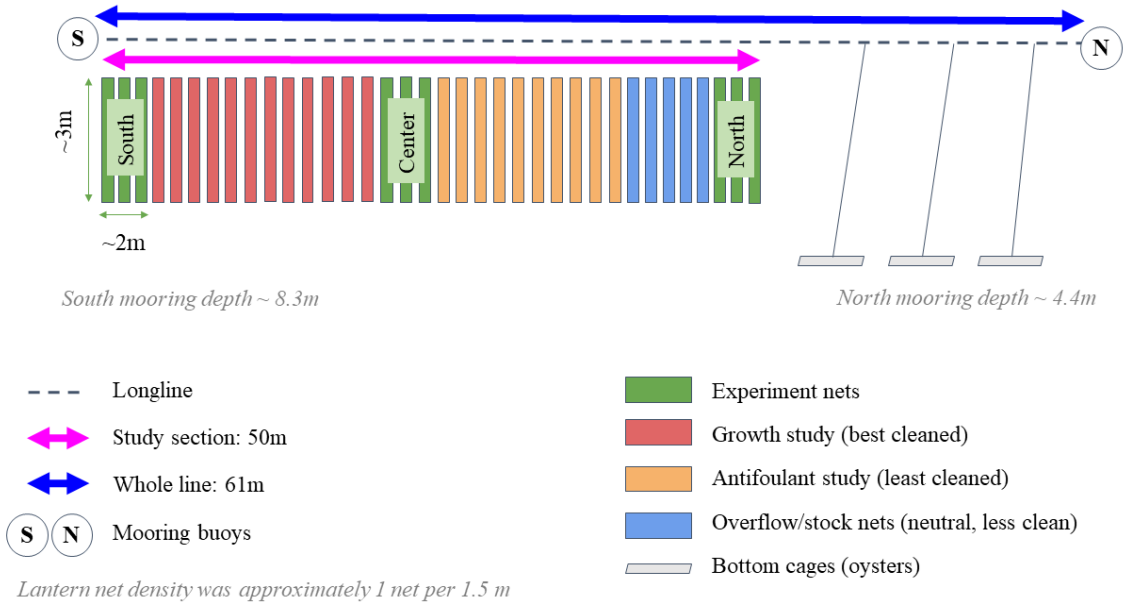

Figure 8. Layout of aquaculture farm longline indicating what portion was lantern nets, what groups those nets were from, and what portion of the line was bottom oyster cages. Nets from this study, "Experiment nets", are shown in green and labeled by sample group as "South", "Center", and "North". The growth study (most often cleaned nets) is shown in red between the "South" and "Center" sample groups of this experiment. The Netminder study (never cleaned nets) is in yellow, and immediately after the "Center" sample group in the north direction. The "overflow" group of nets is shown in blue, between the Netminder group and the "North" sample group from this experiment. Bottom oyster cages are shown to the north of the "North" sample group. The stated mooring depths are from the mean water depth of the moored ADCP and the underway ADCP along-longline transects.

A diagram of the farm longline displays nine lantern nets that were filled with Atlantic Sea Scallops, *Placopecten magellanicus*, from general farm stock (Figure 2), with 15 scallops per tier for 150 per net. These were split along the longline into three groups of three nets each to form the "South", "Center", and "North" sample groups. Utilizing three nets per group yielded an adequate sample size for statistics per location (450 scallops per sample group, 45 scallops per tier in each group), as well as providing replication in case of unforeseen circumstances that could confound results. The nets of the "South" group were the last objects on the longline

before the south mooring buoy, while the “Center” nets were approximately halfway between this and the “North” group, which started ~15 m up the longline. Lantern nets were cylindrical and 10-tier, approximately 0.3 m tall per tier. Throughout this study, measurements of in-water weights, scallop heights, submerged scallop weights, and photos of biofouling were recorded per lantern net, per sample group within 72 hours of the second neap tide (usually the day before or after underway ADCP field work) for consistency of tidal conditions. Specific methods are in *Chapter 3*.

As previously mentioned, there were other lantern net groups on the farm that were unassociated with the present work but likely influenced the local hydrodynamics due to their varying rates of cleaning (i.e. biofoulant growth). These included a growth study experiment, a Netminder anti-foulant coating experiment, and several “overflow” lantern nets with extra scallops used to stock the rest of the farm. The presence of these additional groups of nets gave the longline a realistic stocking density. However, each of the other groups had nets cleaned at differing rates; the growth study was cleaned most often, the Netminder experiment was never cleaned, and the “overflow” nets were cleaned occasionally (Figure 8).

Moored and Underway ADCPs

To quantify the effects of drag on tidal asymmetries and local velocities, as well as to determine the incident angles of the hourly principal component of flow and hourly mean flow, a 1200 kHz Teledyne RDI Acoustic Doppler Current Profiler was moored at the bottom of Lowes Cove approximately 8m from the longline. The instrument was programmed in Mode 12 (highest resolution) in geographic coordinates (North and East) and collected data in 10-minute bursts each hour at 1 Hz, with bin size 0.25 mm. The average depth at its position (from instrument data) was 6.7 meters, after a correction of 0.8 m was applied. The ADCP was compass calibrated on land and positioned by divers on the seafloor to ensure upward orientation.

To quantify velocities around the longline throughout a representative tidal cycle, a set of three, bi-directional transects (blue, red, and magenta in Fig. 3) was performed hourly, for twelve to thirteen consecutive hours (light dependent) within 24 hrhr of the second neap tide of each month. The tracks of the three transects encompassed outer [Lowes] Cove, inner [Lowes] cove and along the farm longline (front and back) as shown in Figure 9. Data were taken in both directions so that results could be averaged to minimized bias in the direction of boat movement (Fong & Monismith, 2004). For the transects closest to the longline, the track from south-to-north was on the cove side, while the track from north-to-south was on the headland side (see Figure 9). The underway ADCP was mounted, downward facing, in a Teledyne riverboat throughout data collection. Underway data were collected at 1 Hz with bin size 0.15 mm.

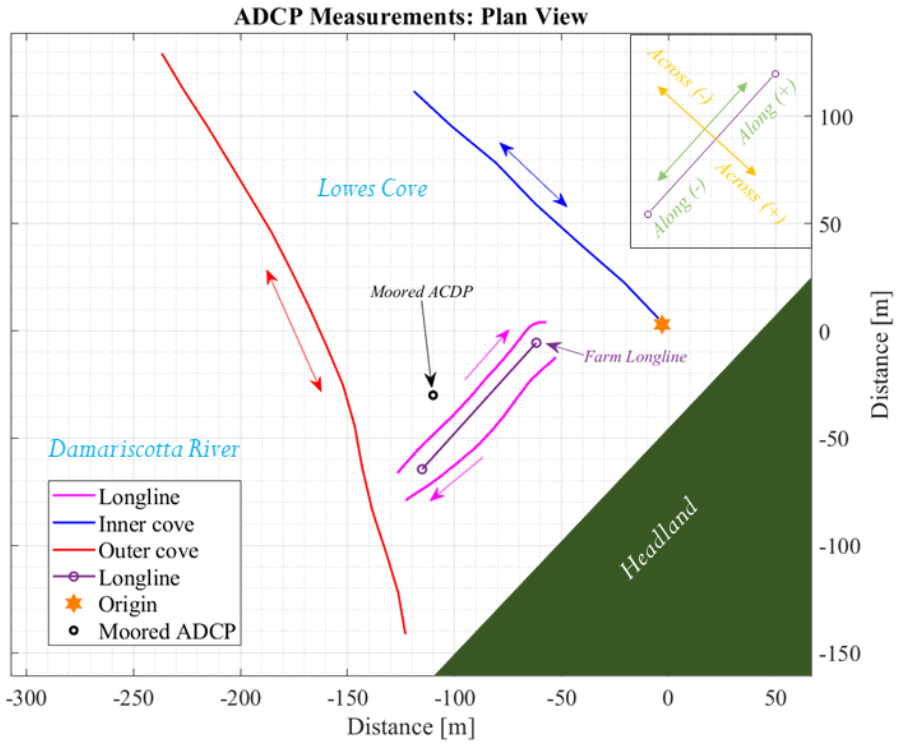

Figure 9. Plan view of underway ADCP transects and approximate location of the moored ADCP, along the aquaculture farm longline. Double arrows indicate that data was collected in both directions on the adjacent track of identical color. Single arrows indicate tracks taken in one direction, specifically the tracks along the longline were south-to-north on the cove side and north-to-south on the headland side.

Data Processing

LOBO (Land/Ocean Biogeochemical Observatory) Buoy and KIWI Wind

Chlorophyll a, turbidity, salinity, and temperature were recorded at 1 m depth and hourly intervals on the LOBO buoy to the southwest of the farm lease. These time series were smoothed on a 24hr window to remove noise, on daily and tidal scales, as well as diurnal oscillations. Four temperature outliers (24.77℃, 24.81℃, 37.51℃ and 38.15℃) as well as all temperatures greater

than 24℃, were replaced with NaNs. Gaps from outlier removal and missing data were filled with linear interpolation. Water current speed and direction (also 1 m depth) from the LOBO were not denoised; it was assumed that north for the current meter was true North, so a correction of +15.1° was not applied. Wind speed and direction were recorded at approx. 16.15 m elevation, at Wiscasset airport, 11.2 km distance from Lowes Cove in 10 min intervals. Wind data had minimal processing, i.e. was not smoothed or manually checked for outliers.

Moored ADCP

Data from the moored ADCP were used for environmental assessment, incident angles of current, tidal asymmetries, normalized velocity magnitudes, and scaled median monthly velocities, and were standardized (by statistics definition of standardize) to account for a mid-time series instrument change and projected onto σ-grid coordinates, which is useful for timeseries analysis in environments with large tidal ranges. In the σ coordinate system, the water column is split into a constant number of vertical bins so that the grid follows variations in topography, where displacement is the independent variable (Wang, et al., 2014; Song & Haidvogel, 1994). For this study, the σ-grid accounted for changes in water level at the set mooring location versus changes in topography, and time was the independent variable instead of displacement, with zero (0) as the seafloor and one (1) as the water surface.

The north and east velocities were rotated to the angle of the farm from true North (48.21°), so that positive-north became positive *along-farm* (into Lowes Cove) and positive-east became positive *across-farm* (toward the headland), according to the aerial view shown in

Figure 3. All data with *across-farm* (*Figure 9*) values less than zero were categorized *after-farm* as these velocities experienced the effects of the longline before being sensed by the beams of the moored ADCP. A five-bin σ-grid was used for the tidal asymmetries and normalized velocity magnitudes, while a twenty-bin σ-grid was used to calculate vertical profiles of the scaled medians (explained later in this section) . The higher twenty-bin resolution was ideal for the scaled medians because depth was the primary independent variable of interest and notable trends would be aliased at low resolution. In contrast, time was the primary independent variable for the tidal asymmetries and normalized velocity magnitudes, so five-bin resolution was adequate.

To quantify tidal asymmetries in velocity due to farm drag in the moored observations a continuous wavelet analysis with "Morlet" as a mother function (Torrence & Compo, 1998) was coupled with zero-crossing to extract the magnitudes of semidiurnal (2 times per day) and quarter diurnal (4 times per day) tidal frequency bands from the *across-farm* velocities. These bands are presented as tidal species (prefixed with a D); each species encompasses several tidal harmonics within the band of similar frequencies. For example, the D2 and D4 bands are composed of harmonic constituents centered around 12.42-hour and 6.21-hour frequencies, respectively, and can include the M2, S2, N2, and M4, S4, N4 harmonics. These tidal species amplitudes were used to calculate tidal asymmetries in the across-farm velocities as a time series of ratio D4/D2 The ratio D4/D2was low-pass *Lanczos* filtered with cutoff frequency of 1/(24*15) hours to remove variations from spring/neap bi-weekly cycles, as well as lower frequencies. A low-pass *Lanczos* filter with cutoff period of 6.21 hr and 336-hours (14 days) smoothing (to remove forcing of frequencies at or below the D4 band and to apply smoothing to remove noise

at and above spring-neap tidal scales, respectively) were also applied to the *normalized after-farm, across-farm* velocities, $\widetilde{\boldsymbol{V}_A}$. Normalized in this context referred to statistically standardizing this time series (subtracting mean and dividing by the standard deviation).

To understand changes in the flow adjacent to the farm on a monthly scale, the vertical profile of the median of the *after-farm* velocity magnitudes was calculated for the *i*th month, then scaled by flow volume during said month, with *Month 1* as August, *Month 2* as September, and *Month 3* as October (approximately, as each was the time span between biological measurements that were on the second neap tide, which was in the final days of each month). These were calculated as $\widehat{V_i} = \frac{\widetilde{V_i}}{\bar{V}_i n_i}$ where $\widetilde{V_i}$ was the median of the *after-farm* velocity magnitudes (hourly), divided by the count of observations categorized *after-farm* per month, n_i, per each of the three months of field work data collection. The median was used (for this metric) instead of the mean as the appropriate measure of central tendency because the velocities were not normally distributed. Dividing $\widetilde{V_i}$ by n_i removed the effects of fluctuations, such as those from increased discharge due to a local rainstorm, from the metric. Confidence intervals (95%) for the scaled medians were calculated through two-level bootstrapping and the student-t method. The student-t method was used to account for skewness.

Per *k* hourly burst, the incident angle of the principal component of flow, θ_k, was calculated from the north ($\boldsymbol{U_k}$) and east ($\boldsymbol{V_k}$) velocities through linear regression by the equation:

$$\boldsymbol{V_k} = \beta_k \boldsymbol{U_k} \tag{14}$$

Where β_k was the coefficient estimate of linear regression and the angle, $\angle\theta_k$ followed as:

$$\angle\theta_k = \ arctan\ (\beta_k) + 15.1° \quad (15)$$

Where 15.1 degrees is the exact correction from magnetic to true north coordinates for Walpole, ME during 2021. While the mean incident angle of flow $\angle\emptyset_k$ was calculated from north ($\boldsymbol{U_k}$) and east ($\boldsymbol{V_k}$) velocities and corrected to true North coordinates as:

$$\angle\emptyset_k = \ arctan2\left(\overline{\boldsymbol{U_k}/\boldsymbol{V_k}}\right) - 15.1° \quad (16)$$

Both angles were calculated per hour, as velocity data were recorded geographic coordinates and at some hours the principal component dictated flow orientation vs at others the mean incident angle was more indicative of flow orientation. Classification of flood vs ebb flow was determined by positive or negative values of the *along-farm* velocity, therefore tidal stage was localized to the farm versus in terms of the larger estuary. The difference of $\angle\theta_k$ and $\angle\emptyset_k$ to farm orientation (48.21° from true North) yielded from subtraction of equivalent angles (see Appendix C). Peak flood and peak ebb were determined from the data, indirectly by greatest absolute value of currents in flood and ebb directions, and also directly, from the highest correlations of velocity values within the third (peak ebb) or first quadrant (peak flood) when north vs east velocities were plotted on a Cartesian plane. Additional methods and illustrations for these angles are in Appendix C.

Underway ADCP

Data were filtered by error velocities less than 10 m/s and discharge less than 10 m^3/s, and percent good above 60%. Joyce corrections for ship motion were applied per run, per track

(Joyce, 1989). Each transect track was interpolated onto a uniform grid with 0.5 m horizontal spacing and 0.25 m vertical spacing. To minimize bias due to boat direction (Fong & Monismith, 2004), a pair of runs, one run per direction, was interpolated onto the uniform grid then averaged together to yield one robust transect per track per hour.

The dissipation rate of turbulent energy, ε, can be approximated: $\varepsilon \sim u^3/L$, where u is the instantaneous velocity and L is the length scale of the largest eddy (Davidson, 2015). Dissipation is a metric of diffusion, which controls the spread of particulates throughout the water column, such as the plankton for microfouling and for shellfish nutrition. For this study, a proxy $\varepsilon^*$was calculated as $\varepsilon^* \sim \frac{\bar{u}^3}{L}$, with $\bar{u}$ as the 5x2m, 2-dimensional, volumetric-averaged velocity magnitude of the longline transect tracks, averaged throughout a tidal cycle on Aug 1st, 2021.

Biological data methods

A detailed derivation and description of methods for biological quantities is in Chapter 3. The relation of estimated submerged biofoulant weight, $E_{B_{ij}}{}^*$, to the whole net relative weight $R_{W_{ij}}$, to the submerged weight of all scallops in the net $E_{S_{ij}}$, was found as (see Chapter 3):

$$R_{W_{ij}}^2 = K_i \left[E_{S_{ij}} + E_{B_{ij}}{}^* \right] \tag{17}$$

This relation demonstrated stability with increasing both *n* and *p*. Note that $E_{B_{ij}}{}^*$ will be an overestimate of the real submerged biofoulant weight, $E_{B_{ij}}$, when the density of the scallops, ρ_S, is greater than the density of the biofoulants, ρ_B. However, it will be an underestimate when the

reverse is true. An expansion of the relation, including its limitations, follows in (*Chapter 3*) and sensitivity analysis methods are detailed in the *Uncertainty Analysis* section.

Biological growth rates

The relative growth rate (*RGR*) of shellfish heights (*H*), submerged shellfish weights (E_S), and relative biofouling weights (E_B) was calculated according to (Hoffmann & Poorter, 2002) as:

$$RGR = \frac{\overline{ln(X_2)} - \overline{ln\,(X_1)}}{t_2 - t_1} \quad (18)$$

where $\overline{ln(X_n)}$ was the sample group mean of the natural log of measurements, *X*, on month *n*, and t_n was the time in days since the start of the experiment. The mean growth rates of the same data were calculated as:

$$MGR = \frac{\overline{X_2} - \overline{X_1}}{t_2 - t_1} \quad (19)$$

Uncertainty Analysis

For any measured parameter in an experiment, there is uncertainty that corresponds to the level of precision of both the measurement instrument and the researcher. To account for this uncertainty, a form of Monte Carlo simulation is proposed to generate a distribution for confidence intervals. Each crane scale weight value, *k*, was allowed to vary randomly within a given ε-neighborhood $0 < \varepsilon \leq p$, where p was a chosen level of precision. For example, if *k* was the in-air weight of the chain recorded as C_0 = 41.78 kg with *p* of 10% it was assumed that the actual value of C_0 may have been as small as 37.60 kg or as large as 45.96 kg. Accordingly, a new value x_k was independently generated from a uniform distribution per recorded weight

value *k* as: $x_k = k \pm \varepsilon$ with $k - p \leq x_k \leq k + p$. The entire analysis of E_S and E_B^* was then performed with the new set of x_k values. This was repeated for *n* count of replications, with *n* varying from 100 to 100,000. Results were expressed as means with 95% confidence interval: $\overline{E_B^*} \pm 1.96 * \frac{\sigma}{\sqrt{n}}$ and $\overline{E_S} \pm 1.96 * \frac{\sigma}{\sqrt{n}}$ with σ as the standard deviation and *n* the number of replications corresponding to their particular mean, $\overline{E_B^*}$ or $\overline{E_S}$. Tested levels of *p* included 0.1 (crane scale units), 1% *(0.01k)*, 5% *(0.05k)* and 10% (*0.1k*). Results for *n* = 1000 replications are shown in multiple figures across this chapter.

Regression Analysis

Many regression models were tested to quantify the link between the normalized after-farm velocities, $\widetilde{\boldsymbol{V}_A}$, and the filtered D4/D2 ratio time series (the hydrodynamics), with the biological data: the weight of the scallops (E_S) and the estimated weight of the biofoulants ($E_{B_{ij}}{}^*$). Independent variables included wind speed, wind direction, moored ADCP depth (corrected for blanking distance), predicted river discharge (Appendix A), as well as E_S and $E_{B_{ij}}{}^*$. Specific methods are described in Appendix B.

Results

Ambient Characteristics

Additional data sources helped inform the larger environmental picture at Lowes Cove. River discharge, predicted for the time series from multiple sources (see Appendix A) varied from a minimum in early August 2021 of 0 m^3/s up a maximum in late September 2021 of 5.7 m^3/s (data not shown, per agreement with KEI Power). The river experienced several pulses of higher discharge during the first half of September (~5m m^3/s), and a longer-term increase from the last week of September into the first week of October (~2-5.7 m^3/s). This final month of the time series had more high discharge events that would have also pulsed water out-estuary, many of which corresponded to multi-day storms. Velocity data (1 m depth) from a current meter (Nortek Aquadopp) on the LOBO buoy just outside of Lowes Cove (155 m southwest of the longline) were more commonly directed south and south-west in the direction of river discharge, or, seaward, with maximum of 0.224 m/s (Figure 10), except during flood tides (maximum 0.404 m/s). Current speed and direction were only available until August 26th, however the WET Labs WQM sensors (1 m depth) or Chlorophyll a, Turbidity, Salinity, and Temperature) were active throughout September as well. Flow was oriented into the cove (northwest) for less than 20% of the time series (Figure 10), corresponding to flood tide. Magnitudes ranged from 0-0.4 m/s, with the majority from 0.05-0.25 m/s (*Figure 10*).

A closer look at the vertical structure of velocities within Lowes Cove was possible from the moored ADCP. The mean water depth measured by the instrument was 6.7 m, and examples

of tidal range were 1.6 m during the second neap of September, and 3.8 m during the first Spring of October. The top half of the water column was used to compare ADCP flows with the LOBO.

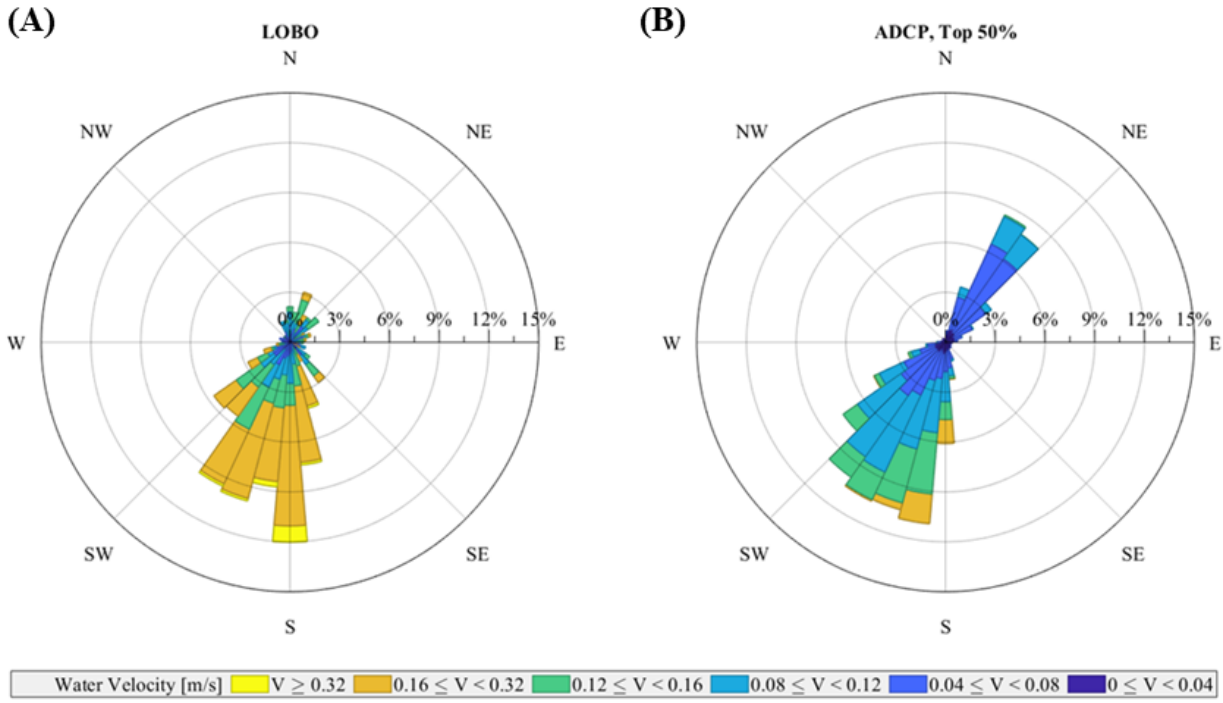

Figure 10. Current roses from Aug 1 - 26, 2021 for the LOBO current meter and the top 50% of the water column from the ADCP. Orientations are with respect to true North.

The predominant flow, inclusive of all tidal and subtidal velocities, was primarily into and out of Lowes Cove, for a northeast, southwest orientation with mean of 160.1° counterclockwise from true North (Figure 10b). Ebb velocities were almost twice (1.8x) those of flood (means of approximately 0.16 m/s, and 0.09 m/s, respectively), in accordance with the findings that the estuary is ebb dominant (Lieberthal et al., 2019), however in this case velocities are considered

versus barotropic characteristics, therefore that ebb velocities in the system should be shorter in time span but larger in magnitude, than flood velocities (Friedrichs & Aubrey, 1988). However, there were more velocities classified as ebb than flood for both the LOBO and the top 50% of the moored ADCP, which disagrees with the ebb dominant classification. Yet it is important to note that this was only a point measurement from 1 m depth at the LOBO buoy, and because of the orientations shown in *Figure 10*, flood encompassed all measurements with positive north velocities (Top 50% of moored ADCP), or all speeds with direction of $> 270°$ or $< 90°$ (LOBO), with ebb being the opposites. In comparison with the velocities at the LOBO buoy, the typical speeds (0.08-0.16 m/s) in the Top 50% of the moored ADCP were around half of those commonly experienced by the LOBO (0.15-0.25). Flood velocities in this portion of the water column averaged 0.06 m/s, while ebb averaged 0.09 m/s, for an ebb to flood ratio, or asymmetry, of 1.5, which is less than the 1.8 of the LOBO. As the major axis of orientation of the flow was in/out of Lowes Cove, which was close to parallel with the farm orientation, velocities parallel to the farm longline were higher magnitude than across farm throughout tidal cycles. The maximum (depth averaged) of local velocities was 0.2 m/s.

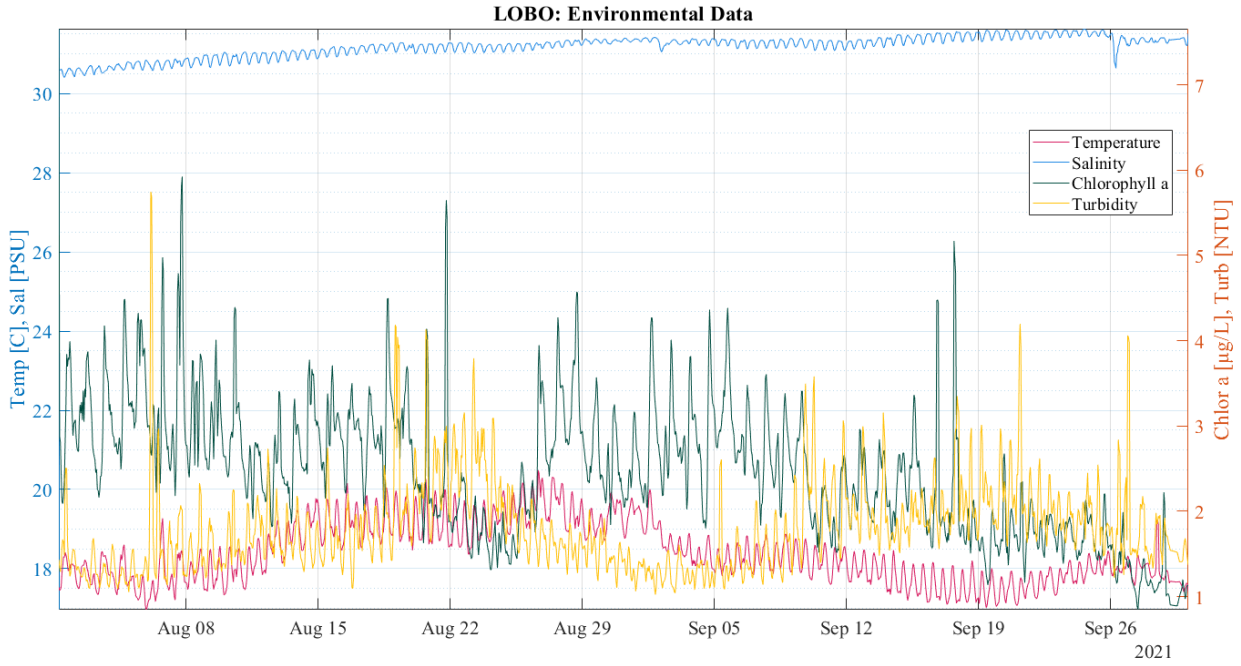

Figure 11. Chlorophyll a, salinity, turbidity, and temperature from the LOBO buoy, approximately 155 m to the southwest of the southern end of the lantern net longline, in the channel of the Damariscotta River.

Salinity (1 m depth) was within the 30-32 PSU range throughout the time series and demonstrated a slow increase over the two-month period, with min/max in August of 30.4/31.4 PSU, while in September it was 30.6/31.6 PSU (Figure 5). Salinity had notable decreases on September 2nd and 26th, corresponding to regional daily precipitation accumulation of 3.6 cm and 8.0 cm (Appendix D) and river discharge pulses (approximately $\geq 5m^3/s$) within 48 hours of each. Water temperature (1 m depth) ranged from 17-19.3°C in the first half of August, and from ~18.1-20.5°C in the second half of August, then dropped back below 19°C for the majority of September. *Chlorophyll a* (1 m depth) varied dramatically throughout the time series, showing an overall decrease from an average of 2.8$\mu g/L$ in August dropping to 2.2 $\mu g/L$ in September which would have indirect impact on shellfish growth from the decrease in food availability. The

variance and value of the turbidity (1 m depth) time series decreased from Aug 24th to September 5th, relative to the rest of August and September. The month of August had almost no precipitation or discharge pulses, and this would decrease the amount of suspended sediment in the water column, especially by the end of the month. However, Aug 31st to September 9th had several discharge pulses (data not shown, see Appendix A), which when associated with precipitation and barometric pressure (Appendix D) describe a stormy period from Aug 31st to Sept 10th. After the first few days this storm restored turbidity conditions to be similar to their previous conditions. Regardless, there was a slight decrease in turbidity over the time series, with min, mean, max as (1.1,1.8,5.7) and (1.0, 1.8, 4.2) NTU for August and September, respectively.

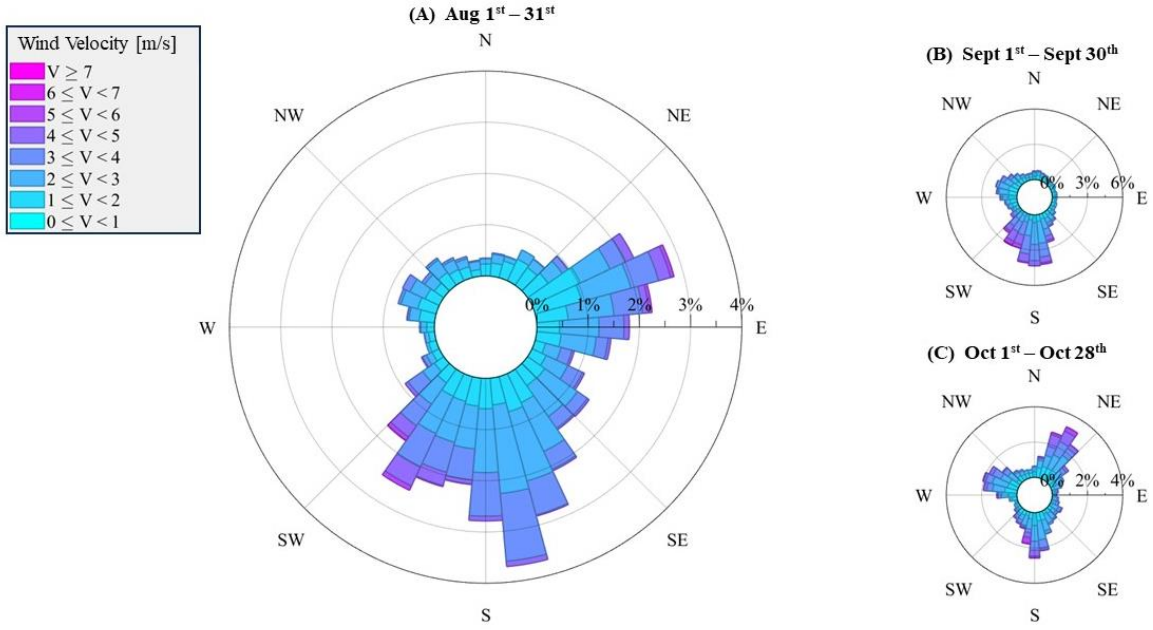

Figure 12. Wind speed and direction from KIWI airport in Wiscasset, ME. This was approximately 11.2 km from the Darling Marine Center. Directions correspond to the origin of the wind. The majority of wind in (A) August 1st – 31st, was from the 90° span of southwest/south/southeast (<6 m/s), with about a third from the east/northeast (<6 m/s). In (B) Sept 1st – 30th, the proportion of wind from the south increased (some winds past 7 m/s) with the remainder primarily switching to west/northwest (< 5/s). However (C) Oct 1st -28th, showed slightly unequal balance between, in order of greatest to least proportion, north-northeast (6 m/s), south (some winds past 7 m/s), and west-northwest (<6 m/s).

Remote and local wind stresses have been shown to drive changes in estuary sea level, barotropic currents, and (water) surface slope, with the relative dominance of these effects determined by estuary length and subtidal wavelength (Garvine, 1985). Accordingly, seasonal changes in wind direction could alter Damariscotta Estuary water levels and the flow regime of Lowes Cove. There was a noteworthy directional change in wind across the months, where winds from the south were far more prevalent in the first two months than in the third month (Figure 12). Speeds higher than 5 m/s were split between the northeast and the southwest August, for somewhat of a balance into and out of the estuary. In contrast, wind speeds higher than 5 m/s were concentrated from the south during September, which is into the estuary. In October, winds were primarily from the northeast, south, and northwest, with wind speeds higher than 5 m/s., for a more balanced into/out of estuary effect. Maximum speeds also increased over the time series, from 6.17 m/s in August, to 6.69 m/s in September, and finally to 7.20 m/s in October.

Hydrodynamic effects on farm environment

To understand the effects of the local cove hydrodynamics on the biofouling of the farm, the first month of the dataset was investigated because most foulants would have settled after two weeks, at least in miniature form (Nurioglu et al., 2015). After this, the mass and structure of the foulants themselves would affect the flow, which would affect their growth, making causation almost impossible to quantify. Therefore, the initial velocity conditions along the longline were used as a reference to local velocities prior to any growth on experimental nets, as quantified

through the top 5m of the longline transects tracks from Aug 1 (in 2m horizontal averages). The bi-weekly averages of the incident angles, $\angle\theta$ and $\angle\emptyset$ (detailed in *Methods* and *Appendix C*), from the first month (Aug 1 to Aug 31) were used to quantify the orientation of the farm with respect to currents and particulate transport. Additionally, the farm wake was tracked throughout the tidal cycle through both Aug 1st and Aug 31st using calculated $\angle\emptyset$, together with underway and moored ADCP data.

August 1st transects gave an initial assessment of the currents experienced by the longline. When the along- and across-farm velocities along the longline were examined, the overall velocity magnitude (combining along- and across-farm components) dropped from 0.12 m/s at the south mooring, to 0.08 m/s at the north end of the experiment (*Figure 13*, (E)). There is a linear rise in bathymetry from 8.3 m to 4.4 m (moored ADCP water level) along the longline, indicating that bottom friction was a factor in the along-farm decrease, especially considering tidal range of up to 3.8 m. Considering hours when the farm was in its own wake, when $\emptyset_0$ was less than or equal to 20° (see next section), Figure 13 (B) shows that along-farm velocity, $\boldsymbol{U}$, was largest on the south half of the longline, where flood velocities averaged above 0.1 m/s. $\boldsymbol{U}$ then decreased to 0.08 m/s by the Netminder experiment, and increased back to 0.1 m/s before dropping to 0.06 m/s on the north end of the longline. Under the same wake conditions, Figure 13 (C), the across-farm velocity, $\boldsymbol{V}$, was bidirectional: at the southernmost end of the longline, across-farm flow was 0.03 m/s, moving toward the center of the cove. However, around 8 m up the longline it reversed direction to increase up to almost 0.06 m/s toward the headland by 21 m from the southernmost mooring, before decreasing to relatively zero by the end of the Netminder experiment (~36 m), until the northernmost mooring. The dissipation rate of turbulent energy,

ε^*, was 0.6 orders of magnitude higher on the southern half of the longline where velocities are largest versus the northern where velocities are weaker (Figure 13 (E)). These velocities and dissipation patterns were expected to influence the phytoplankton uptake of the scallops, and settlement patterns of the biofouling through advection and diffusion, respectively. Notable reduction in ebb velocity, moving north to south on the longline, was also notable in *Figure 13* (B). However, less current reduction along the longlined was evident, as expected, when all hours velocities were phase averaged, regardless of farm orientation difference to incident current angles Figure 13 (A, C).

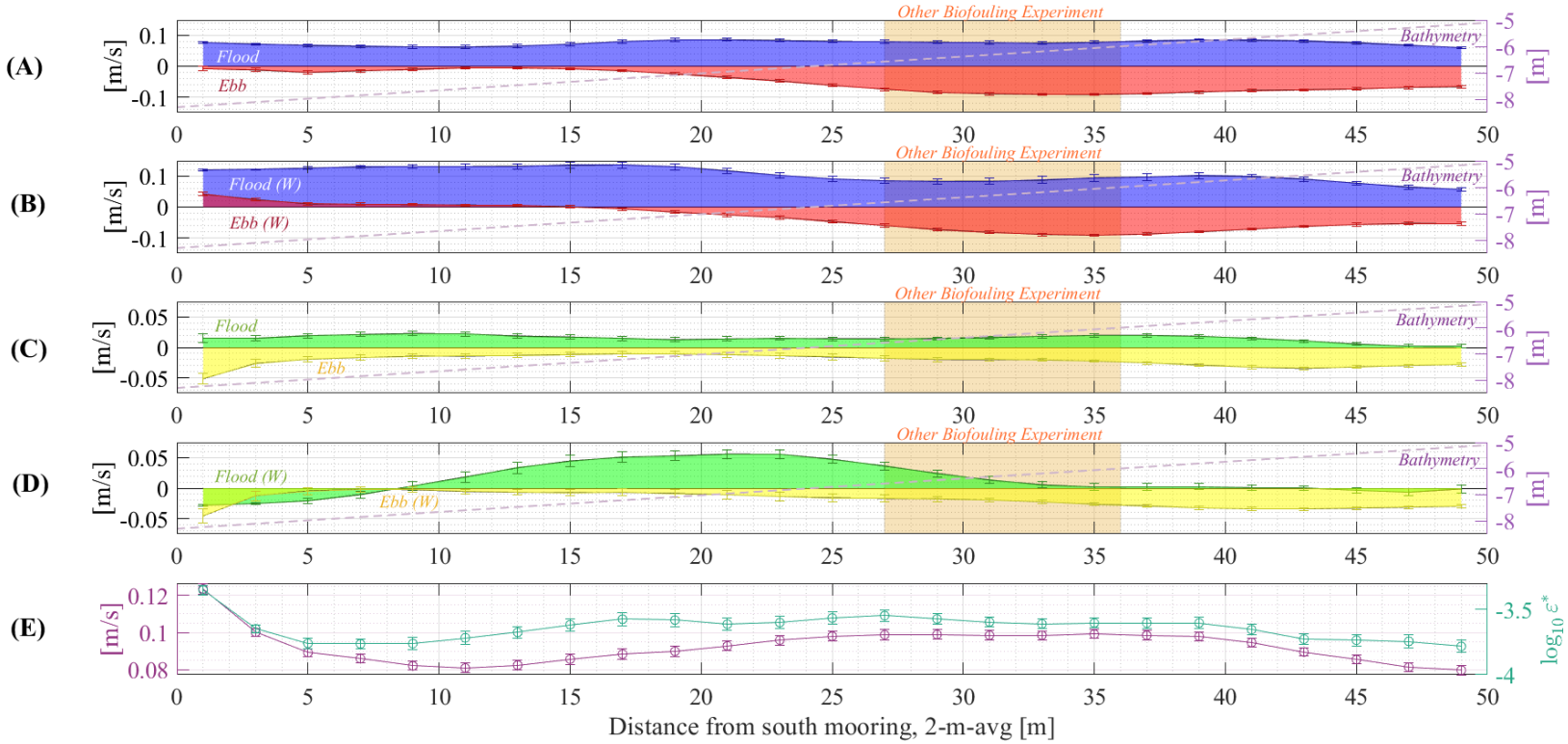

Figure 13. Local flow around farm from longline transects, where headland and cove sides were averaged per hour, then depth averaged in 2 m horizontally averaged bins per tidal phase experienced by the farm: (A) along-farm velocities averaged for flood (blue) and ebb (red) phases, (B) subset of along-farm velocities averaged for flood (blue) and ebb (red) phases when $\emptyset_0$ was less than or equal to 20°, (C) across-farm velocities averaged for flood (blue) and ebb (red) phases, (D) subset of across-farm velocities averaged for flood (blue) and ebb (red) phases when $\emptyset_0$ was less than or equal to 20°, (E) estimated dissipation of TKE (ε^*) and velocity magnitude averaged for all phases of the tide. Units for all series except ε^* are [m/s] while ε^* is [m^2/s^3] in log_{10} scale. Characteristic length, L, for calculation of (ε^*) was 6.7m.

Incident flow angles

The incident angle of the principal component of flow, θ_k, and the mean incident angle of flow, $\emptyset_k$, from the moored ADCP near the farm, showed variation from the first to the second half of August which could have effect on advection of nutrients for the scallops and transport of the microorganisms which initiate biofouling. The range from the minimum to maximum of both types of incident angles was greater during ebb (approx. 200°) than during flood (approx. 150°). The absolute difference between each type of incident angle and the orientation of the farm (θ_0 and $\emptyset_0$), demonstrated whether subsequent farm nets would be expected to be within the wake of the previous nets; this was likely if the absolute difference is less than or equal to 20° (Rabaud & Moisy, 2013). The 20° is a rounded cutoff for the Kelvin angle (19.47°), which defines the outermost possible edge of any wake generated by an object in flow (Rabaud & Moisy, 2013; Verberck, 2013). Kurtosis demonstrates how concentrated, or narrow and tall, the peak of a distribution is. In terms of θ_0 and $\emptyset_0$, kurtosis was a measure of how closely aligned with the farm the incident angles were throughout each two week window, with higher kurtosis meaning greater alignment. For example, if the distribution of $\theta_0$and $\emptyset_0$ were centered below 20° with a low kurtosis, the farm could be in its own wake at some hours but would not be in its own wake for many more. In contrast, for the previous condition but with high kurtosis, the farm would be in its own wake for the majority of the time. This makes kurtosis vital for determining farm wakes.

The absolute difference of the incident angle of mean flow, $\angle\emptyset$, to the the orientation of the longline (hereafter refered to as $\emptyset_0$) had a distribution centered below 15° for flood

throughout all of August (Figure 14; median 14.7° and 12.7° for first two weeks and second two week, respectively), however during ebb the distribution of $\emptyset_0$ was centered higher than 20° for the whole month (27.6° to 25.3° by second week). Meanwhile, kurtosis of the distribution of $\emptyset_0$ increased from 3.8 to 4.6 for ebb, and 4.5 to 6.0 for flood from the first to the second halves of the month, .respectively. These angle differences and kurtosis values imply that the mean incident angle of flow became more aligned to the farm during the second half of August, for both flood and ebb velocities.

The importance of θ_0 is debatable in terms of farm wake, however it is important for comparison with $\emptyset_0$ and advection of particulates to and around the area local to the longline, as it gives indication of the long axis of the tidal ellipse, and therefore, orientation of tidal excursion (Okubo, 1978; Valle-Levinson, 2013). The median of θ_0 values during flood was relatively unchanged, and was below 20° throughout August (13.7° first half, 12.6° second half). From the first to second half of the month the kurtosis during ebb decreased from 4.1 to 3.9, while during flood it increased from 4.1 to 4.7, suggesting that in the first half of August velocities during ebb became less aligned with the longline, while in the second part of the month velocities become more aligned with the longline. During of the first and second half of August, θ_0 was less than or equal to 20° for 77.6% and 81.9%, respectively, of hourly velocities categorized as flood. In contrast, during hourly velocities classified as ebb, θ_0, was less than or equal to 20° for 12.6% and 10.0% of the velocities, respectively.

In theory, the direction of the wake generated by the longline was $\angle\emptyset$, therefore whenever $\emptyset_0$was less than 20°, the farm was likely in its own wake. The distribution of $\emptyset_0$ was less concentrated to the peak for ebb than during flood, complementing scatterplots of the east

versus north velocities (not shown) that demonstrated higher variance of velocity during ebb than

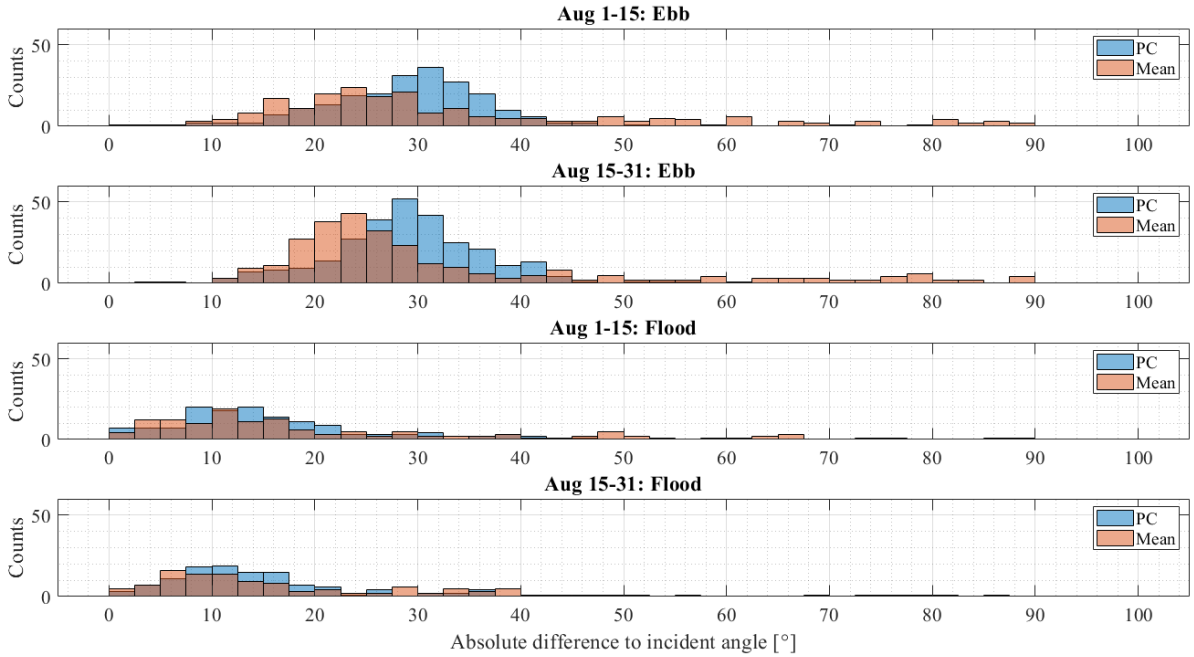

Figure 14. Differences of incident angles to the orientation of the longline. Data were divided by flood and ebb, and by the first two weeks and last two weeks of August 2021.

flood (*Figure 14*). During the first half of the month of August, $\emptyset_0$ was less than or equal to 20° for 64.9% of flood velocities; this slightly increased to 65.5% in the last two weeks of August (*Figure 14*). Hourly velocities designated as ebb demonstrated an opposite pattern, as $\emptyset_0$ was less than or equal to 20° for 20.6% and 18.2%, medians 29.8° and 29.0°, for the first and second halves of August, respectively (*Figure 14*). In general, the flood velocities aligned more with the farm orientation as time progressed, while ebb velocities became less aligned as time progressed.

Existence and Consistency of Farm Wake

For either date (Aug 1st or Aug 31st) the hours that had the highest velocity reduction expressed across the greatest number of 5 m bins were categorized as having the "best" wakes. One of

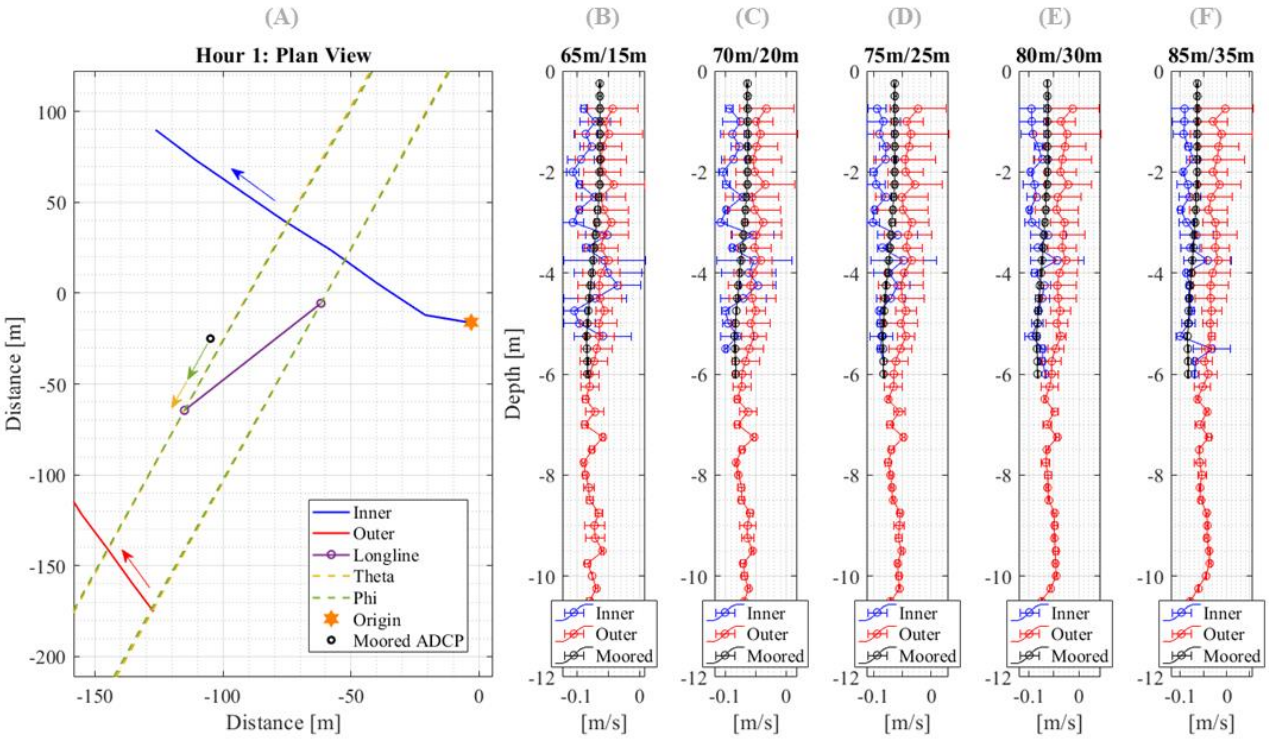

Figure 15. *Wake from longline on Aug 31st, during 6-6:40am local time. The arrows from the moored ADCP marker indicate the incident angles of, ∅ (phi in green) and primary principal component of flow, θ (theta in yellow). Transects are colored for outer cove (red) and inner cove (blue). Right panel titles are the starting distance from the eastern edge of the outer/inner transect, respectively.*

these the first hour of transects (ebb velocity) on Aug 31st, is shown in Figure 15.

In theory, a farm wake should have been detectable when two criteria were both met:

a) The window tangential to the longline moorings created from the incident angle of the mean flow, ∠∅, intersected both the inner and outer cove transect tracks (left panels of Figure 15, *Figure 16*, and Figure 17).

b) The incident angles $\angle\theta$ and $\angle\emptyset$ were more parallel than orthogonal to each other throughout hours of the tidal cycle.

However, when the inner and outer [Lowes] cove transects were averaged into vertical profiles per 5 m, there was a lack of signficant (95% CI, relaced with σ as per personal communication, B. Halteman, 2023) leeward wake even in hours that exhibited both criteria (a) and (b). Instead, hours with the "best wakes" not only met the both theoretical criteria (a) and (b), but also demonstrated what will hereafter be referred to as criteria (c), a high correlation of the raw north and east velocities with $\angle\emptyset$, when they were considered on a Cartesian plane with respect to true

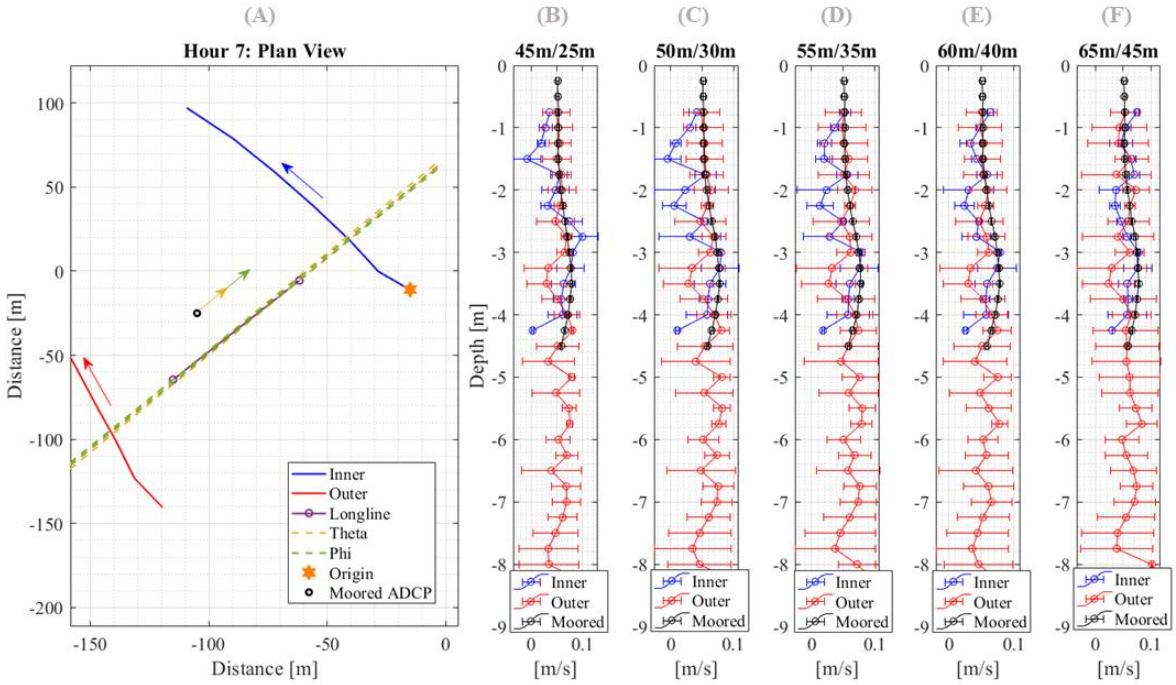

Figure 16. Wake from longline on Aug 31st, during 12-12:40am local time. The arrows from the moored ADCP marker indicate the incident angles of, $\angle\emptyset$ (phi in green) and primary principal component of flow, $\angle\theta$ (theta in yellow). Transects are colored for outer cove (red) and inner cove (blue). Right panel titles are the starting distance from the eastern edge of the outer/inner transect, respectively.

North (plots not shown). Hours near peak flood demonstrated these notable wakes on Aug 31st (Hour 7 in *Figure 16*; Hour 6 not shown).

Hours during peak ebb velocities did not always show quantifiable wake. On Aug 31st peak ebb (with reference to the moored ADCP) was during Hours 1, 12 and 13. Though both Hours 12 and 13 (Aug 31) satisfied criteria (a) and (b), their wakes were barely visible (not shown), while, for Hour 1 there was a distinct wake (*Figure 14*). Hours 5, 8, and 10 (Aug 31) all demonstrated relatively high reduction factor wakes during flood (5 & 8) and ebb (10) while satisfying (a) and (c) but not (b) (Not all hours shown; Hour 8 shown in Figure 17).

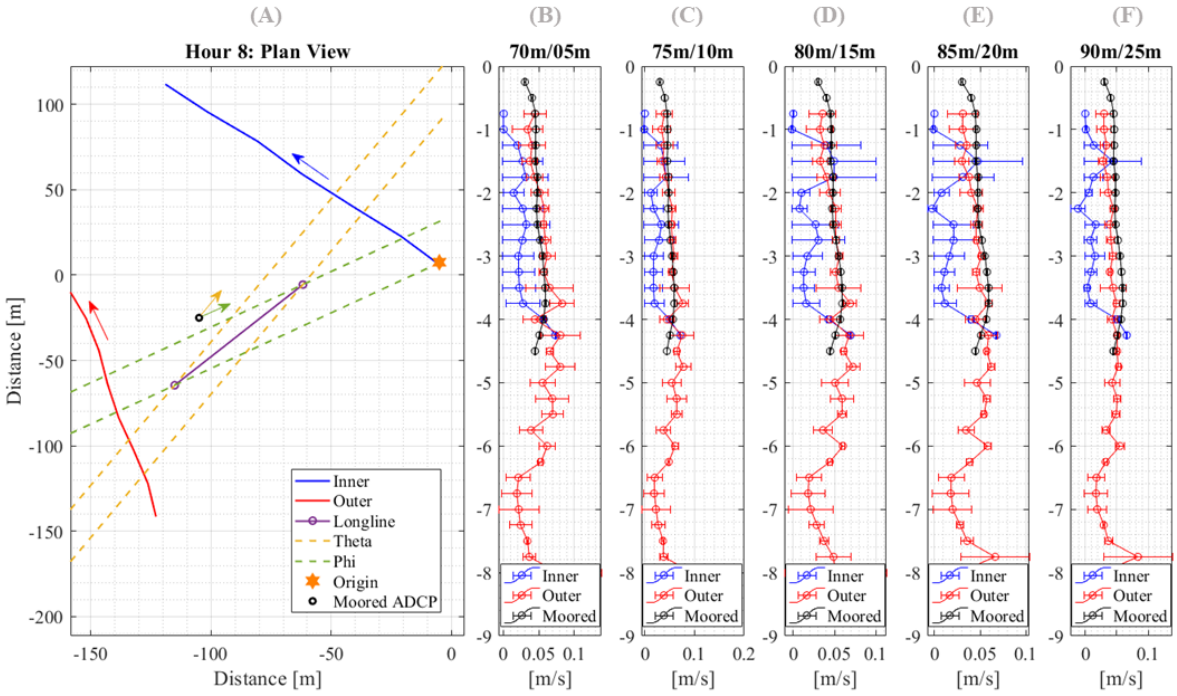

Figure 17. *Wake from longline on Aug 31st, during 1-1:40pm local time. The arrows from the moored ADCP marker indicate the incident angles of, ∅ (phi in green) and primary principal component of flow, θ (theta in yellow). Transects are colored for outer cove (red) and inner cove (blue). Right panel titles are the starting distance from the eastern edge of the outer/inner transect, respectively.*

Multiple observations emerged from examination of the wakes:

1. Hours meeting criteria (a) and (c), i.e. intesection of expected wake path with transects and high correlation of velocities to $\angle\emptyset$, demonstrated wakes more consistently than those satisfying criteria (a) and (b), even in cases when $\angle\theta$ and $\angle\emptyset$ were approximately equal angles. This was evident on Aug 31st from Hour 8 (Figure 17) and Hour 10 (not shown) versus Hour 1 (Figure 15).
2. Wakes were detected more often during flood velocities than during ebb, which corresponds with the previous flow angle findings that demonstrated $\emptyset_0$ was less than 20° more often during flood than during ebb.
3. Significant wakes were present within more transect hours, and across more bins, on Aug 31st when compared with Aug 1st . Almost no wakes were detectable on Aug 1st. This caused heavy reliance on the later date for interpretation, and is elaborated on in the *Discussion*.

Observations of farm wake and incident flow angles could have biological impact. For example, when the mean incident flow angle closely aligned with the farm during flood velocities, the velocity reduction from the wake of subsequent nets could have effected transport of shellfish nutrients and biofouling larvae along the longline.

Biological observations

The four photos taken of the sides of each net per month enabled species identification and detection of biofouling community trends between and across sample groups. Biofouling organisms observed on the farm included marine biofilm (slime), various colors of tunicates and ascidians, maroon algae (potentially *Bangia fuscopurpurea*), fine-haired, bright green algae (possibly *Cladophora spp.*), the clubbed tunicate *Styela clava*, and sea grapes (*Molgula spp.*). Community did not vary distinctively along the longline, with the same species distribution present across nets of all three sample groups. The overall biofouling of the nets was observed month-to-month as marine slime dominant with other macrofouling in its smallest stages, a balance of marine slime and mid-sized macrofouling, and absence of marine slime dominated by macrofouling now larger size (Figure 18). This change in community type over time would equate to a change in solidity of the nets (solidity being defined as the percent solid of the surface area of a net (Loland, 1991), with month two having the highest solidity as it had both marine slime and mid-sized macrofouling (per. communication then list the experts by name). If this experiment were performed earlier in the year, such that mussels and barnacles could also settle onto the nets (these species colonize earlier in the year than mid-summer), solidity due to biofouling would only decrease throughout the time series (personal communication, D. Morse, 2023).

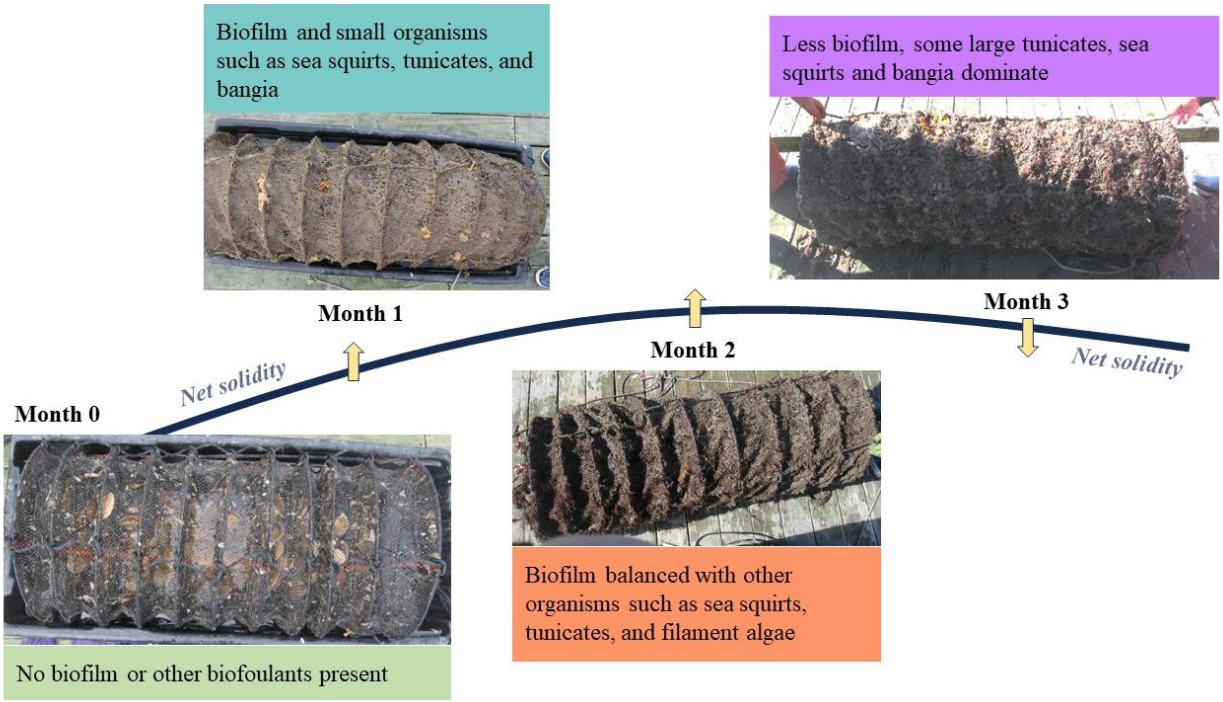

Figure 18. Progression of biofouling community on the lantern nets of this study, as evidenced by Net #38 and Net #39, which were nearer to the center of the studied portion of the longline. A representative curve of net solidity, directly proportional to net occlusion.

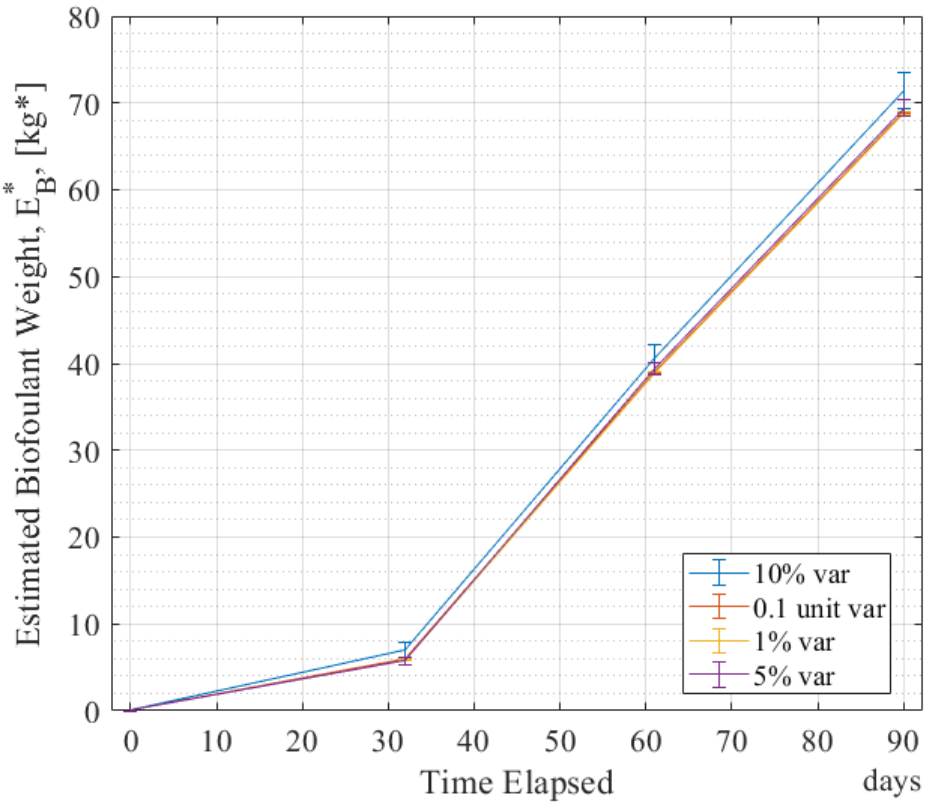

Figure 19. Mean relative biofouling weights for the whole longline over the time series, from sensitivity cases at 1000 replicates per tested precision level, p (see Uncertainty Analysis).

Values of E_B^* generated of by the Monte Carlo uncertainty analysis demonstrated the beginning of a logistic curve, with a gradual increase up to 6-7kgs* across the first month of the experiment, and an increase of approximately 30-35 kgs* for each consecutive month, not corrected for density differences between sea scallops and biofoulant species at each time point (Figure 19). The curves were all very similar across the uncertainty analysis, showing that (1) the analytical model is robust, at least when using the mean of the whole longline to yield adequate sample size and (2) the data trend shows what biologists would expect (i.e. the start of a logistic growth curve). Values were most sensitive to the highest level of precision tested *(p = 10%*), as

evidenced by an almost 10-kg shift in E_B^* for the time series relative to the other three levels of p tested. As the estimated biofoulant weight, E_B^*, was not corrected for density, comparisons could be made among biofoulants and among shellfish, but not between the species, especially as the two were significantly distinct in quantity over the time series, as demonstrated by the 10% variation with 1000 replicates case (Figure 20).

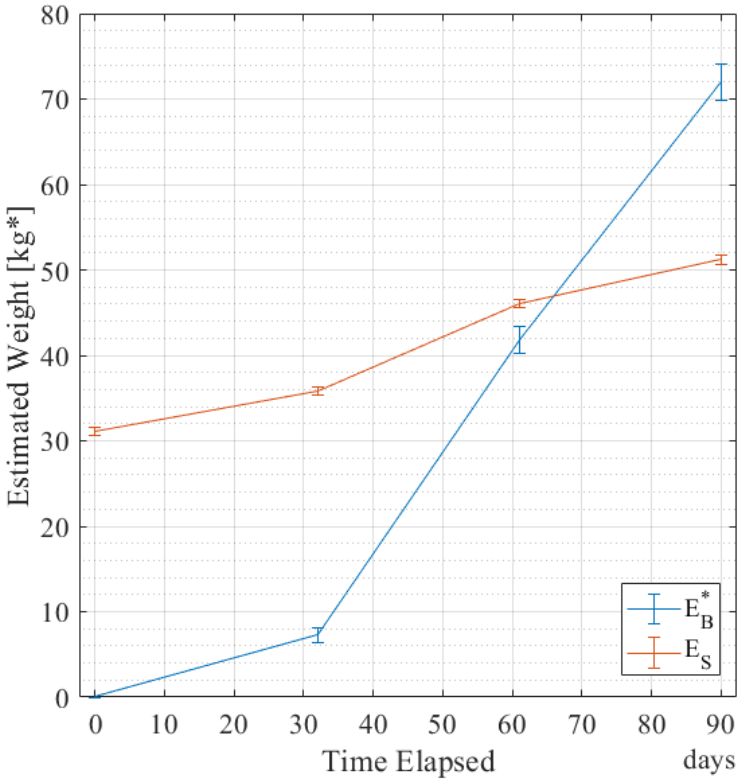

Figure 20. Time series comparison of E_B^* and E_S with p=10% and 1000 replicates.

Relative growth rates (RGRs) were significantly different across north and south groups when 10% variation was allowed with 1000 replicates (Figure 21). The relative growth rate (RGR) of the biofoulants was significantly higher in the north (0.074 ± 0.0010) than in the south

(0.068 ± 0.0010), though less than 0.01 different, while for scallops the RGR was almost three times higher in the south (0.0068 ± 0.0013) than in the north (0.0024 ± 0.0014). The mean growth rate (MGR) reinforced the RGR results as it was almost four times higher in the south (0.099 ± 0.0135) than in the north (0.028 ± 0.0138) for the scallops, while for the biofoulants the north (0.136 ± 0.0174) had an MGR approximately twice that of the south (0.07 ± 0.0178) . Shellfish heights did not demonstrate notable growth patterns across depth and north-south group variation. Detailed results and limited interpretation are in Chapter 2.

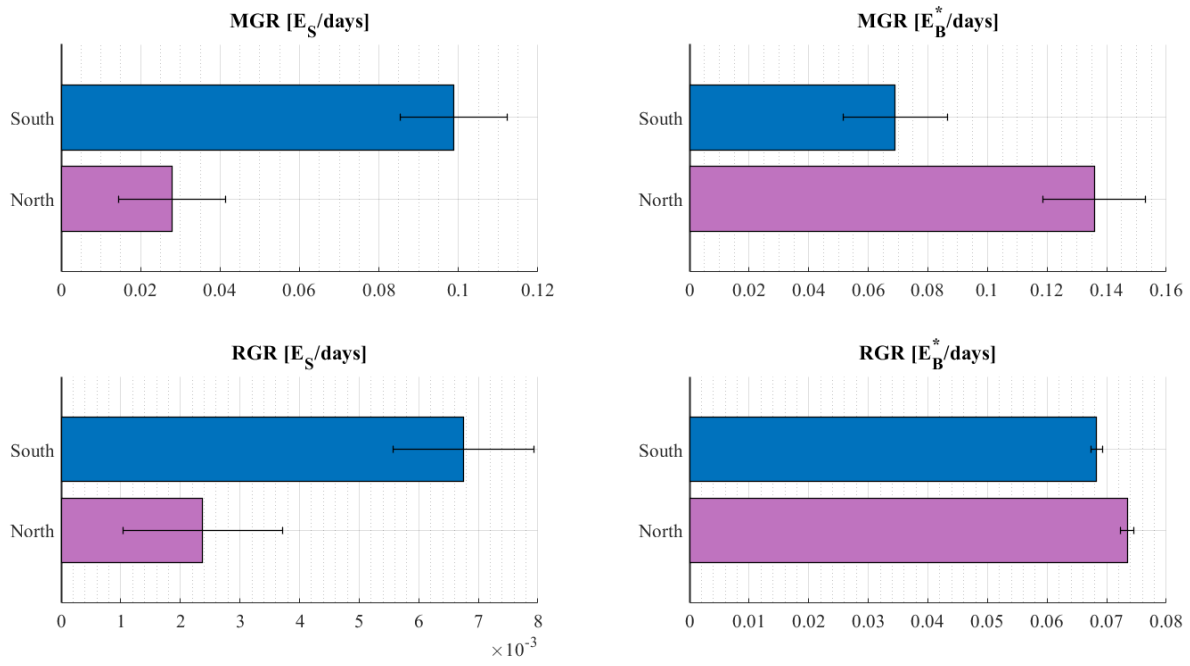

Figure 21. Mean growth rates and relative growth rates calculated from E_B^* and E_S, with 95% confidence intervals from the uncertainty analysis with 10% precision level and 1000 replicates.

Biological influences on hydrodynamics

Tidal Asymmetries of Across-farm Velocities

Change in tidal asymmetries over the study varied by depth bin (*Figure 22*, upper left). During the first month of data collection, there was a notable increase in bins corresponding to the top 60% of the water column, however this appeared cyclical for all but the uppermost bin. In the second month, there was an approximately 1.5 magnitude, mirrored, sinusoidal fluctuation between the 0-20%, 21-40% and 41-60% bins, which can be described as an exchange. It is notable that 61-80% bin also showed some of this transfer, though at about 2/3 of the magnitude of the higher bins, while the lowest bin, directly above the seafloor, showed neglibible change througout the time series. Most notable is the high magnitude decrease in the top bin (0-10%) in the final month, especially as unlike the previous month, the effect was not transferred to the lower water column. Considering the entire time series, there was a decrease in the asymmetry of the second bin (21-40%) even as the top bin (0-20%) showed increases until the final month. The three lowest bins showed fluctuations per month, but no overall time series trends.

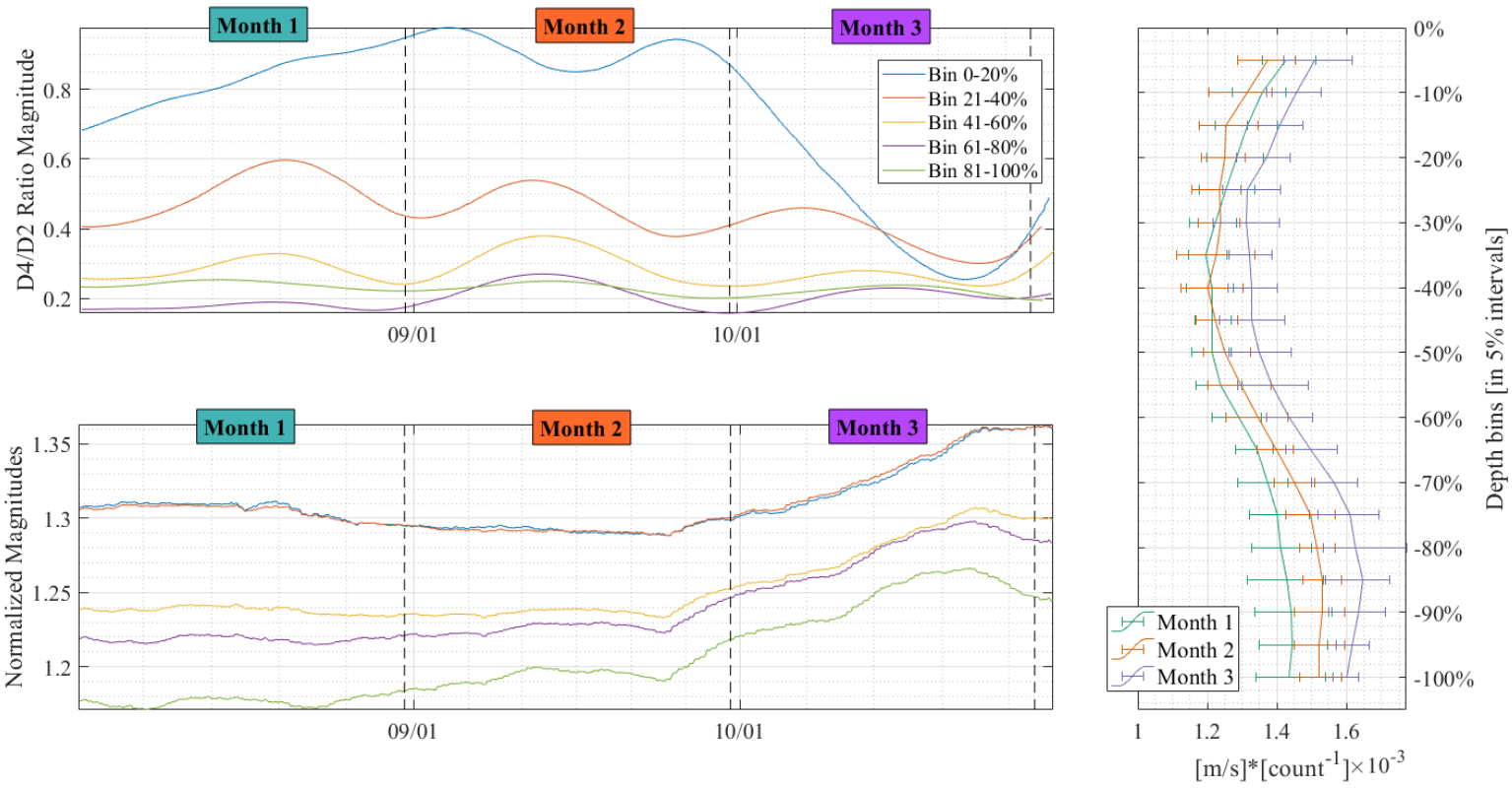

Figure 22. (Upper left) Ratio of D4/D2 bands over time and (lower left) normalized after-farm velocities over time, both on five-bin σ-coordinate grids, each bin corresponding to 20% of the water column. Legend in the upper plot applies to both left plots. Months of the experiment are labelled to correspond both with biological data results and with the right-hand panel. Black dashed vertical lines on ADCP transect days. (Right) scaled monthly medians of after-farm magnitudes of velocity ($\hat{V}$) over each of the three months of data collection.

Instantaneous After-Farm Velocities

Normalized magnitudes of the after-farm, across-farm velocities, hereafter referred to as $\widetilde{\boldsymbol{V}_A}$, reinforce the interpretation of the tidal asymmetry time series (*Figure 22*, lower left). This ($\widetilde{\boldsymbol{V}_A}$) quantifies water velocity perpendicular to the farm, that experienced the effects of the lantern nets before being recorded by the moored ADCP. Across the first two months of the experiment, these velocities demonstrate a decrease of around 0.015 in the top 40% of the water column, with an increase of similar magnitude experienced in the lower 40% of the water column. Thus, the same "mirrored, sinusoidal fluctuation" or "exchange" demonstrated in the second month by the tidal asymmetries is visible in ($\widetilde{\boldsymbol{V}_A}$) on a monthly timescale across months 1-2. It is notable that the center bin of the water column did not see this "exchange". In the final month of the experiment there is a dramatic increase in ($\widetilde{\boldsymbol{V}_A}$), approximately 0.07 units for all bins, on the same timescale as the dramatic decrease in the top bin of the D4/D2 ratios.

Scaled-median Flows

These questions exchange in flow and tidal asymmetries on a monthly timescale were addressed by quantifying the scaled median per month of the after-farm velocity magnitudes, which are hereafter referred to as $\widehat{V_l}$. In the upper water column, $\widehat{V_l}$ decreases from month one to month two, then increases again in month three (*Figure 22*, right panel). Though this difference lacks statistical significance, it is still notable, especially considering that it is from field observations. As with the previously mentioned $\widetilde{\boldsymbol{V}_A}$, the middle of the water column experienced the effects of the lantern nets infrequently throughout each tidal cycle, so that any quantifiable effects were

cancelled out by each other. However the lower water column, which was consistently below the lantern nets, demonstrates increasing $\widehat{V_t}$ from month to month, indicating acceleration of flow under the farm.This increase is only significant between month one and month three, however as with the porosity effects, the pattern is still notable. This metric was limited in explanatory power, as it only partially accounts for the effects of discharge and wind through its calculation (see *Methods*), by accounting for any changes in the volume of water classified as "after-farm". However, it cannot account for an increase in river current speed that would occur as a result of the higher discharge events of September and early October. To encompass all velocities, no low-pass filter was applied, and this makes the metric vulnerable to noise, which may have widened the 95% confidence intervals in the two-level bootrapping required to develop them. Hence the determination the overall patterns are more important for evidence of effects on hydrodynamics than whether or not the error bars intersect.

Regression Modeling

Statistical modeling was used to directly address the possible wind and ambient oceanographic effects on after-farm velocities $\widetilde{\boldsymbol{V_A}}$ and the D4/D2 ratios; a battery of regressions were tested and applied according to the methods in Appendix B.

Table 2. Model fit metrics for tidal asymmetry bands (D4/D2 ratios)

Sigma Grid Bin	**Knots**	**Adjusted R^2**		**MSE**	
		With	Without	With	Without
0-20% (Bin 1)	24	0.9892	0.8841	0.06891188	0.01411143
21-40% (Bin 2)	17	0.8842	0.6575	0.03468588	0.002731716
41-60% (Bin 3)	31	0.7213	0.6259	0.001184301	0.001766878
61-80% (Bin 4)	31	0.8544	0.8211	0.001486285	0.001017258
81-100% (Bin 5)	28	0.7592	0.6589	0.001639574	0.0001047181

Table 3. Model fit metrics for after-farm velocity magnitudes ($\widetilde{V_A}$)

Sigma Grid Bin	Knots	Adjusted R^2		MSE	
		With	Without	With	Without
0-20% (Bin 1)	4	0.9971	0.8434	1.610125e-05	0.006686602
21-40% (Bin 2)	4	0.9974	0.8468	2.087719e-05	0.006896012
41-60% (Bin 3)	4	0.996	0.8427	8.243908e-05	0.005927369
61-80% (Bin 4)	4	0.9944	0.8194	0.0002092551	0.005562344
81-100% (Bin 5)	4	0.9939	0.7967	0.000340773	0.004936328

The same final equation was determined for both the tidal asymmetry and after-farm velocity regressions; however, knot counts for the b-splines utilized for the non-linear relation with the oceanographic predictors varied (Table 2, Table 3), as detailed in Appendix B. Before inclusion of the biological predictors, mean squared error (MSE) for the after-farm velocity magnitudes was at least one order of magnitude less than that of the tidal asymmetry for all depth bins; this model will hereafter be referred to as Model 1. After inclusion of the biological predictors, or Model 2 (the weight of the scallops, the estimated weight of the biofoulants, and their interaction), the difference was three orders of magnitude less for the top 60% of the water column, while maintaining one order of magnitude less for the bottom 40%. Adjusted R^2 values demonstrated that almost all variance within the along-farm velocities could be accounted for from Model 2, while for the tidal asymmetry bands only the top 20% of the water column had more than 90% variance accounted for by the model. For the after-farm velocities change in Adjusted R^2 was in increase from Model 1 to Model 2 of around 15% for the top 60% of the water column, of 17.5% for the fourth bin (61-80%), and of 19.7% for the bin nearest to the sea floor. For the tidal asymmetries there was a less consistent change in adjusted R^2 from Model 1

to Model 2. From top of the water column to the seafloor there was an increase of: 10.5%, 22.7%, 9.5%, 3.3% and 10%, respectively.

Discussion

The hydrodynamics had a significant effect on biofouling and shellfish growth across the first month of the time series. During initial conditions before biofoulants had settled on the lantern nets, the along-farm currents were distinctly lower on the north half compared to the south half of the longline, likely due to shallower bathymetry, phased lag in tidal currents with the rest of Lowes Cove, and wake effects of the lantern nets. This along-farm velocity reduction had implication for turbulence and therefore mixing, which promoted less turbulent conditions where velocities were lowest (i.e. on the downstream end of the farm). The shellfish growth rate was largest where velocities were largest over the first month (i.e. the southern side), which is consistent with Kirby-Smith (1972) who found that higher velocities transport higher volumes of plankton past the bivalves for nutrient uptake, as well as flushing waste from surroundings. Whereas biofouling accumulation is expected to be more prevalent in areas with lower velocities and reduced turbulence, therefore allowing for settlement. The biofouling growth rate over the same period was greater where current velocities and turbulence were reduced. The reduction in along-farm velocities over the length of the longline throughout August corresponds with the farm nets being in the wake of subsequent nets for 65% of hourly velocities classified as flood. During flood (into Lowes Cove), flow encounters the southern nets before the northern nets as it rounds the headland to enter the cove. Ebb velocities (out of Lowes Cove) had a wider distribution of orientations than those of flood, as they could fan out of the cove mouth and at the

edge of the cove, at time parallel the main channel of the Damariscotta. Therefore, it makes sense that ebb had fewer instances (<20%) of the farm being in its own wake. However,, ebb velocities would not be delivering new material for biofouling settlement and shellfish uptake, so instances of their wake are less important for shellfish growth.

Once biofouling developed on the scallop nets after the first month, it had a significant effect on surrounding hydrodynamics through and frictional drag. Over the course of the three months, the species makeup of the biofouling community caused net solidity to increase then decrease, meanwhile the mass of the scallops and of the biofoulants only increased. Conservation of mass of the water flowing through the farm was demonstrated through the monthly scaled median velocities; these showed an inverse relation to net solidity in the water column (adjacent to the farm), and a direct relation (acceleration) to flow in the lower water column under the farm. Frictional drag was evident in the current velocities in August and September, evidenced by increasing D4/D2 ratios in the upper water column in the presence of lantern nets, indicating growing tidal asymmetries with time, which were enforced by the decreasing magnitude of after-farm velocities in the upper water column. This suggests that as biofouling weight increased logistically, the flow reduction behind the farm became more prevalent from drag effects. Conversely, D4/D2 ratios and after-farm velocities in the lower layer increased as surface friction effects increased, indicating that flow acceleration under the farm is also dependent on biofouling accumulation at the surface. These qualitative connections of biology and hydrodynamics were reinforced by partially linear regression models to overcome confounding impact of oceanographic factors in the final month of the time series. When the influence of oceanographic factors was controlled for in the models, scallop and (estimated) biofoulant

weights had statistically significant impacts on after-farm velocities across all depth bins; this was echoed in the tidal asymmetries but with lower statistical significance.

Overall linkages

Aquaculture farms produce a reduction in their ambient flow velocity in accordance with structural contact area and characteristic drag coefficient(s) (Loland, 1991). This wake is often dictated by the Kelvin angle (19.47°) except in presence of shear flow with surface effects, when the angle will be narrower (Ellingsen, 2014; Rabaud & Moisy, 2013). It is likely that Lowe's cove experienced horizontally shear flow due to its complex morphology and proximity of the longline to the headland; this characteristic is suggested by the transect data collected in this study, but further study is required to confirm or deny. Thus, it was prudent to assume for this analysis that the wake from the lantern nets would extend less than or equal to 19.47° from either side of the mean incident flow angle when it intersected the longline. Comparison of scatterplots of the moored ADCP velocity and corresponding inner and outer transect tracks on August 1st and 31st demonstrated a reduction factor, *r*, (Loland, 1991) in ambient velocities, otherwise known as a wake, produced by drag effects (Results: Figure 12, Figure 13, and Figure 14).

Empirically and theoretically, orientation of the longline relative to the ambient flow velocity affects the development of the wake itself (Loland, 1991), and determines whether that wake will coincide with other nets on the longline or not. If the longline is less than 20 deg from the incident angle that induces a wake, the ambient velocity can be expected to reduce by a reduction factor, where U_i is the velocity at screen *i*, r^i is the reduction factor experienced at screen *i*, and U_∞ is the free flow velocity (Loland, 1991):

$$U_i = U_\infty r^i \quad (20)$$

This is important for conceptual consideration of the difference of $\angle\theta$ and $\angle\emptyset$ to the orientation of the farm throughout the month of August 2021. A wake angle narrower than 19.47° would make its detection more difficult in field observations and may explain why a statistically significant wake was not identified across all transect hours.

Various studies have demonstrated community density effects on seston feeding for shellfish (Coleman et al., 2021; Côté J. et al., 1993; Parsons et al., 2002; Tu, et al., 2022). Specifically, the feeding habits of the animals exposed to the nutrient input first will affect the seston available for the next shellfish to consume (Tu, et al., 2022). Across the first month of biological data it was clear that the end of the longline that shellfish were cultivated on had a significant effect on their growth rate. Given that the transportation of seston occurs through ambient flow, the orientation of the farm to the incident flow angles likely played a causal role in the discrepancy of shellfish growth rates from nets on the southern half of the longline (RGR ~0.0068) to the north nets (RGR~0.0024), as the shellfish on the northern end would be in the feeding shadow of all nets to the south, inclusive of the three other lantern net groups (growth study, Netminder study, and overflow stock) on the longline. These finding indicate that orienting a farm longline to be more than 20° from the mean incident angles throughout a tidal cycle would be preferable. However, this could increase the tensions on the mooring lines which would in turn increase equipment requirements (and thus, costs) for the farm, as farm orientation parallel with incident wave (Zhao, et al., 2019) and current angles (personal communication with T. Dewhurst, 2023) mitigates mooring line tensions. The effects of the incident angles of flow, θ and $\emptyset$, on mooring line tensions are not quantified or further discussed, as they were outside the

scope of this work, yet they are important to any real-world application of the ideas of this work. Regardless, the overall goal of aquaculture farms is to grow high quality marine animals and this study has demonstrated that is not optimized when a farm is in its own wake in a semi-sheltered environment.

Drag effects on tidal velocities appear with increasing mass, both in shellfish and biofouling, on the longline, especially in the first month. Tidal asymmetry notably increased in the upper water column during the first month of data collection (*Figure 22*, upper left), which corresponded to biofouling colonization and shellfish growth. The consequence of flow reduction in the upper layer was flow acceleration in the lower layer, which increased with biofouling and shellfish mass accumulation as expected from similar suspended aquaculture studies (Gibbs et al., 1991; Loland, 1991; Plew et al., 2005;). If significant enough, flow acceleration could lead to local scouring under the farm, like that observed in the bathymetry under a floating oyster farm in the Damariscotta estuary (Liu, 2021). However, the acceleration under the farm may have an overall positive impact on the ecological system surrounding the farm and is therefore important to successful aquaculture farming, as it forces the excrement of the scallops to be dispersed, which is important for cycling of elements (such as nitrogen) throughout the marine ecosystem and avoidance of benthic eutrophication (Cranford et al., 2003, and references therein; Nilsson & Rosenberg, 2000; Pearson & Rosenburg, 1978, and references therein). Without adequate flushing underneath the farm, scallop waste could settle on the benthic layer and create a chemical, and therefore ecological, imbalance in the area local to the farm, instead of being utilized by the larger Damariscotta estuary ecosystem (Cranford et al., 2003, and references therein; Nilsson & Rosenberg, 2000; Pearson & Rosenburg, 1978, and

references therein). This necessity to ensure balanced cycling is true of suspended aquaculture in general and is the reason integrated multi-trophic farms are becoming more common (Government of Canada, 2022).

After the first month of the experiment, asymmetry remained relatively constant only monthly times scales, yet was modulated on fortnightly time scales, likely due to spring-neap variation. In the final five weeks, tidal asymmetry markedly decreased, while in the presence of increasing biofouling weight and scallop mass, due to external forcing. From September 23rd through October, frequent storms accompanied by offshore wind and increased river discharge may have led to increased out-estuary flow, which would be strongest in the upper water column as its freshly precipitated contents would be less dense than the rest of the Damariscotta. These seaward flows likely reduced the flows before the farm, leading to less flow to be reduced by the farm in across-farm flows and, thereby, less asymmetry. This is reinforced by the regression models, which demonstrating that at least 63% of the variance in the tidal asymmetry bands was from the oceanographic factors including but not limited to: river discharge, wind, water levels and their interaction terms (for a full list see Appendix B), while for the normalized after farm velocities, at least 80% of the variance was composed of these factors.

Further examinations

A decrease in scallop growth rate across the time series was expected as chlorophyll content drops with the onset of fall, that includes decreasing water temperature and fewer hours of sunlight, as was noted from the LOBO instrument data. As chlorophyll is indicative of nutrients for shellfish growth, it would be expected that scallop growth rate decreased in the third month

relative to the first two months. Additionally, water temperatures were higher during this experiment than is optimal for sea scallop growth, which is 10-15C (Coleman et al., 2021). This implies that growth across the whole longline would be inhibited in comparison with scallop growth in colder waters. The relationship of current speed and orientation with scallop growth was specifically studied by Kirby-Smith (1972) and Wildish & Sualnier (1993). Kirby-Smith found that scallop growth was almost eliminated when ambient currents reached 0.125m/s, and though growth increased with decreasing velocity, this trend was reversed at 0.21 cm/s since flux was not high enough to remove waste and provide shellfish sustenance (Kirby-Smith, 1972). Wildish and Saulnier found that current speeds below 0.03 m/s and above 0.06 m/s were not optimal for scallop feeding, and that above 0.3 m/s the shellfish closed to nutrient uptake (Wildish & Saulnier, 1993). In this study, the northern end of the longline average current magnitudes remained below 0.1 m/s, dropping to 0.08 m/s at the northmost mooring, while the southern half magnitudes increased up to 0.12 m/s by the southernmost mooring. Shellfish growth across the first month was significantly higher in the southern half of the longline, which implies that the lower threshold of current magnitude causing a decrease in growth may be nearer to 0.08m/s than to the 0.0021 m/s of Kirby-Smith (1972) or the 0.03 m/s of Wildish & Saulnier (Kirby-Smith, 1972; Wildish & Saulnier, 1993). The results of this study agree do agree with the findings of Kirby-Smith, that higher velocity up to 0.125 m/s was beneficial for scallop growth, but this is debatable from the results of Wildish & Saulnier (Wildish & Saulnier, 1993; Kirby-Smith, 1972). It is more likely these growth rates were caused by less seston being advected to the northern end of the longline than the southern, due to subsequent lantern nets being in their own wake, and influence of bathymetry on tidal currents. This means that the

amount of food present may have been the controlling factor on shellfish growth, so that the magnitude of velocities impacted scallop feeding efficacy indirectly by nutrient prevalence versus directly through active delivery of nutrients to each scallop.

More wakes were detected on August 31 than on Aug 1st, with consideration to the same tidal stages and a longline stocked with scallop-filled lantern nets present on both days. The increase in wakes could be due to the increased mass on the longline from both shellfish and biofoulants inducing higher reduction factors from frictional drag, as well as a change in ambient water velocities for the time period, but it could be from other effects. The most significant wakes were expected during peak flood and peak ebb, as wake intesity, and thus the reduction factor, is directly proportional to the ambient velocity (Davidson, 2015; Loland, 1991). Scatterplots of the north versus east velocities showed less correlation with $\emptyset$ and θ on Aug 1st than aug 31st, implying that there was less defined direction of flow during the periods of data collection of the moored ADCP on the earlier date (i.e. more random distribution when plotted on the Cartesian plane). The lower correlation would lead to more error in the calculation of $\emptyset$ and θ; as these angles are foundational for finding the wakes, lackluster results from August 1st were reasonable. Additionally, data were colleted only 10 minutes per hour, so the 10-min window of data collection may not have corresponded to the peak ebb and flood flows as well on August 1st as it did on August 31st.

More biofouling weight was accumulated on the northern half of the longline versus the southern, during the first month. This directly connects with the reduced velocities and reduced proxy dissipation rate at the northern versus the southern nets. It is reasonable to conclude that while advection from the tide and river discharge were present to distribute plankton throughout

the water column and along the longline (Okubo, 1978), local velocities were slow enough to allow those plankton to colonize surfaces to a larger extent that possible in the south, since higher velocities imply higher critical stresses, which could prevent settlement (Menesses et al, 2017). When coupled with the significantly lower velocity magnitudes throughout tidal cycles, this lower dissipation proxy would be expected to yield a higher settlement of fouling across resident lantern nets, as lower velocities would allow micro-organisms to settle and colonize instead of being flushed from the area through turbulent mixing and higher flows (Abelson & Denny, 1997; Menesses et al., 2017).

Limitations

The biological growth rates from the first to second measurement months were appropriate to quantify and compare as there was no biofoulant mass at the start of the time series. Throughout the time series, comparisons across locations could be made of the scallop growth rates and the biofoulant growth rates independently of each other. However, because of a lack of precise density data required for correction to obtain the true weight of biofoulants, $E_{B,}$ it would be inappropriate to compare growth rates between the weight of the scallops (E_S), and the estimated weight of the biofoulants (E_B^*) to each other.

The water depth decreased from the southern to northern half of the longline by approximately 3.9 meters. The shallowing bathymetry would have bottom friction effects on the velocities adjacent to the farm, having a slowing down velocities in addition to any imposed by farm wake. The effects of bathymetry on the flow field, were not studied in this work. This was

in part due to inadequate field data collection on Aug 1st, but was also not planned for in the project scope.

Conclusion

This study examined the interactions of hydrodynamics, biofouling, and scallop growth on a lantern net longline in a semi-sheltered environment from mid-summer to early fall in midcoast Maine. After the initial month of the study, accumulation of biofoulants on the two halves of the longline was inversely proportional to local velocity magnitude, as well as the proxy dissipation rate along the farm longline across the tidal cycle. Relative growth rate (RGR) of scallops was in direct contrast to that of biofoulants, as the RGR on the northern end of the longline (0.0024) was around one-third that of the southern end (0.0068). The spatial variation in local velocity, and its effects on scallop and biofoulants was in part explainable from farm wake patterns throughout the tidal cycle, however is likely due in part to bottom friction from site bathymetry. Effects of the farm on hydrodynamic environment included (1) increasing tidal asymmetries as the frictional drag from the farm increased, as quantified with an increasing D4/D2 ratio (controlling imbalances between flood and ebb velocities), (2) conservation of [water] mass surrounding the farm, as water slowed in the upper water column when it was impeded by lantern nets of increasing solidity from biofouling and accelerated underneath the farm. It is recommended that further research on the orientation of lantern nets to incident flow angles be considered, as well as accelerations from conservation of mass around the longline structure, as this study demonstrated that former plays a role to optimize shellfish growth and mitigate

biofouling settlement, while the latter could mitigate the settlement of farm detritus common on the benthos beneath aquaculture farms and/or in severe cases, induce bathymetric scour.

CHAPTER 4: CONCLUSIONS & RECOMMENDATIONS

The goal of this thesis was to investigate the linkages between hydrodynamics and biofouling, in tandem with shellfish growth, on an Atlantic Sea Scallop farm with lantern net cultivation methods in the Gulf of Maine. This objective was met through a ninety-day study on and around the principal longline of the experimental aquaculture farm of the Darling Marine Center where: (1) nine lantern nets with 150 Atlantic sea scallops each were deployed in three net groups at the southern central and northern ends of the 50 m expanse of the longline that hosted scallop lantern nets at approximately 1 net per 1.5 meters; (2) hydrographic surveys were made on both sides of the longline, and crossing the inner and outer dimensions of Lowes Cove with an underway ADCP; (3) a moored ADCP was utilized to measure ambient current velocities beside the longline; (4) a novel method for in-water weights of lantern nets was developed and performed for quantification of biofouling and scallop weight per net, monthly over the time series, and following this, (5) an analytical model was derived to relate in-water weights of the whole nets to distinct weights of of the scallops and the biofoulants.

With respect to the effects of hydrodynamics on farm biofouling and shellfish growth in the first month of the time series, results demonstrated that an increase in shellfish weight was greater at the south end of the farm, where flow velocity was above 12 cm/s throughout the tidal cycle, proxy rate of dissipation of turbulent kinetic energy (TKE) was an almost order of magnitude higher, and bathymetric depth was far greater than the northern half. In contrast, biofouling weight accumulation was higher across the northern end of the farm, where flow velocity was at or below 10 cm/s throughout the tidal cycle, proxy rate of dissipation of TKE was

almost an order of magnitude lower, and bathymetric depth was so low that nets rested on the sea floor during lowest tide. A study of the wakes developed by the lantern net longline across the tidal cycle at the start of August 2021 and the end of the same month demonstrated that wakes were most commonly detectable at flood velocities. Additionally, it was shown that subsequent nets of the longline would be in the wake of previous nets for around 65% of flood tide velocities. These wakes would have an additive (with bathymetry), but alterable effect to slow velocities moving from Outer to Inner Lowes Cove, putting lantern nets in the shadow zone of feed for each other and reducing velocity to ease biofouling settlement. Tidal phases along the longline also demonstrated that there may be lateral shear flow in Lowes Cove, so that flow near the farm is opposite to the overall tidal phase farther toward the center of the Cove. To maximize shellfish health/growth and minimize biofouling, it is recommended to consider whether the Darling Marine Center farm could be reoriented, as even a 10-degree shift could have a notable impact on the velocities experienced by the scallops on the longline.

With respect to the effects of biofouling on hydrodynamics ambient to the farm, results demonstrated that tidal asymmetry in the upper water column increased with the onset of biofouling, and that as overall shellfish and biofouling weights increased, there was an exchange of asymmetry magnitudes in areas of the water column at and directly below the farm, that was not notable nearest to the seafloor. This means that friction from the farm decreased flow in the upper water column, connecting with the wake effect to reduce flow to lantern nets farther from Lowes Cove mouth. Flow was also accelerated beneath the farm, which is excellent for preventing buildup of shellfish waste on the seafloor. Monthly trends in after-farm flow demonstrated an inverse relationship with net solidity in the upper water column where the

lantern nets were located, while in the lower water column as flow accelerated as the collective weight of the farm increased. It is important to note that in the hydrodynamic data, there was evidence to indicate that some benthic acceleration (bottom intensification) may be from local bathymetric effects and not entirely from the presence of the farm, and strong enough below-farm acceleration could cause benthic scour. Further research, ideally with a moored ADCP at the farm site throughout the year, inclusive of times when nets are present and absent, could potentially be used to untangle the interactions of bathymetry and farm drag on tidal flows.

With regards to acting as a foundational study for future research on the linkages of hydrodynamics, biofouling, and shellfish growth, the methodology of this study, lessons learned in field applications and the data, are the most valuable aspects. The field methods and analytical relationship presented here for biofouling weights may be useful to future researchers and farmers but require refinement for (a) simplification of field methods, if possible, and (b) further testing of the analytical biofouling/in-water weight model through additional field data and numerical simulation. All data, both hydrographic and biological, will be made available to the researchers of the Darling Marine Center for usage in future aquaculture and other marine research. To the author's knowledge, prior to this study there was no hydrographic survey data collected on the scale and precision of tidal cycles across months, or continuous vertical profiles, close to the experimental aquaculture farm and around Lowes Cove. It is the hope of the author that this data is a useful reference for future research across aquaculture and other marine topics at the site.

BIBLIOGRAPHY

Abarzua, S., & Jakubowski, S. (1995). Biotechnological investigation for the prevention of biofouling. I. Biological and biochemical principles for the prevention of biofouling. *Mar. Ecol. Prog. Ser., 123*, 301-312. Retrieved from https://www.int-res.com/articles/meps/123/m123p301.pdf

Abelson, A., & Denny, M. (1997). Settlement of marine organisms in flow. *Annual Review of Ecology and Systematics, 28*, 317. Retrieved from https://www.proquest.com/docview/219570057?parentSessionId=9uOrNy0JvPOMiDKJNwAhfzjnqxWKcLSNWKp6AaCBhY0%3D&pq-origsite=summon&accountid=14583

Adams, C. M., Shumway, S. E., Whitlach, R. B., & Getchis, T. (2011). Biofouling in Marine Molluscan Shellfish Aquaculture: A Survey Assessing the Business and Economic Implications of Mitigation. *Journal of the World Aquaculture Society, 42*(2), 242-252. doi:https://doi-org.wv-o-ursus-proxy02.ursus.maine.edu/10.1111/j.1749-7345.2011.00460.x

Anderson, C., & Connolly, S. (2022, June 7). *Salmon...A Pacific Northwest Icon*. Retrieved from U.S. Fish & Wildlife Service: https://www.fws.gov/story/2022-06/salmona-pacific-northwest-icon

Armijo, L. C. (2007). *Processing Acoustic Doppler Current Profiler Data for Score 1.* Naval Postgraduate School. Retrieved from https://www.met.nps.edu/~psguest/OC3570/CDROM/summer2007/Armijo/report.pdf

Bagnall, P. (2022, Dec 14). Mi'kmaq Farms to quadruple fish production with expansion in 2023. *Bangor Daily News*, p. online. Retrieved from https://www.bangordailynews.com/2022/12/14/news/aroostook/mikmaq-farms-brook-trout-production-xoasq1i29i/

Bannister, J. S., Sievers, M., Bush, F., & Bloecher, N. (2019). Biofouling in marine aquaculture: a review of recent research and developments. *Biofouling, 35*(6), 631-648. doi:doi:10.1080/08927014.2019.1640214

Barber, B. J., Getchell, R., & Schick, D. (1988). Reduced fecundity in a deep-water population of the giant scallop \Plactopecten magellanicus in the Gulf of Maine, USA. *Mar. Ecol. Prog. Ser., 42*, 207-212. Retrieved from int-res.com/articles/meps/42/m042p207.pdf

Bashevkin, S. M., & Mahardja, B. (2022). Seasonally variable relationships between surface water temperature and infow in the upper San Francisco Estuary. *Limnology and Oceanography, 67*(3), 684-702. doi:https://doi.org/10.1002/lno.12027

Bears, K. (2018). The Dynamics of Mixing and Subtidal Flow in a Maine Estuary. *Electronic Theses and Dissertations*, 2877. Retrieved from https://digitalcommons.library.umaine.edu/cgi/viewcontent.cgi?article=3956&context=etd

Bullard, S. G., Davis, C. V., & Shumway, S. E. (2013). Seasonal Patterns of Ascidian Settlement at an Aquaculture Facility in the Damariscotta River, Maine. *Journal of Shellfish Research, 32*(2), 255-264. Retrieved from https://doi.org/10.2983/035.032.0202

Cengel, Y. A., & Cimbala, J. M. (2018). *Fluid Mechanics: Fundamentals and Applications* (Fourth Edition ed.). New York, NY: McGraw-Hill Education.

Clark, M. (2021, August 23). Sea Scallops Farmed in Maine Aren't Just Sustainable. They're Helping Their Habitat. *The New York Times*. Retrieved from https://www.nytimes.com/2021/08/23/dining/maine-sea-scallops.html

Coleman, S., Cleaver, C., Morse, D., Brady, D. C., & Kiffney, T. (2021). The coupled effects of stocking density and temperature on Sea Scallop (Placopecten magellanicus) growth in suspended culture. *Aquaculture Reports, 20*, 100684. Retrieved from https://doi.org/10.1016/j.aqrep.2021.100684

Corson, T. (2009, Sept 16). Learning From Maine's Lobster Wars. *The Atlantic*, p. online. Retrieved from https://www.theatlantic.com/health/archive/2009/09/learning-from-maines-lobster-wars/26613/

Côté, J. H., Himmelman, J. H., & Claereboudt, M. R. (1994). Separating effects of limiting food and space on growth of the giant scallop Placopecten magellanicus in suspended culture. *Marine Ecology Progress Series, 106*(1-2), 85-91. Retrieved from https://www.int-res.com/articles/meps/106/m106p085.pdf

Côté, J., Himmelman, J. H., Claereboudt, M., & Bonardelli, J. C. (1993). Influence of Density and Depth on the Growth of Juvenile Sea Scallops (Placopecten magellanicus) in Suspended Culture. *Canadian Journal of Fisheries and Aquatic Sciences, 50*(9), 1857-1869. Retrieved from https://doi.org/10.1139/f93-208

Cranford, P., Dowd, M., Grant, J., Hargrave, B., & McGladdery, S. (2003). Ecosystem level effects of marine bivalve aquaculture. In B. T. Hargrave, P. Cranford, M. Dowd, B. Grant, S. McGladdery, & L. E. Burridge (Eds.), *A scientific review of the potential environmental effects of aquaculture in aquatic ecosystems* (pp. 51-95). Retrieved from https://www.researchgate.net/publication/236218368_Ecosystem_level_effects_of_marine_bivalve_aquaculture

Davidson, P. A. (2015). *Turbulence: An Introduction for Scientists and Engineers* (Second Edition ed.). New York, NY: Oxford University Press.

Doochin, H. S. (1951). Marine Boring and Fouling in Relation to Velocity of Water Currents. *Bulletin of Marine Science, 1*(3), 196-208. Retrieved from https://www.ingentaconnect.com/contentone/umrsmas/bullmar/1951/00000001/00000003/art00003#

Edmondson, C. H., & Ingram, W. M. (1939). Fouling Organisms in Hawaii. *Occasional Papers of Bernice P. Bishop Museum, Honolulu, Hawaii, XIV*(14), 251-300. Retrieved from http://hbs.bishopmuseum.org/pubs-online/pdf/op14-14.pdf

Ellingsen, S. Å. (2014). Ship waves in the presence of uniform vorticity. *Journal of Fluid Mechanics, 742*, R2. doi:doi:10.1017/jfm.2014.28

Fitridge, I. D., Dempster, T., Guenther, J., & de Nys, R. (2012). The impact and control of biofouling in marine aquaculture: a review. *Biofouling, 28*(7), 649-669. Retrieved from https://doi.org/10.1080/08927014.2012.700478

Fong, D. A., & Monismith, S. G. (2004). Evaluation of the Accuracy of a Ship-Mounted, Bottom-Tracking ADCP in a Near-Shore Coastal Flow. *Journal of Atmospheric and Ocean Technology, 21*(7), 1121-1128. doi:https://doi.org/10.1175/1520-0426(2004)021<1121:EOTAOA>2.0.CO;2

Fredsoe, J., & Sumer, B. M. (2006). *Hydrodynamics Around Cylindrical Structures (Revised Edition).* World Scientific Publishing Company. Retrieved from http://ebookcentral.proquest.com/lib/umaine/detail.action?docID=1679304

Friedrichs, C. T., & Aubrey, D. G. (1988). Non-linear Tidal Distortion in Shallow Well-mixed Estuaries: a Synthesis. *Estuarine, Coastal and Shelf Science, 27*(5), 521-545. Retrieved from https://doi.org/10.1016/0272-7714(88)90082-0

Gansel, L. B., Blöcher, N., Floerl, O., & Günther, J. (2017). Quantification of biofouling on nets: a comparison of wet weight measurements and optical (image analysis) methods. *Aquacult Int, 25*, 679-692. doi:https://doi.org/10.1007/s10499-016-0062-5

Gansel, L. C., Plew, D. R., Endresen, P. C., Olsen, A. I., Misimi, E., Guenther, J., & Jensen, Ø. (2015). Drag of Clean and Fouled Net Panels -- Measurements and Parameterization of Fouling. *PLoS ONE, 10*(7), e0131051. doi:https://doi.org/10.1371/journal.pone.0131051

Garvine, R. W. (1985). A Simple Model of Estuarine Subtidal Fluctuations Forced by Local and Remote Wind Stress. *Journal of Geophysical Research, 90*(C6), 11945-11948. Retrieved from https://agupubs-onlinelibrary-wiley-com.wv-o-ursus-proxy02.ursus.maine.edu/doi/pdf/10.1029/JC090iC06p11945

Gibbs, M. M., James, M. R., Pickmere, S. E., & Woods, P. H. (1991). Hydrodynamic and water column properties at six stations associated with mussel farming in Pelorus Sound, 1984-85. *New Zealand Journal of Marine and Freshwater Research, 25*, 239-254. Retrieved from https://www.tandfonline.com/doi/epdf/10.1080/00288330.1991.9516476?needAccess=true&role=button

Government of Canada. (2009, Feb 3). *Global Consequences of Overfishing*. Retrieved from Fisheries and Oceans Canada: https://www.dfo-mpo.gc.ca/international/isu-global-eng.htm

Government of Canada. (2022, 09 20). *Integrated Multi-Trophic Aquaculture*. Retrieved from Fisheries and Oceans Canada: https://www.dfo-mpo.gc.ca/aquaculture/sci-res/imta-amti/index-eng.htm

Guo, X., & Luo, Y. (2016). Scallops and Scallop Aquaculture in China. *Developments in Aquaculture and Fisheries Science, 40*, 937-952. doi:DOI:10.1016/B978-0-444-62710-0.00022-5

Hammack, E. A., Fong, M. T., & Stockstill, R. L. (2009). *Calculating Forces on Components of Hydraulics Structures.* US Army Corps of Engineers, ERDC/CHL. Retrieved from https://erdc-library.erdc.dren.mil/jspui/bitstream/11681/2050/1/CHETN-IX-21.pdf

Harbo, R. M. (2022). Tunicates, Sea Squirts, Ascidians. In R. M. Harbo, *Whelks to whales: Coastal marine life of the Pacific Northwest, newly revised and expanded* (Third ed.). Harbour Publishing Co. Ltd. Retrieved from https://ebookcentral.proquest.com/lib/umaine/reader.action?docID=6896581&ppg=433&pq-origsite=summon

Harder, T. (2020, Nov 18). *Tales from a tribal trout farm*. Retrieved from The Fish Site: https://thefishsite.com/articles/tales-from-a-tribal-trout-farm

Hardin, G. (1968). The Tragedy of the Commons. *Science, New Series, 162*(3859), 1243-1248. Retrieved from https://www.jstor.org/stable/1724745

Hart, D. R., & Chute, A. S. (2004). *Essential fish habitat source document. Sea Scallop, Placopecten magellanicus, Life History and Habitat Characteristics.* U.S. Department of Commerce: National Oceanic and Atmospheric Administration. Retrieved from https://repository.library.noaa.gov/view/noaa/4031

Hart, D. R., & Rago, P. J. (2006). Long-Term Dynamics of U.S. Atlantic Sea Scallop Placopecten magellanicus Populations. *North American Journal of Fisheries Management, 26*, 490-501. doi:DOI: 10.1577/M04-116.1

Harte, M., Tiller, R., Kailis, G., & Burden, M. (2019). Countering a climate of instability: the future of relative stability under the Common Fisheries Policy. *ICES Journal of Marine Science, 76*(7), 1951-1958. Retrieved from https://doi.org/10.1093/icesjms/fsz109

Hennen, D. R., & Hart, D. R. (2012). Shell Height-To-Weight Relationships for Atlantic Sea Scallops (Placopecten magellanicus) in Offshore U.S. Waters. *J. of Shellfish Research, 31*(4), 1133-1144. doi:https://doi.org/10.2983/035.031.0424

Hoffmann, W. A., & Poorter, H. (2002). Avoiding Bias in Calculations of Relative Growth Rate. *Ann Bot., 90*(1), 37-42. doi:10.1093/aob/mcf140

Jiang, H.-z., Ji, Y.-p., & Zhang, M.-l. (2023). Modeling impact of culture facilities on hydrodynamics and solute transport in marine aquaculture of North Yellow Sea. *Water Science and Engineering, 16*(1), 26-35. doi:https://doi.org/10.1016/j.wse.2022.10.005

Joyce, T. M. (1989). On In Situ "Calibration" of Shipboard ADCPs. *American Meterological Society, 6*, 169-172. doi:https://doi.org/10.1175/1520-0426(1989)006<0169:OISOSA>2.0.CO;2

Kaplan, K. A., Hart, D. R., Hopkins, K., Gallager, S., York, A., Taylor, R., & Sullivan, P. J. (2017). Evaluating the interaction of the invasive tunicate Didemnum vexillum with the Atlantic sea scallop Placopecten magellanicus on open and closed fishing grounds of Georges Bank. *ICES Journal of Marine Science, 74*(9), 2470-2479. Retrieved from https://doi.org/10.1093/icesjms/fsx076

Kirby-Smith, W. W. (1972). Growth of the Bay Scallop: The Influence of Experimental Water Currents. *J. Exp. Mar. Biol. Ecol., 8*(1), 7-18. doi:https://doi.org/10.1016/0022-0981(72)90051-2

Lieberthal, B., Huguenard, K., Ross, L., & Liu, Z. (2019). Intratidal Variability of Water Quality in the Damariscotta River, Maine. *Water, 11*(12), 2603. doi:https://doi.org/10.3390/w11122603

Lin, J., Li, C., & Zhang, S. (2016). Hydrodynamic effect of a large offshore mussel suspended aquaculture farm. *Aquaculture, 451*, 147-155. doi:https://doi.org/10.1016/j.aquaculture.2015.08.039

Liu, Z. (2021). *Hydrodynamic Impacts of Expanding Aquaculture.* University of Maine. Retrieved from https://digitalcommons.library.umaine.edu/etd/3379

Liu, Z., & Huguenard, K. (2020). Hydrodynamic Response of a Floating Aquaculture Farm in a Low Inflow Estuary. *Journal of Geophysical Research: Oceans, 125*, e2019JC015625. Retrieved from https://doi.org/10.1029/2019JC015625

Loland, G. (1991). *Current Forces on and flow through fish farms.* The Norwegian Institute of Technology, Division of Marine Hydrodynamics. Trondheim: The Norwegian Institute of Technology.

Loy, E., & Cai, Y. (2017, May 6). Squamish Nation's yearly salmon distribution takes new form. *CBC News*, p. online. Retrieved from https://www.cbc.ca/news/indigenous/squamish-first-nation-yearly-salmon-distribution-takes-new-form-1.4093477

Lui, B., Fu, D., Zhang, Y., & Chen, X. (2020). Experimental and numerical study on the wave force calculation of a partially immersed horizontal cylindrical float. *International Journal of Naval Architecture and Ocean Engineering, 12*, 733-742. doi:https://doi.org/10.1016/j.ijnaoe.2020.08.002.

MacKenzie, A. F., Basque, K., Maltby, E. A., Hodgson, M., Nicholson, A., Wilson, E., . . . Wyeth, R. C. (2021). Effectiveness of several commercial non-toxic antifouling technologies for aquaculture netting at reducing mussel biofouling. *Aquaculture, 543*, 736968. doi: https://doi.org/10.1016/j.aquaculture.2021.736968

MacKenzie, B. R., & Leggett, W. C. (1993). Wind-based models for estimating the dissipation rates of turbulent energy in aquatic environments: empirical comparisons. *Marine Ecology Progress Series, 94*(3), 207-216. Retrieved from http://www.jstor.org/stable/24832707

Maine Department of Agriculture, Conservation & Forestry. (2021). *Whaleback Shell Midden*. Retrieved from Bureau of Parks and Lands: https://www.maine.gov/dacf/parks/discover_history_explore_nature/history/whaleback/index.shtml

McAlice, B. J., & Petrie, W. M. (1969). *An environmental survey of the Damariscotta River estuary, Lincoln County, Maine.* Augusta, Maine: Maine Department of Economic Development. Retrieved from https://digitalcommons.usm.maine.edu/cgi/viewcontent.cgi?article=1105&context=me_collection

Menesses, M., Belden, J., Dickenson, N., & Bird, J. (2017). Measuring a critical stress for continuous prevention of marine biofouling accumulation with aeration. *Biofouling, 33*(9), 703-711. Retrieved from https://doi.org/10.1080/08927014.2017.1359574

Michalak, I., & Messyasz, B. (2021). Concise review of Cladophora spp.: macroalgae of commercial interest. *J Appl Phycol, 33*, 133-166. Retrieved from https://doi.org/10.1007/s10811-020-02211-3

Morgan, S. G., Shanks, A. L., MacMahan, J. H., Reniers, A. M., & Feddersen, F. (2018). Planktonic Subsidies to Surf-Zone and Intertidal Communities. *Annual Review of Marine Science, 10*, 345-369. doi:doi:https://doi.org/10.1146/annurev-marine-010816-060514

Morison, J. R., Johnson, J. W., & Schaaf, S. A. (1950). The Force Exerted by Surface Waves on Piles. *J Pet Technol, 2*, 149-154. Retrieved from https://watermark.silverchair.com/spe-950149-g.pdf?token=AQECAHi208BE49Ooan9kkhW_Ercy7Dm3ZL_9Cf3qfKAc485ysgAAAzEwggMtBgkqhkiG9w0BBwagggMeMIIDGgIBADCCAxMGCSqGSIb3DQEHATAeBglghkgBZQMEAS4wEQQMvurpwBW4ZFu-bW-BAgEQgIIC5DjXwyAQAuzk5gCbX7iupyY_KtKHSkDeShOi0NQS_v

Morse, D. L., Cowperthwaite, H. S., Perry, N., & Britsch, M. (2020). *Methods and Materials for Aquaculture Production of Sea Scallops (Placopecten magellanicus).* NOAA IR. Retrieved from https://repository.library.noaa.gov/view/noaa/38586

Newell, R., & Branch, G. (1980). The influence of temperature on the maintenance of metabolic energy balance in marine invertebrates. In J. H. Blaxter, F. S. Russell, & M. Yonge (Eds.), *Advances in Marine Biology* (Vol. 17, pp. 329-396). London, UK: Elsevier. doi:https://doi.org/10.1016/S0065-2881(08)60304-1

Nilsson, H. C., & Rosenberg, R. (2000). Succession in marine benthic habitats and fauna in response to oxygen deficiency: analysed by sediment profile-imaging and by grab samples. *Mar Ecol Prog Ser*, 139-149. Retrieved from https://www.int-res.com/articles/meps/197/m197p139.pdf

NOAA Fisheries. (2020, Nov 9). NOAA Fisheries Science Helps Maine's Pioneering Sea Scallop Farmers. *News*, p. online. Retrieved from https://www.fisheries.noaa.gov/feature-story/noaa-fisheries-science-helps-maines-pioneering-sea-scallop-farmers

NOAA Fisheries. (2022, Nov 28). *Puget Sound Salmon and Steelhead Fisheries*. Retrieved from Sustainable Fisheries: https://www.fisheries.noaa.gov/west-coast/sustainable-fisheries/puget-sound-salmon-and-steelhead-fisheries

Nurioglu, A. G., Esteves, A. C., & De With, G. (2015). Non-toxic, non-biocide-release antifouling coatings based on molecular structure design for marine applications. *Journal of Materials Chemistry B, 3*, 6547-6570. Retrieved from https://pubs.rsc.org/en/content/articlepdf/2015/tb/c5tb00232j

Okubo, A. (1978). Horizontal Dispersion and Critical Scales for Phytoplankton Patches. In J. Steele (Ed.), *NATO Conference Series. Spatial Pattern in Plankton Communities* (Vol. 3). Boston, MA: Springer. Retrieved from https://doi.org/10.1007/978-1-4899-2195-6_2

Palanisamy, S. K., Thomas, O. P., & McCormack, G. P. (2018). Bio-invasive ascidians in Ireland: A threat for the shellfish industry but also a source of high added value products. *Bioengineered, 9*(1), 55-60. doi:10.1080/21655979.2017.1392421

Parker, B. B. (2007). *Tidal Analysis and Prediction.* U.S. Department of Commerce: National Oceanic and Atmospheric Administration. Retrieved from https://tidesandcurrents.noaa.gov/publications/Tidal_Analysis_and_Predictions.pdf

Parsons, G. J., Shumway, S. E., Kuenstner, S., & Gryska, A. (2002). Polyculture of sea scallops (Placopecten magellanicus) suspended from salmon cages. *Aquaculture International, 10*, 65-77. Retrieved from https://doi.org/10.1023/A:1021324610930

Pearson, T. H., & Rosenburg, R. (1978). Macrobenthic succession in relation to organic enrichment and pollution of the marine environment. *Oceanogr. Mar. Biol. Ann. Rev., 16*, 229-311. Retrieved from https://www.researchgate.net/publication/243785865_Pearson_TH_Rosenberg_R_Macrobenthic_succession_in_relation_to_organic_enrichment_and_pollution_of_the_marine_environment_Oceanogr_Mar_Biol_Ann_Rev_16_229-311

Perry, A. (2010). Rethinking The Adequacy Of Informal Property Rules: Some Evidence From Maine's Lobster Fishery. *Ocean and Coastal Law Journal, 15*(1), 85-93. Retrieved from https://core.ac.uk/download/pdf/234109027.pdf

Pershing, A. J., Alexander, M. A., Brady, D. C., Brickman, D., Curchitser, E. N., Diamond, A. W., . . . Wang, Y. (2021). Climate impacts on the Gulf of Maine ecosystem: A review of observed and expected changes in 2050 from rising temperatures. *Elementa: Science of the Anthropocene, 9*(1), 00076. Retrieved from https://doi.org/10.1525/elementa.2020.00076

Petersen, J. K., Schou, O., & Thor, P. (1997). In situ growth of the ascidian Ciona instestinalis (L.) and the blue mussel Mytilus edulis in an eelgrass meadow. *Journal of Experimental Marine Biology and Ecology, 218*(1), 1-11. Retrieved from https://doi.org/10.1016/S0022-0981(97)00064-6

Petraitis, P. S. (1991). Recruitment of the mussel Mytilus edulis L. on sheltered and exposed shores in Maine, USA. *Journal of Experimental Marine Biology and Ecology, 147*(1), 65-80. Retrieved from https://doi.org/10.1016/0022-0981(91)90037-W

Pilditch, C. A., & Grant, J. (1999). Effect of variations in flow velocity and phytoplankton concentration on sea scallop (Placopecten magellanicus) grazing rates. *Journal of Experimental Marine Biology and Ecology, 240*(1), 111-136. Retrieved from https://doi.org/10.1016/S0022-0981(99)00052-0

Plew, D. R., Stevens, C. L., Spigel, R. H., & Hartstein, N. D. (2005). Hydrodynamic implications of large offshore mussel farms. *IEEE Journal of Oceanic Engineering, 30*(1), 95-108. doi:doi: 10.1109/JOE.2004.841387

Plew, D. R., Stevens, C. L., Spigel, R. H., & Hartstein, N. D. (2005). Hydrodynamic Implications of Large Offshore Mussel Farms. *IEEE Journal of Oceanic Engineering, 30*(1), 95-108. Retrieved from https://ieeexplore-ieee-org.wv-o-ursus-proxy02.ursus.maine.edu/stamp/stamp.jsp?tp=&arnumber=1435580

Rabaud, M., & Moisy, F. (2013). Ship wakes: Kelvin or Mach angle? *Physical review letters, 110*(21), 214503. Retrieved from https://journals-aps-org.wv-o-ursus-proxy02.ursus.maine.edu/prl/pdf/10.1103/PhysRevLett.110.214503

Rbouvier Consulting. (2019). *Market Analysis of Maine Farm-Raised Sea Scallops.* Retrieved from https://www.ceimaine.org/wp-content/uploads/2019/02/Market-Analysis-of-Maine-Farm-Raised-Sea-Scallops.pdf

Reames, E. (2012). *Nutritional Benefits of Seafood.* Souther Regional Aquaculture Center. Retrieved from https://aquaculture.ca.uky.edu/sites/aquaculture.ca.uky.edu/files/srac_7300_nutritional_benefits_of_seafood.pdf

Schmitt, C., & Hartin, S. (2016). Marine Sciences at the University Of Maine, 1960-2015. *Maine History, 50*(2), 60-75. Retrieved from https://digitalcommons.library.umaine.edu/mainehistoryjournal/vol50/iss2/4

Schuech, R. M.-D., & Menden-Deuer, S. (2014). Going ballistic in the plankton: Anisotropic swimming behavior of marine protists. *Limnology and Oceanography: Fluids and Environments, 4*(1), 1-16. doi:https://doi.org/10.1215/21573689-2647998

Scrosati, R. A., & Holt, J. K. (2021). Recruitment and Post-recruitment Dynamics of the Barnacle Semibalanus balanoides on a Wave-Exposed Headland in Atlantic Canada. *Front. Mar. Sci., 8*, 1-7. Retrieved from https://doi.org/10.3389/fmars.2021.799514

Smith, F. G. (1946). Effect of Water Currents upon the Attachment and Growth of Barnacles. *Biological Bulletin, 90*(1), 51-70. doi:https://doi.org/10.2307/1538061

Song, Y. H., & Haidvogel, D. (1994). A semiimplicit ocean circulation model using a generalized topography-following coordinate system. *J. Comput. Phys., 115*, 228-244. Retrieved from http://iodlabs.ucsd.edu/falk/roms_class/song-1994.pdf

Squamish Tribe. (2023). *Salmon*. Retrieved from Finfish: https://suquamish.nsn.us/home/departments/fisheries/finfish/#:~:text=Since%20time%20immemorial%2C%20the%20Suquamish,and%20beyond%20to%20harvest%20salmon.

Tanaka, K. R., Torre, M. P., Saba, V. S., Stock, C. A., & Chen, Y. (2020). An ensemble high-resolution projection of changes in the future habitat of American lobster and sea scallop in the Northeast US continental shelf. *Biodiversity Research, 26*(8), 987-1001. Retrieved from https://doi.org/10.1111/ddi.13069

Tettelbach, S. T., Tetrault, K., & Carroll, J. (2012). Efficacy of Netminder® silicone release coating. *Aquaculture Research, 45*(2), 1-9. doi:doi:10.1111/j.1365-2109.2012.03220.x

Thompson, B., Perry, M. J., & Davis, C. (2006). *Phytoplankton in the Damariscotta River Estuary.* National Oceanic and Atmospheric Administration (NOAA). Retrieved from https://repository.library.noaa.gov/view/noaa/38812

Thompson, B., Perry, M. J., Davis, C., & University of Maine. (2006). *Phytoplankton in the Damariscotta River Estuary.* Maine Sea Grant. Retrieved from https://repository.library.noaa.gov/view/noaa/38812/noaa_38812_DS1.pdf

Torrence, C., & Compo, G. P. (1998). A Practical Guide to Wavelet Analysis. *Bulletin of the American Meteorological Society, 79*(1), 61-78. Retrieved from https://paos.colorado.edu/research/wavelets/bams_79_01_0061.pdf

Trotter, B. (2018, Nov 15). Sea Squirts Are Thriving In The Gulf Of Maine, And 'There's Nothing You Can Do About It'. *Bangor Daily News*, p. electronic. Retrieved from https://www.mainepublic.org/environment-and-outdoors/2018-11-15/sea-squirts-are-thriving-in-the-gulf-of-maine-and-theres-nothing-you-can-do-about-it

Tu, G., Liu, H., Ru, Z., Yang, W., Sun, T., Xing, L., & Ding, Y. (2022). Refined three-dimensional numerical simulation of velocity field and seston flux within a scallop-fishing net cage. *Ocean Engineering, 253*, 111199. Retrieved from https://doi.org/10.1016/j.oceaneng.2022.111199

United Nations. (n.d.). *Department of Economic and Social Affairs, Sustainable Development*. Retrieved from Goals: 2: End hunger, achieve food security and improved nutrition and promote sustainable agriculture: https://sdgs.un.org/goals/goal2

United Nations. (n.d.). *What is sustainable development?* Retrieved from The Sustainable Development Agenda: https://www.un.org/sustainabledevelopment/development-agenda/#:~:text=What%20is%20sustainable%20development%3F,to%20meet%20their%20own%20needs.

United States Census Bureau. (2023, 08 08). *U.S. and World Population Clock*. Retrieved from World Population: https://www.census.gov/popclock/world

Uribe, E., & Etchepare, I. (2002). Effects of Biofouling by Ciona intestinalis on Suspended Culture of Argopecten purpuratus in Bahia Inglesa, Chile. *Bull. Aquacul. Assoc. Canada, 102*(3), 93-95. Retrieved from https://www.researchgate.net/profile/Eduardo-Uribe/publication/285455119_Effects_of_biofouling_by_Ciona_intestinalis_on_suspended_culture_of_Argopecten_purpuratus_in_Bahia_Inglesa_Chile/links/5dc4b239299bf1a47b1f8318/Effects-of-biofouling-by-Ciona-intesti

Uzun, D., Demirel, Y. K., Coraddu, A., & Turan, O. (2019). Time-dependent biofouling growth model for predicting the effects of biofouling on ship resistance and powering. (ELSEVIER, Ed.) *Ocean Engineering, 191*, 106432. Retrieved from https://www.sciencedirect.com/science/article/abs/pii/S0029801819305803

Valle-Levinson, A. (2013). Some basic hydrodynamic concepts to be considered for coastal aquaculture. In L. G. Ross, T. C. Telfer, L. Falconer, D. Soto, & J. Aquilar-Manjarrez (Ed.), *Site selection and carrying capacities for inland and coastal aquaculture* (pp. 147-158). Stirling, the United Kingdom of Great Britain and Northern Ireland: FAO Fisheries and Aquaculture Proceedings No. 21. Rome, FAO. 282 pp. Retrieved from https://www.observatorio-acuicultura.es/sites/default/files/images/adjuntos/libros/site_selection_fao.pdf#page=159

Verberck, B. (2013). Wake up. *Nature Physics, 9*, 390. Retrieved from https://doi.org/10.1038/nphys2687

Vinagre, P. A., Simas, T., Cruz, E., Pinori, E., & Svenson, J. (2020). Marine Biofouling: A European Database for the Marine Renewable Energy Sector. *Journal of Marine Science and Engineering, 8*(7), 495. Retrieved from https://doi.org/10.3390/jmse8070495

Wahl, M. (1989). Marine epibiosis. I. Fouling and antifouling: some basic aspects. *Mar. Ecol. Prog. Ser., 58*, 175-189. Retrieved from https://www.int-res.com/articles/meps/58/m058p175.pdf

Walton, T. (2002). *Tidal Velocity Asymmetry at Inlets.* US Army Corps of Engineers: Coastal and Hydraulics Laboratory (U.S.), Engineer Research and Development Center (U.S.). Retrieved from https://hdl.handle.net/11681/1953

Wang, Q., Danilov, S., Sidorenko, D., Timmermann, R., Wekerle, C., Wang, X., . . . Schröter, J. (2014). The Finite Element Sea Ice-Ocean Model (FESOM) v.1.4: formulation of an ocean general circulation model. *Geoscientific Model Development, 7*(2), 663-693. doi:https://doi.org/10.5194/gmd-7-663-2014

Wang, X., Xie, J., Luo, Y., Wang, X., Guo, G., & You, X. (2023). Experimental Investigation of the Hydrodynamic Characteristics of Longline Aquaculture Facilities under Current and Wave Conditions. *Fishes, 2023*(8), 204. Retrieved from https://doi.org/10.3390/fishes8040204

Washington State Department of Health. (n.d.). *Health Benefits of Fish*. Retrieved from https://doh.wa.gov/community-and-environment/food/fish/health-benefits

Wildish, D. J., & Saulnier, A. M. (1993). Hydrodynamic control of filtration in Plactopecten magellanicus. *Journal of Experimental Marine Biology and Ecology, 174*(1), 65-82. doi:doi:https://doi.org/10.1016/0022-0981(93)90251-I

Zang, Z., Ji, R., Hart, D. R., Jin, D., Chen, C., Liu, Y., & Davis, C. S. (2023). Effects of warming and fishing on Atlantic sea scallop (Placopecten magellanicus) size structure in the Mid-Atlantic rotationally closed areas. *ICES Journal of Marine Science, 80*(5), 1351-1366. Retrieved from https://doi.org/10.1093/icesjms/fsad063

Zhao, Y.-P., Yang, H., Bi, C.-W., Chen, Q.-P., Dong, G.-H., & Cui, Y. (2019). Hydrodynamic responses of longline aquaculture facility with lantern nets in waves. *Aquaculture Engineering, 86*, 101996. doi:https://doi.org/10.1016/j.aquaeng.2019.101996

APPENDICES

APPENDIX A: Prediction of Discharge Time Series

A partial time series of discharge was available for July 12, 2021, through November 29, 2021, from KEI Power, who are the owners and operators of the Newcastle Dam. The data provided was recorded inconsistently every 2-3 days, so interpolation was required to make a daily time series. USGS gauge height data were available in 15-min intervals from the nearby Sheepscott River and daily total precipitation was available on Weather Underground (TWC, 2023) from 7-mile-distant KIWI airport in Wiscassett, ME.

All datasets were imported into MATLAB and the Sheepscott River dataset was converted from 15-min intervals to daily mean. The three datasets were normalized according to standard statistical practice (subtracting the mean and dividing by the standard deviation) and trimmed to the bounds of the Newcastle dataset. The MATLAB function *ScatteredInterpolant* was used to predict discharge from three variables (time, precipitation, and the Sheepscott gage height). As the effect of same-day precipitation on river flow would be compounded or even superseded by any precipitation the previous day, a one-day lagged version of the KIWI precipitation data was also tested as a predictor. This testing included various versions of the predicted series with the precipitation variable as: (Model 1) the same-day precipitation, (Model 2) the one-day lagged precipitation, (Model 3) the mean of the lagged and the same-day and, (Model 4) the geometric mean of the absolute values of the same-day and one-day lag precipitation.

To test machine learning applications to the data, a basic linear regression predictor with cross-validation was also tested for prediction. This was not robust (low accuracy when compared to known values) due to (a) short time series and (b) non-linearity of the relation between the environmental predictors and the Damariscotta River discharge.

The last option (Model 4) yielded the most realistic results for gap interpolation, based on its similar functional shape to the Sheepscott River discharge. Using said dataset for decision-making comparison was appropriate as the Sheepscott River discharge was recorded at a much higher frequency of measurement and immediately to the west of the Damariscotta, therefore it provided a realistic model of functional form of regional river discharge.

The final predicted discharge was un-normalized by multiplying by the standard deviation of the original Newcastle data and adding the mean of the same. It was then checked for outliers---as it still predicted some negative values. When there was a negative value predicted, the value from (Model 1) was used unless it also was negative in which case the value was changed to 0 m^3/s for that observation. The final dataset of predicted discharge was converted from *cfs* to m^3/s to be utilized as environmental reference data for the larger biofouling and hydrodynamics study. The final time series was also used for the regression model in the same study, specifically for determining the effects of biofouling and shellfish on tidal asymmetries and variation in short-term velocities local to the experimental aquaculture farm longline.

The final time series is not shown as per written communication with KEI Power.

APPENDIX B: Regression Modeling

A multitude of regression models were tested for satisfying the underlying assumptions of multivariate linear regression, maximization of adjusted R^2 and minimization of mean squared error (MSE) between original data and predicted values. Optimal results were from Equation (21), where either the D4/D2 or normalized magnitudes of after farm velocities ($\hat{V}$) were represented by the dependent variable, Y_t, and predictor variables on the right-hand side indicated by $\boldsymbol{X_t}$ and marked in *Table 4* with ** in their variable notation, with g in Equation (21) expressing application of basis or b-splines to the predictor variables it encompasses.

$$Y_t = E_B^* S_t Y_t = g(\boldsymbol{X_t}) + \sqrt{E_{B_t}^*} + \sqrt{E_{S_t}} + \sqrt{E_B^* S_t} \quad (21)$$

This allowed the application of a partially linear model, with b-splines accounting for the trigonometric cycling of depth, wind direction, and wind speed across the time series.

Table 4. Variables utilized in regression models.

Variable	Description	Units	Source
W_t**	Present wind speed	m/s	KIWI airport
W_{t-1}**	Wind speed one day previous	m/s	KIWI airport
T_t**	Present wind direction	radians	KIWI airport
T_{t-1}**	Wind direction one day previous	radians	KIWI airport
H_t	Present depth	m	Moored ADCP

Table 3 continued

H_{t-1}**	Depth from one day previous	m	Moored ADCP
$W_t \times T_t$**	Interaction of present wind speed and direction	NA	Calculated
$W_{t-1} \times T_{t-1}$**	Interaction of wind speed and direction, one day previous	NA	Calculated
$W_t \times T_t \times H_{t-1}$**	Interaction of present wind speed and direction, with depth from one day previous	NA	Calculated
$W_{t-1} \times T_{t-1} \times H_{t-1}$**	Interaction of wind speed, wind direction, and depth all from one day previous	NA	Calculated
D_t**	Discharge	m^3/s	Appendix B
H_r**	Residual depth	m^3/s	Appendix B
E_B^*	Predicted time series of E_B^*	kg*	Chapter 2
E_S	Predicted time series of E_S	kg	Chapter 2
E_B^*	Interaction of predicted E_B^* and E_S, calculated as $(E_B^* \times E_S)$	NA	Calculated

Initially, b-splines were used to model the wind speed, wind direction and water depth each as a dependent variable with and time elapsed in days as a predictor. This smoothed the data to eliminate outliers before each series was used as an independent variable. Distribution of these variables versus the after-farm velocities and D4/D2 ratio demonstrated a clear pattern after day 54 of the time series, with more randomization before that date. This aligned with the dramatic increase in both the after-farm velocities and the D4/D2 ratio after September 23, 2021 (see *Figure 22* in Chapter 3), and with the hypothesis that environmental effects were overpowering predictors which were causing those dramatic increases. Knot count was optimized (minimum MSE) for the b-splines of each of these predictors, then one-day lagged versions were created, along with interaction terms as shown in (Table 4). To eliminate collinearity, present day depth was modeled as a predictor of the lagged variables and interaction terms, including a one-day lag of depth. The residuals were used in place of the original present-day depth for the final model. The scallop and biofoulant weights were fit to exponential curves, optimized twice with least squares to allow manual correction to the proper starting values of each series. The best fit equation found for estimated biofoulant weight (E_B^*) in kg* was:

$$E_B^*(t) = 1.2667e^{0.0489t} - 1.2667 \quad (22)$$

While the best fit equation for sea scallop weight in kg was:

$$E_S(t) = 0.4711e^{0.0057t} \quad (23)$$

It was assumed that the first day of the scallop time series was day 730, while for the biofoulants the first day was counted as day zero.

Various data transformations were tested for the final model, including but not limited to squaring the left-hand-side (i.e. the after-farm velocities or D4/D2 ratios), taking the square root,

b-spline, or natural log of the scallop and the biofouling weights. Natural splines were also tested, as well as various other transformations. The dependent variables (after-farm velocities or D4/D2 ratios), were modelled first only with the oceanographic predictors, including discharge predicted according to Appendix A. This yielded a base model, and residuals for examination of appropriate fit. These residuals were also plotted with biological predictors, to aid in determining which data transformation would be appropriate. There were also multiple linear regressions performed with these biological predictors with the residuals as dependent variables, to optimize the explanatory power of the scallop and estimated biofoulant weight through model form selection. The final models were partially linear, with the base oceanographic model variables having the same b-spline transformation optimized in their original model, and the biological variables each being transformed by taking their square root. Note that the biofoulant and scallop interaction term product was taken before its square root was calculated. The physical explanation for the b-spline is that wind-direction, wind speed, and water depth are cyclic and need to be explained by trigonometric regression prior to linear model application. Splines account for the cycle form by fitting a curve with a specific knot count. This contrasts with the biological variables, which nature dictates should have a direct, linear impact on the after-farm velocities and D4/D2 ratios through the drag force. As velocity is squared in the calculation of drag force, it was hypothesized that the square root of the biological variables would have the most predictive power; of the transformations tested this was confirmed.

Appendix C Incident Flow Angle Methods

This appendix provides detailed information of how the orientations of the incident flow angles ($\angle\emptyset$ and $\angle\theta$), relative to the bearing angle of the farm ($\angle F = 48.21°$ clockwise from true North) were calculated, as each angle had a different reference system, initially.

Let the ray, $\vec{F}$ designate the bearing angle ($\angle F$) created by the farm moorings with respect to true North, assigning the southernmost mooring of the longline as the origin of the coordinate system (*Figure 23*). For each ray of the incident angles ($\angle\emptyset$ and $\angle\theta$ which were calculated according to the methods in Chapter 3) let the original ray forming the angle be continued into a straight line, $\overleftrightarrow{\emptyset}$ or $\overleftrightarrow{\theta}$, that passes through the center of the compass rose to form a 180° angle dividing the 360° in two equal halves.

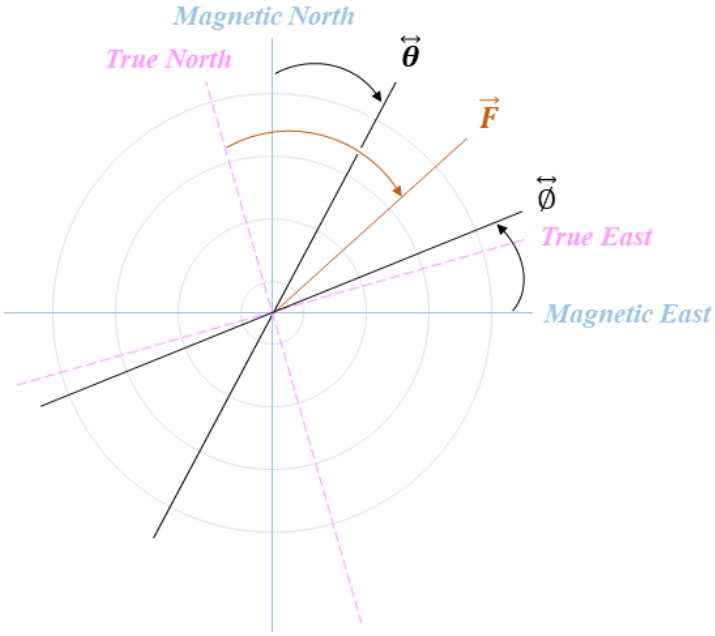

Figure 23. Cartoon of incident angles ($\angle\emptyset$ and $\angle\theta$), and the bearing angle of the farm ($\angle F$) designated by their respective rays and line, shown with respect to a both magnetic and true North coordinates and the southernmost mooring as the coordinate system origin. Note that $\angle F$, $\angle\emptyset$, and $\angle\theta$ started with different references of measurement; the zero and positive direction per each angle is indicated by respective arrows.

Let the part of this straight line that is not the original ray be called the "opposite ray". Consider that per each incident angle ($\angle\emptyset$ or $\angle\theta$) the "original rays" and the "opposite rays" represent the

same orientation of the flow relative to the farm in each hour as they are collinear. From the incident angles ($\angle\emptyset$ and $\angle\theta$) calculated from the moored ADCP burst data the following characteristics were observed.

- $\angle\emptyset$ was measured with magnetic east as zero, counterclockwise positive, and oftentimes was a negative angle.
- $\angle\theta$ was measured with magnetic north as zero, clockwise as positive, and was typically a positive angle.
- Between the opposite ray and the original ray of each hour, the ray with the least absolute difference to the farm angle will be less than 90° in positive or negative direction to $\vec{F}$, which designates the bearing angle ($\angle F$) created by the farm moorings with respect to true North. The line $\overleftrightarrow{F}_{90}$ bounds the area of the coordinate plane that is 90° less or 90° greater than $\angle F$.

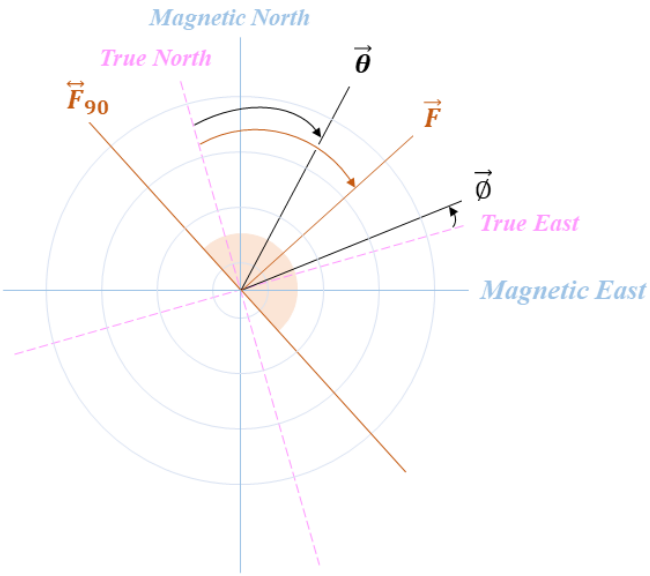

Figure 24. This cartoon is consecutive to Figure 23. It illustrates the line $\overleftrightarrow{F}_{90}$ and Steps 1-2 of Methods (following page).

Flow Angle Methods

1. To convert each of the angles ($\angle\emptyset$ and $\angle\theta$) to true North coordinates, add 15.1° to initial values of $\angle\theta$ and subtract 15.1° from initial values of $\angle\emptyset$ (*Figure 24*).
2. To convert $\angle\emptyset$ and $\angle\theta$ to their closest equivalent angles (*Figure 24*):
    - If $\angle\emptyset > 180° - \angle F$ then subtract 180°
    - If $\angle\emptyset < -\angle F$ then add 180°
    - If $\angle\theta < -(90° - \angle F)$ then add 180°
    - If $\angle\theta < (90° + \angle F)$ then subtract 180°
3. Recall that $\angle\emptyset$ also needs to be changed from counterclockwise positive from magnetic East as zero, to clockwise positive starting at magnetic North as zero. This is performed by calculating $\angle\emptyset' = 90° - \angle\emptyset$ (*Figure 25*).
4. Finally, the absolute values of the difference of this new, $\angle\emptyset'$, and $\angle\theta$, to the farm angle $\angle F$ can be calculated as (as stated in Chapter 3):

$$\angle\emptyset_0 = |\angle F - \angle\emptyset'| \quad (24)$$

$$\angle\theta_0 = |\angle F - \angle\theta| \quad (25)$$

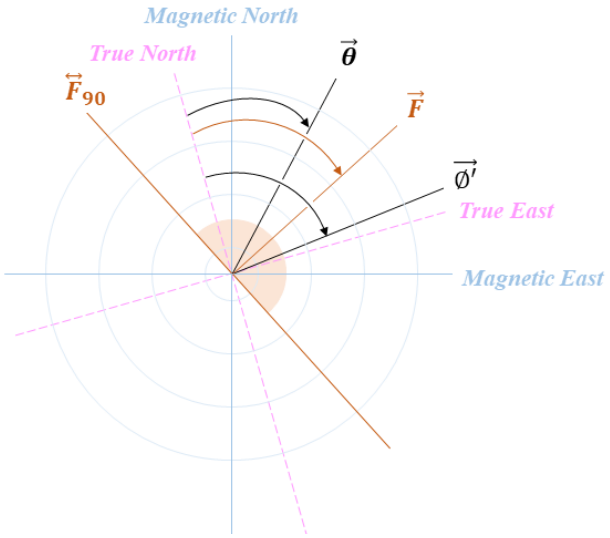

Figure 25. This cartoon is consecutive to Figure 24, and illustrates the outcome of Step 3 of Methods.

Appendix D: Supplementary Environmental Data

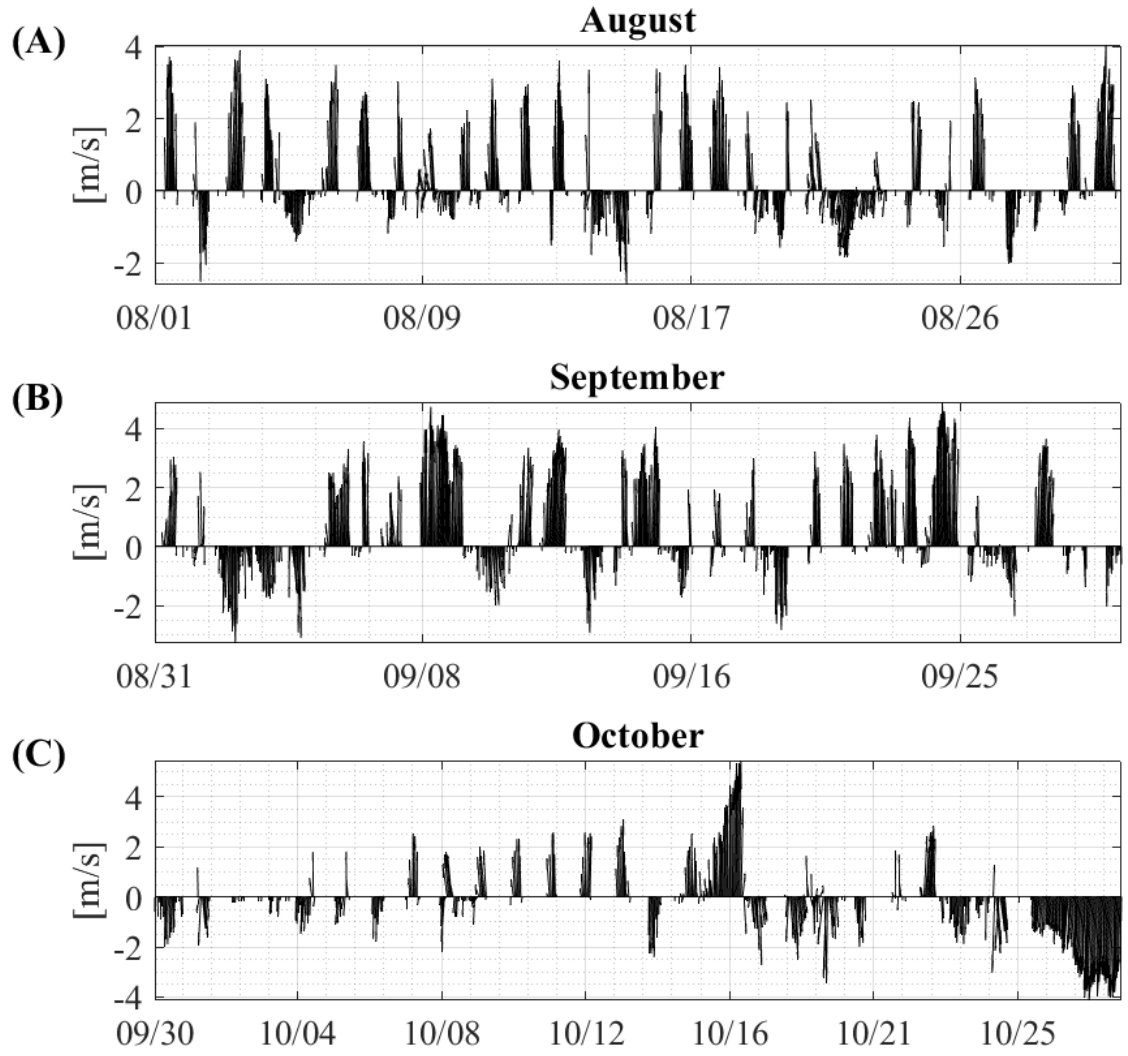

Figure 26. Supplementary wind speed and direction time series from KIWI Airport in Wiscasset, Maine, expressed as daily time series for each month of data collection. Data were corrected from counterclockwise from East, to clockwise from North, and reversed direction by adding 180° (as wind data were recorded in direction proceeding from, not to). Note that the airport is ~11.2 km from Lowes Cove, as the crow flies.

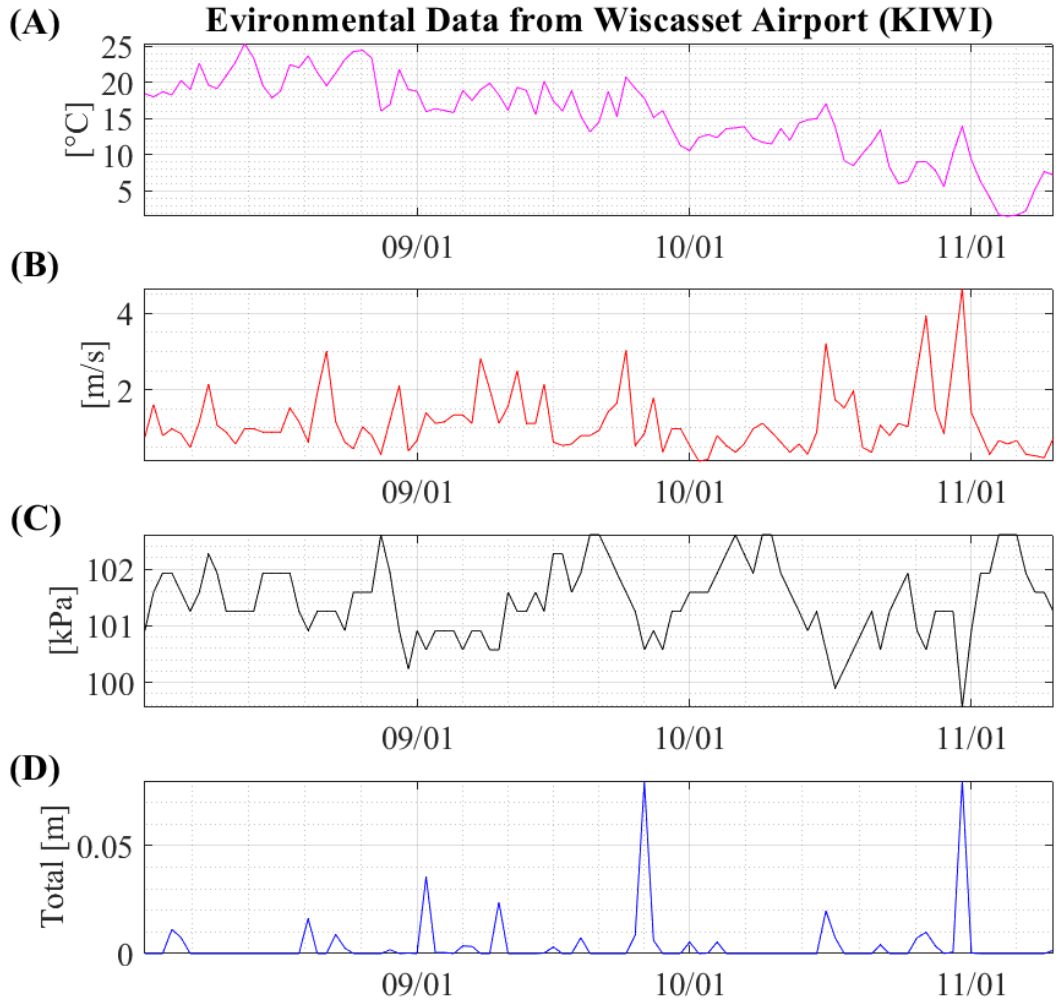

Figure 27. Supplementary environmental data from KIWI Airport in Wiscasset, Maine, expressed as daily time series of: (A) Mean daily air temperature in ℃, (B) Mean daily wind speed in meters per second (m/s), (C) Barometric pressure at sea level in kPa, and (D) Total daily precipitation (m). Note that the airport is ~11.2 km from Lowes Cove, as the crow flies. Also note that temperature decreases, but precipitation events increase in frequency over the time series.

BIOGRAPHY OF THE AUTHOR

Elisabeth (Lizzy) Younce was born in Washington State though still claims some cultural residency to Montana, where she attended Carroll College to study Applied Mathematics and Foreign Language for International Development. After college, she used her data science skills in research with projects from health economics of Latin America and the Serengeti to oceanographic habitat studies of Chilean Patagonia, where she lived for over a year. She misses the mountains of Montana very much but after living next to a fjord she decided that oceans are important too and moved to Maine to get her Masters degree and become an engineer. She has now moved to Mississippi, to work in the Coastal Hydraulics Lab of the USACE Engineering Research & Development Center and learn as much as possible about hydrodynamic engineering while “playing with big splashy toys”. Her long-term goal is to be a coastal/ocean engineer who works to make the aquaculture industry sustainable worldwide. Elisabeth is a candidate for the Master of Science degree in Civil Engineering from the University of Maine in August 2023.